FINAL TECHNICAL REPORT

AFOSR Grant F49620-93-1-0296
Covering the Period 04/01/93-6/30/96
Program Manager: Dr. James McMichael

NUMERICAL STUDIES OF UNSTEADY COMPRESSIBLE TURBULENT SHEAR FLOWS

Principal Investigators:

Dr. Victor Yakhot
Professor Steven A. Orszag
Department of Mechanical and Aerospace Engineering
Princeton University
Princeton, NJ 08544

December 1996

REPORT DOCUMENTATION PAGE

Form Approved
OMB No. 0704-0188

1. AGENCY USE ONLY (Leave blank)	2. REPORT DATE	3. REPORT TYPE AND DATES COVERED
		Final Technical 4/1/93-6/30/96

4. TITLE AND SUBTITLE
NUMERICAL STUDIES OF UNSTEADY COMPRESSIBLE TURBULENT SHEAR FLOWS

5. FUNDING NUMBERS
G - F49620-93-1-0296
PR-TA - 2307/BS

6. AUTHOR(S)
Dr. Victor Yakhot
Prof. Steven Orszag

7. PERFORMING ORGANIZATION NAME(S) AND ADDRESS(ES)
Princeton University
Department of Mechanical & Aerospace Engineering
Princeton, NJ 08544

8. PERFORMING ORGANIZATION REPORT NUMBER

9. SPONSORING/MONITORING AGENCY NAME(S) AND ADDRESS(ES)
AFOSR/NA
110 Duncan Avenue Room B115
Bolling AFB, DC 20331-8080
Attn: Dr. James M. McMichael

10. SPONSORING/MONITORING AGENCY REPORT NUMBER

11. SUPPLEMENTARY NOTES

12a. DISTRIBUTION/AVAILABILITY STATEMENT
Approved for public release; distribution unlimited.

12b. DISTRIBUTION CODE

13. ABSTRACT (Maximum 200 words) We have shown that in all cases when the integral scale (L_i) of turbulence is of the order of the size of the system (L), flow parameters and characteristics of the turbulence fluctuate strongly on a time scale of one turn-over time. DNS of Kolmogorov flow has been used to establish this effect. Experimental data on jet and mixing layers, where the integral scale is $L_i \approx 1/2L$, supports this basic observation. Strong fluctuations invalidate the ordinary "eddy viscosity" concept which in these cases requires finite time corrections. It has been shown that for those strongly time dependent flows the Smith/Yakhot modification of RNG gives a good description of the flow. The derived equations are being used for investigation of the onset of nonstationarity in flow over bluff bodies, including a rocket-like body at finite angle of attack. We have studied the optimization of physical characteristics of a "spoiler' used to reduce or eliminate vortex shedding using VLES. It has been shown that the process parameters depend on the device length and relative position. The validated theoretical concepts & numerical codes have been used for a set of exploratory simulations of a 3-D flow over a rocket-like body at the Reynolds number $Re \sim 10^7$. A number of 3-D phenomena have been observed.

14. SUBJECT TERMS	15. NUMBER OF PAGES
	98
	16. PRICE CODE

17. SECURITY CLASSIFICATION OF REPORT	18. SECURITY CLASSIFICATION OF THIS PAGE	19. SECURITY CLASSIFICATION OF ABSTRACT	20. LIMITATION OF ABSTRACT
Unclassified	Unclassified	Unclassified	SAR

"Numerical Studies of Unsteady Compressible Turbulent Shear Flows"
Princeton University
AFOSR F49620-93-1-0296

SUMMARY

The goal of this research is to establish the conditions for very large eddy simulations (VLES), i.e. the spontaneous generation of strong time-dependence of the "mean" flow characteristics and derivation of the effective equations of motion for accurate description of strongly nonstationary turbulent flows. The VLES technique is tested on cases of interest to the Air Force.

Funding received from AFOSR to support this project for the period 04/01/93 thru 06/30/96 totaled $546,169. The following personnel contributed to the work effort.

Principal Investigators:

Dr. Victor Yakhot
Prof. Steven A. Orszag.

Personnel Supported:

Dr. Ananias Tomboulides
Dr. J.-G. Liu
Sharon Matarese (administrative)

Student Support: Alexei Chekhlov

Degrees Awarded: 1 Ph.D

"Studies of Forced-Dissipative Turbulence in Model Hydrodynamics" by Alexei Chekhlov, Ph.D. Dissertation, Program in Applied & Computational Mathematics, Princeton University, June 1995.

Recognition Awards: Steven A. Orszag, 1995 G.I. Taylor Medal of the Society of Engineering Science.

Publications/Reports

Kolmogorov's Refined Similarity Hypothesis for Hyperviscous Turbulence (Vadim Borue and Steven A. Orszag), Physical Review E, Vol. 53, No. 1, January 1996.

Convective Instabilities of Two-Dimensional Compressible and Incompressible Flow Over Backward-facing Step (Yansi Zhang, Jian-Guo Liu, Steven A. Orszag), 48th Annual Meeting of the American Physical Society, Vol. 40, No. 12, Irvine, CA, November 1995.

Anomalous Scaling of Passive Scalar (R. H. Kraichnan, V. Yakhot and S. Chen), Phys. Rev. Lett., September 1995.

Kolmogorov Turbulence in a Random-Force-Driven Burgers Equation (Alexei Chekhlov and Victor Yakhot), Phys. Rev. E51(4), R2739-R2742, April 1995.

Spectra of Fluctuations of Velocity, Kinetic Energy and Dissipation Rate in Strong Turbulence (Victor Yakhot), Internal Report, May 1994.

Large-Scale Coherence and "Anomalous Scaling" of High-Order Moments of Velocity Differences in Strong Turbulence (Victor Yakhot), Phys. Rev. E49, 4, April 1994.

Fluctuations of Velocity, Kinetic Energy and Dissipation Rate in Strong Turbulence (Victory Yakhot), Phys. Rev. E50, 20, 1994.

Renormalization Group Modeling and Turbulence Simulations (Steven A. Orszag, Victor Yakhot, William S. Flannery, Ferit Boysan, Dipankar Choudhury, Joseph Maruzewski and Bart Patel), in Near-Wall Turbulent Flows, Editors R.M.C. So, C. G. Speziale and B. E. Launder, Elsevier Science Publishers B.V., 1993.

DESCRIPTION OF ACCOMPLISHMENTS/NEW FINDINGS

Table of Contents

	Page
1. Renormalization Group Modeling and Turbulence Simulations	4
2. Large-Scale Coherence and "Anomalous Scaling" of High-Order Moments of Velocity Differences in Strong Turbulence	20
3. Spectra of Fluctuations of Velocity, Kinetic Energy and Dissipation Rate in Strong Turbulence	62
4. Kolmogorov Turbulence in a Random-Force-Driven Burgers Equation: Anomalous Scaling and Probability Density Functions	74
5. Kolmogorov's Refined Similarity Hypothesis for Hyperviscous Turbulence	86

Renormalization Group Modeling and Turbulence Simulations

Abstract

We review the application of renormalization group methods to the transport modeling of turbulence. A variety of applications of the RNG $K-\mathcal{E}$ transport model are described, including flows with massive separation and strong anisotropy.

1. Introduction to RNG Methods for Turbulence

Renormalization group (RNG) methods are a general framework for "model building" in which the complex dynamics of physical problems is described in terms of so-called "coarse-grained" equations of motion governing the large-scale, long-time behavior of the physical system. For example, a mole of a classical gas involves 6×10^{23} interacting atoms and is described at a basic level in terms of a system of $3 \times 6 \times 10^{23}$ Newton's equations (for each of the three coordinates of each atom). Coarse-graining of this system can be performed at several levels: First, kinetic theory for dilute systems describes the coarse-grained system dynamics in terms of Boltzmann's equation for the probability density function of having an atom with velocity $\mathbf{v}$ at the space-time point $(\mathbf{x}, t)$. Second, further coarse-graining can be done by seeking a set of fluid dynamical equations that describe the average behavior of collections of atoms on space-time scales large compared with a mean free path and collision time. The resulting Navier-Stokes equations form the basis of modern fluid dynamics.

More generally, the RNG approach allows similar coarse-graining of physical phenomena as varied as critical phenomena, high-energy particle physics, and, especially in the context of fluid dynamics, turbulence, combustion, and heat transfer. The key idea is that the RNG method is applicable to scale invariant phenomena lacking externally imposed characteristic length and time scales. For turbulence, this means that the method is applicable to the description of the small scales (small eddies) that should be statistically independent of the

external initial conditions and dynamical forces that create them through various kinds of instability phenomena. In other words, the RNG method gives a theory of the so-called Kolmogorov equilibrium range of turbulence, especially comprising the so-called inertial range of small-scale eddies whose energy spectrum follows the famous Kolmogorov law $E(k) \propto k^{-5/3}$. The importance of the RNG results is, as we shall see, once the inertial range eddies can be accounted for in a quantitatively correct way, we may then obtain coarse-grained equations of motion for the other relevant variables of the turbulence, including, the mean velocity, rms velocities, etc.

In his 1985 Nobel Prize lecture, Kenneth Wilson, the originator of key ideas of renormalization group methods for field theory, stated

> "The renormalization group is one of the fundamental approaches to tackling this problem of what to do when you cannot make your grid small enough to use the fundamental equation. How do you increase the grid spacing beyond the level of a straight numerical approach, yet preserve all of the reliability that working from a fundamental equation can give you?"

Indeed, turbulent flows have eddies that range in size from so-called "energy-containing eddies" of size L, the integral scale, down to eddies of size $L/R^{3/4}$, where $R = v_{\rm rms}L/\nu$ is the Reynolds number. Still smaller eddies exist, but they have exceedingly low excitation due to viscous dissipation. Thus, accurate solution of the three-dimensional Navier-Stokes equations for a turbulent flow requires storage of order $O(R^{9/4})$ and computational work of order $O(R^3)$ [since turbulence also has a range of time scales of order $R^{3/4}$]. If R is large, these computational requirements are enormous, so RNG methods can be effective in reducing the computational requirements.

We use the RNG method to construct $K-\mathcal{E}$ RANS (Reynolds Averaged Navier-Stokes) equations by developing a theory of isotropic small-scale inertial-range eddies so that they may be eliminated from the equations of motion, yielding equations for averaged flow quantities at the integral scale of the turbulence. In this paper, we shall describe how this is done in a heuristic way – further details are given in our original papers on the application of RNG methods to turbulence.

2. Summary of the RNG Method

The basic ideas of the RNG method as developed in [1] are summarized in Figures 1–3. In Figure 1, we indicate the scales of effective excitation in turbulence ranging from a low energy-containing wavenumber $k_0 = 2\pi/L$ to the high wavenumber viscous cutoff Λ. The idea of the RNG method is to remove a narrow band of modes near Λ by representing these modes in terms of lower modes in the interval $k_0 < k < \Lambda e^{-\ell} (\ell << 1)$. When the narrow band of modes is removed, the resulting equations of motion for the remaining modes is a

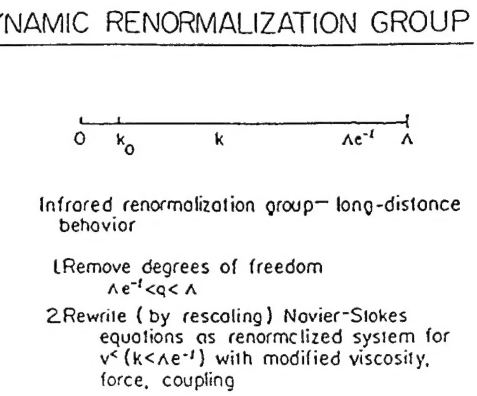

Figure 1

modified system of Navier-Stokes equations in which there is a modified (eddy) viscosity, modified force, and modified nonlinear coupling. Once this first narrow band of modes is removed from the dynamics, the process of removal of degrees of freedom is repeated iteratively, so that more and more modes are removed from the dynamics. In this way, the RNG method gives an effective calculus for the removal of modes from the Navier-Stokes equations, thereby rendering them computable at huge Reynolds numbers.

In Figure 2, we illustrate further the effect of the RNG procedure as the mode removal process continues. The solid band represents the small length scale eddies that are already removed from the dynamics. Their main effect is to increase the viscosity from its molecular value ν_{mol} to an effective eddy viscosity ν_{eddy}, thereby decreasing the effective Reynolds number to R_{eddy}. In Figure 3, we present a block diagram of the main steps in the RNG method. These steps are discussed further below.

Here we begin with a simple dimensional analysis argument that yields the main results for the RNG eddy viscosity for turbulence. The idea is that the eddy viscosity in turbulence is scale dependent $\nu(\ell)$ and that the RNG method constructs this viscosity by iterative removal of narrow bands of degrees of freedom. Thus, the RNG procedure develops directly an equation for $d\nu/d\ell$ rather than an equation for $\nu(\ell)$ itself. In the inertial range, the expression for $d\nu/d\ell$ can depend only on the eddy size ℓ, $\nu(\ell)$ itself, and $\mathcal{E}$, the rate of energy transfer through the inertial range to the dissipating eddies. If we note that leading-order

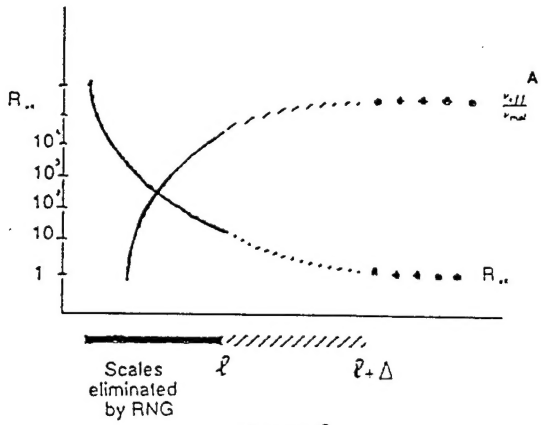

Figure 2

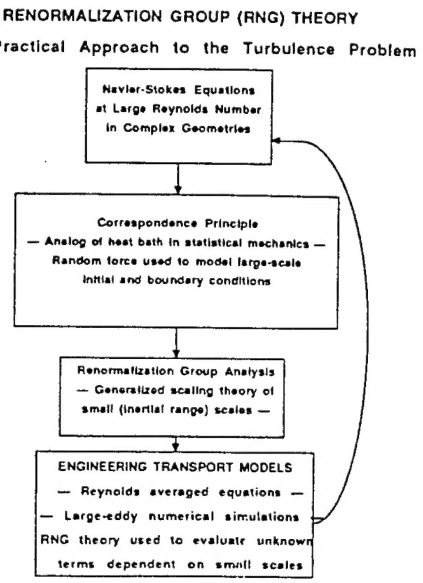

FIGURE 3

term in field theory for $d\nu/d\ell$ is proportional to $\mathcal{E}$ and assume that this result holds to higher order as well, we conclude that the only dimensionally correct expression is

$$\frac{d\nu}{d\ell} = \frac{A\mathcal{E}\ell^3}{\nu(\ell)^2} \tag{1}$$

where $A \approx 1.04 \times 10^{-4}$ is a constant evaluated by the full RNG theory. Integrating this equation over ℓ and using the condition that $\nu = \nu_{\text{mol}}$ when $\ell = \ell_d$, where ℓ_d is the Kolmogorov dissipation scale ($\approx L/R_L^{\frac{3}{4}}$), gives

$$\nu(\ell) = \nu_{\text{mol}} \left[1 + \frac{3A\mathcal{E}}{4\nu_{\text{mol}}^3} (\ell^4 - \ell_d^4) \right] \qquad (\ell \geq \ell_d) \tag{2}$$

Eq. (2) gives an interpolation formula for $\nu(\ell)$ between the molecular viscosity ν_{mol} valid at dissipation scales and the high Reynolds number limit

$$\nu(\ell) \sim \left(\frac{3}{4} A\mathcal{E} \right)^{1/3} \ell^{4/3} \qquad (\ell \gg \ell_d) \tag{3}$$

obtained from Eq. (2) in the limit $\ell \gg \ell_d$.

The result (3) already shows the power of the RNG method. Indeed, if we simply apply (3) to the largest eddies of the turbulence, those at the integral scale L, and eliminate the dissipation (energy transfer) rate $\mathcal{E}$ in terms of the large-scale rate-of-strain $\nabla\overline{\mathbf{U}}$ using the formula

$$\mathcal{E} = \nu_{\text{eddy}}|\nabla\overline{\mathbf{U}}|^2 \tag{4}$$

we obtain

$$\nu_{\text{eddy}} = [0.094L]^2|\nabla\overline{\mathbf{U}}| \tag{5}$$

The result (5) is remarkably close to Prandtl's classical mixing length formula for ν_{eddy}, derived originally as a semi-empirical formula to fit experimental data.

In the application of RNG methods for turbulence modeling, the local turbulent kinetic energy K and the local energy dissipation rate $\mathcal{E}$ are used to eliminate the length scale L (or ℓ) from the dynamics and the RANS equation of motion for $\overline{\mathbf{U}}$ is supplemented by equations for K and $\mathcal{E}$. The RNG method is used to evaluate otherwise unknown terms in these equations for this $K-\mathcal{E}$ model.

The resulting RNG $K-\mathcal{E}$ model differs from classical (or standard) $K-\mathcal{E}$ models in at least six ways:

- At high Reynolds number, the constants in the RNG $K-\mathcal{E}$ model are evaluated by the theory
- New terms appear like a rate of strain term, which is important for treatment of non-equilibrium effects and flows in the rapid distortion limit
- Impulse response modifications, important for non-equilibrium effects, are also taken into account
- Low Reynolds number modifications are given by the RNG theory, so wall functions are no longer required
- Modified boundary conditions are developed from the theory
- Stratification and rotation (swirl) effects are accounted for by extensions of the RNG theory to stratified and rotating flow

Here we give an illustration of some of these results. For example, the eddy viscosity in standard $K-\mathcal{E}$ models is given by [2]

$$\nu_{\text{eddy}} = C_\mu \frac{K^2}{\mathcal{E}} \tag{6}$$

where $C_\mu \approx 0.09$. RNG theory gives this result by eliminating the length scale ℓ between the expression (5) for the high Reynolds number turbulent viscosity and the following expression for the total kinetic energy in isotropic inertial range eddies at scales smaller than ℓ:

$$K = 0.71\mathcal{E}^{2/3}\ell^{2/3} \tag{7}$$

The resulting expression for the eddy viscosity is (6) with $C_\mu = 0.0845$, in good agreement with the "standard" value. However, because the RNG theory also gives the low Reynolds number interpolation formula (4), we obtain the more general expression

$$\nu_{\text{eddy}} = \nu_{\text{mol}} \left[1 + \sqrt{\frac{C_\mu}{\nu_{\text{mol}}}} \frac{K}{\sqrt{\mathcal{E}}} \right]^2 \tag{8}$$

which is valid across the full range of flow conditions from low to high Reynolds numbers.

The high Reynolds number form of the RNG $K - \mathcal{E}$ model is given by [2]

$$\frac{\partial \overline{U}_i}{\partial t} + \overline{\mathbf{U}} \cdot \nabla \overline{U}_i = -\nabla_i p + \frac{\partial}{\partial x_j} \left[\nu_{\text{eddy}} \left(\frac{\partial \overline{U}_i}{\partial x_j} + \frac{\partial \overline{U}_j}{\partial x_i} \right) \right] \tag{9}$$

$$\frac{\partial K}{\partial t} + U_j \frac{\partial K}{\partial x_j} = \nu_{\text{eddy}} S^2 - \mathcal{E} + \nabla \alpha \nu_{\text{eddy}} \nabla K \tag{10}$$

and

$$\frac{\partial \mathcal{E}}{\partial t} + U_j \frac{\partial \mathcal{E}}{\partial x_j} = 1.42 \frac{\mathcal{E}}{K} \nu_{\text{eddy}} S^2 - 1.68 \frac{\mathcal{E}^2}{K} - R + \nabla \alpha \nu_{\text{eddy}} \nabla \mathcal{E} \tag{11}$$

where the rate-of-strain term R is given by

$$R = 2\nu_{\text{eddy}} S_{ij} \overline{\frac{\partial u_l}{\partial x_i} \frac{\partial u_l}{\partial x_j}} \tag{12}$$

This term is expressed in the RNG $K - \mathcal{E}$ model equations as

$$R = \frac{C_\mu \eta^3 (1 - \eta/\eta_0)}{1 + \beta \eta^3} \frac{\mathcal{E}^2}{K} \tag{13}$$

where $\eta = SK/\mathcal{E}$ and $S^2 = 2S_{ij}S_{ij}$ is the magnitude of the rate-of-strain. The RNG theory gives values [3], [4] of the constants $C_{\mathcal{E}_1} = 1.42$ and $C_{\mathcal{E}_2} = 1.68$, and $\alpha = 1.39$, in comparison with the "standard" values $C_{\mathcal{E}_1} \approx 1.4$ and $C_{\mathcal{E}_2} \approx 1.9$, and $\alpha = 1$.

The reduced value of $C_{\mathcal{E}_2}$ in the RNG theory has the interesting consequences of decreasing both the rate of production of K and the rate of dissipation of $\mathcal{E}$, leading to smaller values of ν_{eddy} according to (6). In regions of small η, the term R tends to increase ν_{eddy} somewhat, but it is still typically smaller than its value in the standard theory. However, in regions of large η, the *sign* of R is changed and ν_{eddy} is decreased even more. This feature of the RNG equations is due to the strong anisotropy in regions of large shear and is responsible for some of the marked improvement of the RNG model in the treatment of massive flow separation and anisotropic large-scale eddies (see below).

The RNG procedure also yields low-Reynolds-number modifications that obviate the need for wall-functions in low effective Reynolds number regions of the flow. These low-Reynolds-number modifications appear typically in the form of differential relationships in

which the modeling "constants" become functions of local effective Reynolds number. Here we will not discuss these features of the model. The inverse turbulent Prandtl numbers α, in (10)-(11) are obtained from the RNG scalar heat transport relation.

3. Mathematical Theory of the RNG Method

At a more mathematical level, the main ideas of the RNG method can be summarized in the following way [1]. Consider the nonlinear equation:

$$\frac{\partial \phi}{\partial t} + N(\phi) = \nu_0 \nabla^2 \phi + f \tag{14}$$

where $N(\phi)$ is a non-linear operator, ν_0 is molecular viscosity, and f is a random stirring force. In principle, any other linear terms can be added to this equation. For simplicity, let us assume that the random force f is a gaussian variable. The equation of motion is assumed to be defined on the domain $0 < k < \Lambda_0$. It is assumed that the non-linear term N is large and can be characterized by the dimensionless coupling constant (Reynolds number) $\lambda_0 = \lambda(\nu_0, D_0, \Lambda_0)$ where D_0 is the amplitude of the force correlation function $\langle ff \rangle \propto D_0 k^{-y}$. Using the generalized perturbation methods of quantum field theory, it is possible to formally eliminate the small-scale modes $\phi(k)$ with $\Lambda < k < \Lambda_0$ from the problem and derive another equation of motion defined on the interval $0 < k < \Lambda$:

$$\frac{\partial \phi_\Lambda}{\partial t} + N_\Lambda(\phi_\Lambda) = \nu_\Lambda \nabla^2 \phi_\Lambda + f_\Lambda \tag{15}$$

This new equation has the dimensionless coupling constant

$$\lambda(\Lambda) = \lambda(\nu_0, D_0, \Lambda_0, D(\Lambda), \nu(\lambda), \Lambda)$$

where $D(\Lambda)$, $\nu(\Lambda)$ are the effective transport coefficients and induced random noises which account for the effects of the eliminated modes. We can always define dimensionless variables so that the effective coupling constant is the amplitude of the new non-linear term $N_\Lambda(\phi)$. The new (renormalized) parameters and new non-linearities must be explicitly evaluated from the original dynamic equation. Our goal is to follow the dependence $\lambda(\Lambda)$ upon the variation of the cut off Λ . In a scale invariant range the effective coupling constant and all correlation functions must not depend on the molecular (bare) parameters ν_0, D_0 and Λ_0. Thus, in the limit $\Lambda \to 0$

$$\lambda \to \lambda(D(\Lambda, \nu(\Lambda), \Lambda) \tag{16}$$

and the effective coupling constant goes to a so-called "fixed point":

$$\lambda(\Lambda) = \lambda(\Lambda/C) \tag{17}$$

where $C > 1$ is an arbitrary number. This relation reflects the fact that, in a scale invariant range, $\lambda(\Lambda) \to \lambda^* = const$, independent of the scale Λ . If $\lambda^* \to 0$, then the problem, formulated in the new variables $D(\Lambda)$ and $\nu(\Lambda)$ is linear and exactly solvable. If λ^* is small, then perturbation expansion in powers of λ^* can be used to obtain explicit formulas for the scale-invariant field. In many cases, the fixed point value of the effective coupling constant λ^* is a function of a parameter ϵ which is constructed from the other parameters of the problem. The perturbation expansion in powers of λ^* is then called an ϵ-expansion. The renormalization group with the ϵ-expansion is in principle, a mathematical prescription to derive equations of motion describing the large-scale system dynamics with the small scales removed.

The RNG prescription consists of the following steps:

1. Identify the space of relevant parameters $\{P\}$ governing the system. In the case of homogeneous and isotropic turbulence, $\{P\}$ includes $\mathcal{E}$—the dissipation rate of kinetic energy; ν_0—the molecular viscosity; Reynolds number; etc. This case, however, is the simplest possible: in strongly rotating or stratified flows we have to add vorticity or swirl; buoyancy fluxes, etc.

2. Eliminate a band of small scales and evaluate corrections to the flow parameters, nonlinearities in the equations of motion, noises, etc.

3. Iterate the scale-elimination procedure described above to find new scale depending parameters of the problem $\{P(\Lambda)\}$ and assess their relative importance as functions of Λ .

4. Derive the dimensionless coupling constants $\lambda(\Lambda) \to \lambda^*$ and evaluate the solutions of the equations of motion in the lowest order in expansion in powers of λ^* or ϵ. If this is impossible to do analytically, the resulting equations of motion should be solved numerically.

When this strategy is applied to the Navier-Stokes equation we obtain a series of turbulence models ranging from sub-grid eddy viscosity models to the full $K - \mathcal{E}$ transport model described in the previous section.

4. Applications of the RNG $K - \mathcal{E}$ Model

The RNG $K - \mathcal{E}$ model with the appropriate low-Reynolds-number modifications and boundary conditions has now been used to successfully compute a variety of complex flows. Here we give several examples.

Backward-Facing Step

In Figure 4, we plot streamlines for a 2:3 channel expansion at an inflow Reynolds number of 88,000. At this Reynolds number, the reattachment length is predicted to be at 7.0 step heights, while experiment yields 7.1 step heights. Comparison of other flow quantities with experiment is also quite satisfactory. An important feature of the flow, a small corner vortex, observed in the experiment is accurately predicted by the model. This kind of detailed flow feature can be quite important to the accurate prediction of heat transfer and scalar transport.

Blunt Flat Plate

In Figure 5, we plot the mean-flow streamlines obtained using the standard and RNG $K - \mathcal{E}$ model for flow past a blunt flat plate at a Reynolds number of 21,600. The RNG model gives a separated eddy whose size ($\approx$ 8 half-widths of the plate) agrees well with experiment, while the standard model gives a vanishing small separated eddy, largely due to the fact that the eddy viscosity is too large in the standard model. At a Reynolds number of 50,000, the RNG model predicts a separated eddy of roughly 9.5 half-widths, in good agreement with the experimental result of 9.6 half-widths.

Turnaround Duct (U-Bend)

In Figure 6, the mean-flow streamlines obtained using the standard and RNG model are presented for flow in a turnaround duct at a Reynolds number of 10^5. The RNG model again gives a separated eddy whose size agrees well with experiment, but the standard model misses the flow separation completely (again due to an eddy viscosity that is too large).

(a) streamlines with reattachment X/H = 7.0

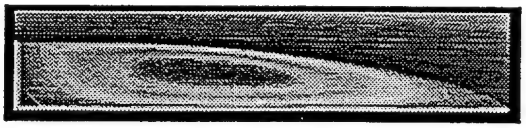

(b) primary eddy

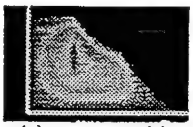

(c) corner eddy

Figure 4: Streamlines for the flow over a backward facing step with expansion ratio of 2:3 at inlet Re = 88,000, computed using the RNG K – $\mathcal{E}$ model.

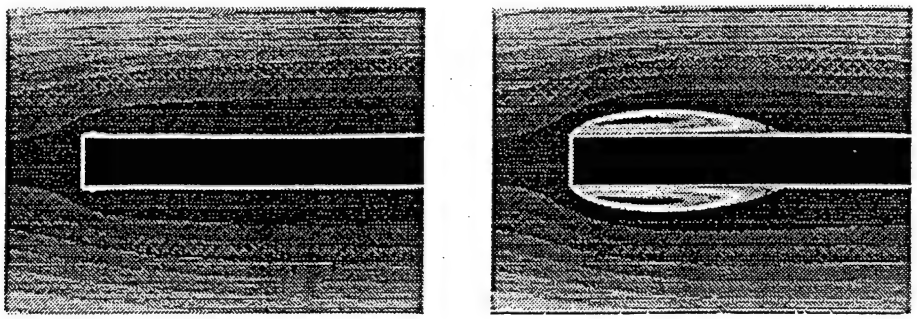

(a) (b)

Figure 5: Streamlines for the flow over a blunt flat plate computed using a) the standard K-ε model b) the RNG K-ε model (Re = 21,600)

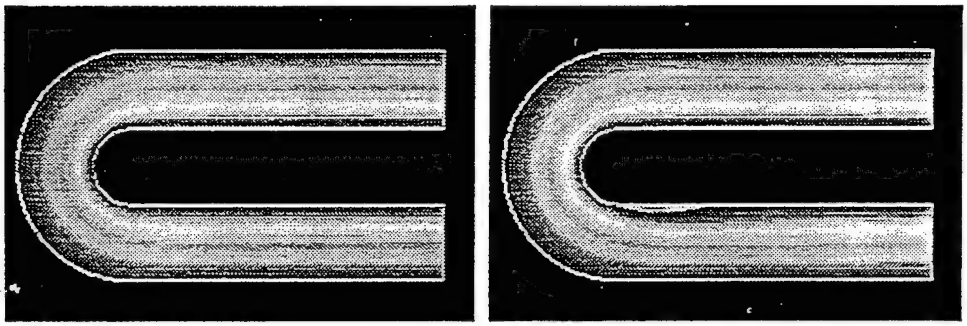

(a) (b)

Figure 6: Streamlines for the flow in a turnaround duct computed using a) the standard K-ε model b) the RNG K-ε model (Re = 100,000)

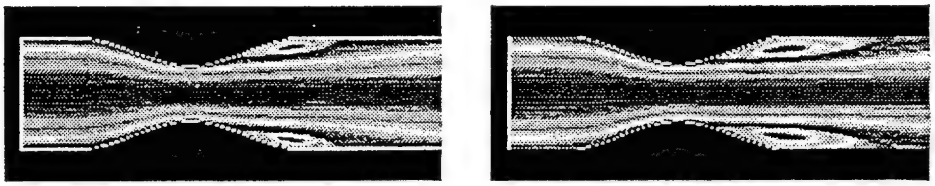

(a) (b)

Figure 7: Streamlines for the flow in a stenosis computed using a) the standard K- ε model b) the RNG K -ε model (Re = 10,000)

Constricted Pipe Flow (Stenosis)

In Figure 7, the mean-flow streamlines obtained using the standard and RNG model are presented for flow in a constricted pipe with Reynolds number 10^4. The pipe has a diameter that varies by a factor 2:1. Again, the RNG model gives a separated eddy whose size agrees well with experiment and that is significantly larger than that predicted by the standard model. *Valve-Port Assembly*

In Figures 8-11, the mean-flow streamlines obtained using the standard and RNG model are presented for flow in a valve-port assembly studied by Gosman and Ahmed with non-dimensional gap widths $L^* = 0.20, 0.25$. The flow visualization is given in Figure 8, which shows flow separation at both gap widths in the crown region of the geometry and flow separation in the gap for the larger gap width. In Figure 9,we show the grid used in our computations which involve a 60×150 mesh. In Figure 10, we plot the mean streamlines for the standard $K - \mathcal{E}$ model – there is no flow separation in either the crown or the gap regions for both gap widths. The results plotted in Figure 11 for the RNG model show that there are separated eddies in both the crown and gap regions whose size agrees well with experiment.

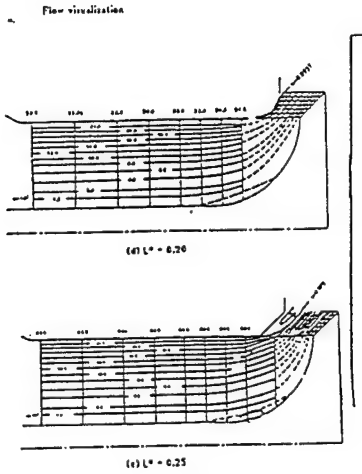

Figure 8

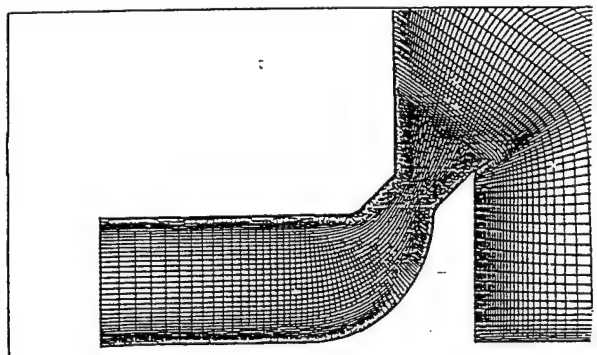

Figure 9

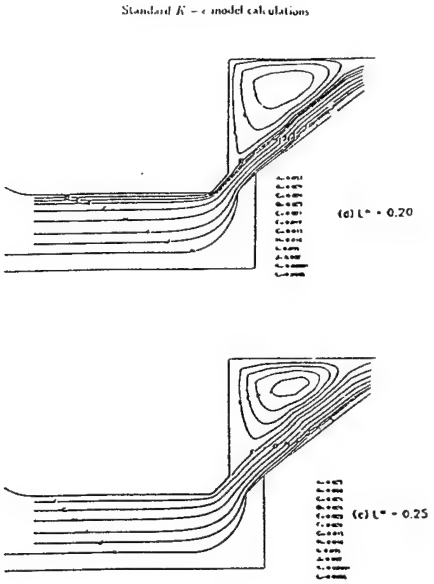

Figure 10

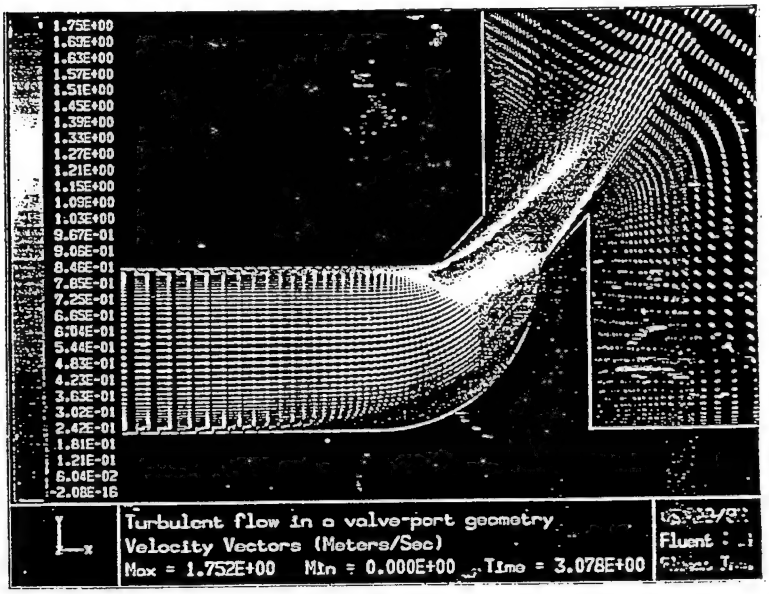

Figure 11

Transitional Flow Past a Cylinder

The RNG model can also describe time-dependent transitional flow phenomena. This is illustrated by the flow field results plotted in Figure 12–14 for flow past a cylinder at a Reynolds number of 14,500. The streamlines plotted in Figure 12 demonstrate the ability of the model to capture the time-dependent coherent flow structures immediately behind the cylinder. The instantaneous turbulence intensity distributions plotted in Figure 13 and time-averaged turbulence intensity plotted in Figure 14 show that the RNG model is capable of predicting time dependent phenomena like vortex shedding. The calculated Strouhal number, $S = 0.185$ is to be compared with the experimental observed value $S = 0.19$.

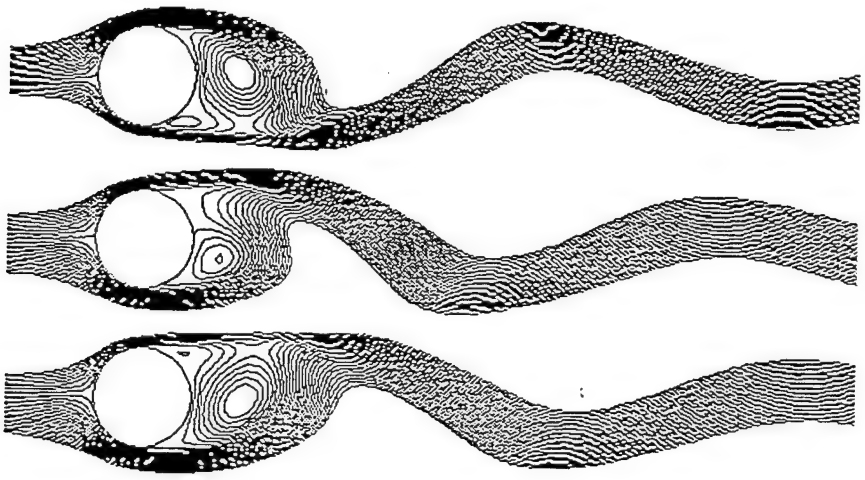

Figure 12: Streamlines in the wake of a cylinder at Re=14,500 computed using the RNG K– ε Model

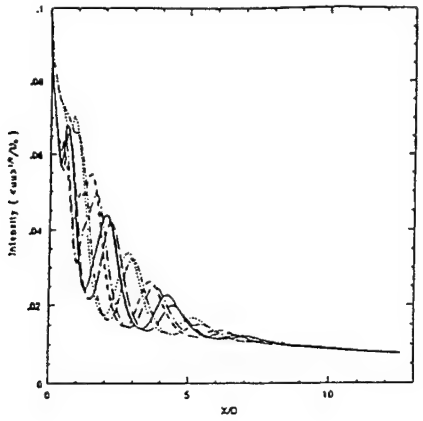

Figure 13: The turbulence intensity in the wake of a cylinder at six time slices over one shedding cycle. (Re = 14,500)

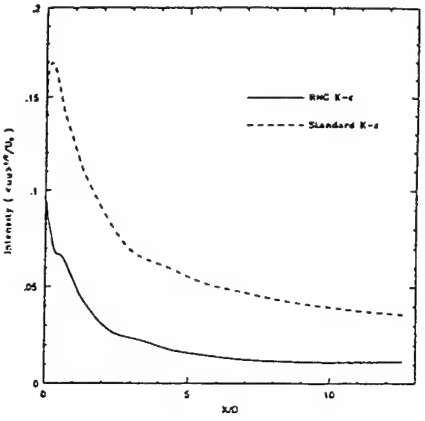

Figure 14: The average turbulence intensity in the wake of the cylinder computed with the RNG K-ϵ model (Re = 14,500).

Flow Past a Model 2D Car

In Figure 15, we show instantaneous streamlines, pressure contours, and K contours for flow past a 2D model car studied by Rieger et. al. [5]. The Reynolds number of the flow is 6.6×10^6. These results obtained by the RNG code describe the time-dependent nature of the vortex shedding process to an accuracy of about 5% (including Strouhal number, drag and lift, and base pressure). In Figure 16, we plow the average surface pressure distribution in comparison with experimental results [5].

The ability of turbulence modeling to accurately describe separated flows is of great practical importance. For example, maxima of heat transfer are observed close to the reattachment points. This is important for the description of combustion-related phenomena.

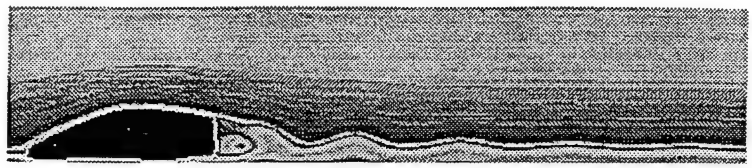

(a) Streamlines

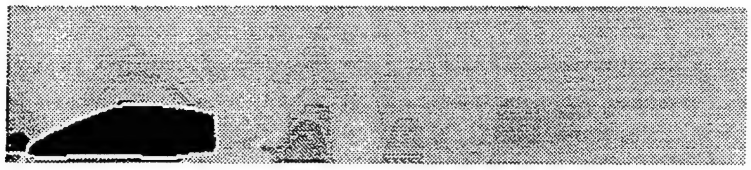

(b) Contours of Pressure

(c) Contours of turbulent kinetic energy

Figure 15: Flow over the Mercedes Benz 2-D Automobile Model Computed Using the RNG K-$\mathcal{E}$ Model.

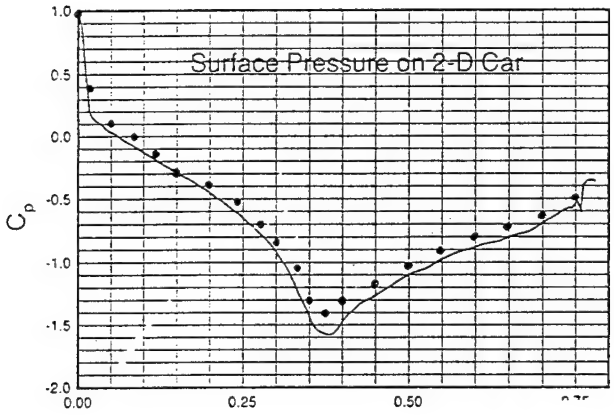

Figure 16. Average surface pressure on the 20 car [5]. The solid line is the results of the RNG $K-\mathcal{E}$ model while the data points are the experimental results.

References

[1]V. Yakhot and S. A. Orszag, "Renormalization group analysis of turbulence: 1. Basic theory", J. Sci. Comput. 1, 3 (1986).

[2]V. Yakhot, S. A. Orszag, S. Thangam, T. B. Gatski, and C. G. Speziale, "Development of turbulence models for shear flows by a double expansion technique", Phys. Fluids, A4, 1510 (1992).

[3]L. M. Smith and W. C. Reynolds, "On the Yakhot-Orszag renormalization group method for deriving turbulence statistics and models", Phys. Fluids A 4, 364 (1992).

[4]V. Yakhot and L. M. Smith, "The renormalization group, the ϵ-expansion and derivation of turbulence models, "J. Sci. Comput. 3, 35 (1992).

[5]H. Rieger, F. Magagnato, W. Fritz, and W. Siebert, "Numerische Simulation turbulenter Strömungen um komplexe Automogilgeometrien-Erfahrungen, Status und Ausblick, VDI Berichte Nr. 1007, pp. 839-857 (1992).

Large-Scale Coherence and "Anomalous Scaling" of High-Order Moments of Velocity Differences in Strong Turbulence.

Abstract

The Hamiltonian formulation of hydrodynamics in Clebsch variables is used for construction of a statistical theory of turbulence. It is shown that the interaction of the random and large-scale coherent components of the Clebsch fields is responsible for generation of two energy spectra $E(k) \propto k^{-\frac{7}{3}}$ and $E(k) \propto k^{-2}$ at scales somewhat larger than those corresponding to the $-5/3$- inertial range. This interaction is also responsible for the experimentally observed gaussian statistics of the velocity differences at large scales, and the nontrivial scaling behaviour of their high-order moments for inertial- range values of the displacement r. The "anomalous scaling exponents" are derived and compared with experimental data.

1 Introduction

A widely accepted formulation of turbulence theory deals with a flow governed by the Navier-Stokes equations (the density $\rho = 1$):

$$\frac{\partial \mathbf{v}}{\partial t} + \mathbf{v} \cdot \nabla \mathbf{v} = -\nabla p + \mathbf{F} + \nu_0 \Delta \mathbf{v}$$

$$\nabla \cdot \mathbf{v} = 0$$

where $\mathbf{F}$ is a forcing function having Fourier-transform $F(k) \neq 0$ only in the interval $k < k_0 \to 0$. This means that kinetic energy is pumped into the system at large scales only. At large enough Reynolds number Re the flow becomes turbulent and, introducing the Reynolds decomposition $\mathbf{v} = \mathbf{U} + \mathbf{u}$, where $\mathbf{U}$ and $\mathbf{u}$ describe the mean and fluctuating components of the velocity field, respectively, the equations of motion can be formally rewritten as

$$\frac{\partial \mathbf{U}}{\partial t} + \mathbf{U} \cdot \nabla \mathbf{U} + \mathbf{U} \cdot \nabla \mathbf{u} = -\nabla P + \mathbf{F} + \nu_0 \Delta \mathbf{U}$$

$$\frac{\partial \mathbf{u}}{\partial t} + \mathbf{u} \cdot \nabla \mathbf{u} + \mathbf{u} \cdot \nabla \mathbf{U} = -\nabla p' + \nu_0 \Delta \mathbf{u}.$$

If $p = P + p'$, these equations are equivalent to the original Navier-Stokes equations. The goal of the theory is to evaluate both $\mathbf{U}$ and $\mathbf{u}$.

Understanding the behaviour of the small-scale velocity fluctuations is one of the main challenges of turbulence theory. It is usually assumed that the statistical characteristics of the flow at small enough scales are independent of the large-scale dynamics. This assumption is basic for comparison of the theoretical predictions with experimental data. However, as seen from the equation for $\mathbf{u}$, the small-scale velocity fluctuations interact with the "dressed" external field U, responsible for turbulence production. This field must be taken into account when we are interested in such fine detail of the flow as deviations from the Kolmogorov theory observed in the high-order moments of the velocity differences, defined below. Moreover, at the not-too-small scales this field can dominate the dynamics, thus considerably simplifying the problem. Investigation of the possible effects of the large-scale, long-living structures on the small-scale properties of turbulence is the goal of this work.

Experimental data on the second order structure function $S_2(x)$ measured in various high-Reynolds number flows support the Kolmogorov prediction

$$S_2 \equiv \overline{(\Delta u)^2} \equiv \overline{\Big(u(X) - u(X+x)\Big)^2} = C_K \bar{\epsilon}^{\frac{2}{3}} x^{\frac{2}{3}} \qquad (1.1)$$

where $\bar{\epsilon}$ is the energy flux in wave-vector space. Relation (1.1), though not derived from mathematically rigorous theory, is readily obtained from various qualitative considerations. For example, at scales much smaller than the energy injection scale the following exact relation holds:

$$S_3 = -\frac{4}{5}\bar{\epsilon}x$$

Relation (1.1) is obtained immediately if the possibility of the "anomalous scaling" arising from the nontrivial dimensionality of $\bar{\epsilon}$ is disregarded.

However, dimensional arguments applied to the high-order moments of velocity differences give $S_n(x) \approx x^{\frac{2}{3}n}$ which contradicts the available experimental data when n is large. So far the observed scaling behaviour of higher-order structure functions remains something of a mystery. Numerous experiments indicate that in the available range of displacements x the functions $S_n(x)$ seem to be rather well fitted by the power laws:

$$S_n = \overline{\Big(u(X) - u(X+x)\Big)^n} \propto x^{\kappa_n - \xi_n} \tag{1.2}$$

where the scaling exponents ξ_n describe deviations from the Kolmogorov values $\kappa_n = \frac{n}{3}$. Further, it was found that the larger the order n, the larger the deviation of ξ_n from the predictions of the Kolmogorov theory.

Another unsolved problem is the shape of the probability distribution function (PDF) of the velocity differences $P(\triangle u)$. It is well established that the single-point PDF is gaussian. In other words,

$$P(\triangle u) \propto exp\Big(-\frac{(\triangle u)^2}{u_{rms}^2}\Big) \tag{1.3}$$

for $x \gg L$, where L is the integral scale of turbulence. Moreover gaussian statistics of velocity differences are observed for separations $x/L = O(1)$. For the scales x corresponding to the inertial range $l_d << x << L$, where l_d is the dissipation scale, the experimentally observed $P(\triangle u)$ seems to be close to exponential:

$$P(\triangle u) \propto exp\Big(-\alpha\frac{|\triangle u|}{u_{rms}}\Big) \tag{1.4}$$

with the dimensionless coefficient $\alpha = 0(1)$. Relations (1.3) and (1.4) represent the most dominant feature of the PDF of velocity differences in the inertial range.

Not less interesting is the behaviour of the fluctuations of the local value of the kinetic energy dissipation rate $\epsilon = \nu(\frac{\partial u_i}{\partial x_j})^2$. The Kolmogorov theory (K41) simply neglected the ϵ-fluctuations assuming $\epsilon(x) = const.$ It was later suggested[1] that the ϵ–fluctuations may be responsible for the experimentally observed deviations from Kolmogorov scaling. It is easy to show that if turbulent transport coefficients obtained from the K41 phenomenology are used for construction of a dimensional argument, the resulting correlation function is:

$$S_2^\epsilon = \overline{\Big(\epsilon(X) - \epsilon(X+x)\Big)^2} \propto x^0 \tag{1.5}$$

Relation (1.5), showing that the ϵ-fluctuations are evenly distributed in space, has never been observed in numerical or physical experiments. Instead, observations suggest

$$S_2^\epsilon \propto x^{-\mu} \tag{1.6}$$

with the "intermittency exponent" μ ranging from 0.1 to $\simeq 1$ depending on the experimental conditions, Reynolds numbers etc. Relation (1.6) shows that the dissipation rate of kinetic energy is concentrated in the localized areas of space having a "spotty" nature. This is often interpreted as spatial intermittency of strong turbulence. Theoretical understanding of this behaviour is a major challenge. Accurate experimental verification of (1.6) is very difficult and at the present time we cannot even be sure that a scaling relation of the type (1.6) exists at all, though it is clear that experimentally observed $S_2^\epsilon(x)$ decreases with x more slowly than predicted by (1.5).

Since the dissipation rate appears in the expression for the Kolmogorov energy spectrum, it is tempting to try to incorporate the ϵ-fluctuations into Kolmogorov-like considerations and express the deviations from the K41 scaling observed in the high-order moments of velocity differences in terms of the intermittency exponent μ. This has been done in various models, often rather loosely related to the Navier-Stokes equation of motion. However, the gaussianity of the large-scale velocity fluctuations has not been

addressed by any model of intermittency known to me. It is remarkable that in various experimental situations, differing by geometry, production mechanisms, Reynolds number etc, the observed PDF of velocity differences was so close to gaussian at the scales $x/L \approx 1$. In my opinion the universality and robustness of this quantity is most surprising and very difficult to explain. In this paper I modify the Clebsch formulation of statistical theory of strong turbulence, developed in Ref:(3), to include the large-scale coherent structures, sometimes responsible for turbulence production. It will be shown that the interaction between coherent and random components of the Clebsch fields is responsible for the observed gaussian statistics of the large-scale velocity differences and for the non-trivial behaviour of the high-order moments. The results will be compared with experimental data.

This paper is organized in a following way. In Sections 2 and 3, closely following Ref.(3), the formulation of hydrodynamics in Clebsch variables is introduced and the Kolmogorov energy spectra corresponding to the constant fluxes of conserved quantities are derived. In Section 4 the interaction of the large-scale coherent and random components is introduced, and it is shown that the theory reduces to the many-body problem in a strong external field. The interaction of the velocity fluctuations with coherent structures is responsible for two additional solutions at scales larger than those corresponding to the Kolmogorov range. The expressions for the probability distribution function of velocity differences, which is gaussian at large scales and close-to-exponential at smaller scales, is derived in Section 5. In Section 6 the derivation of the dissipation rate correlation function, developed in Ref.(3) is presented. The discussion of experimental data and a detailed comparison with the outcome of this paper are presented in the Section 7.

2 Formulation of the Problem

We consider a fluid flow driven at the very large scales $l \gg L \to \infty$. Somewhere at the smallest scales $l \to 0$ an energy sink is assumed, so that a statistically steady state can be achieved. The flow is described by the Navier-Stokes equations:

$$\frac{\partial \mathbf{v}}{\partial t} + \mathbf{v} \cdot \nabla \mathbf{v} = -\nabla p + \mathbf{F} + \nu_0 \Delta \mathbf{v}$$

$$\nabla \cdot \mathbf{v} = 0$$

subject to initial and boundary conditions. We assume that the force $\mathbf{F}(\mathbf{x}, \mathbf{t})$ is an arbitrary deterministic function of position and time acting at large scales only. In various flows $\mathbf{F}$ corresponds to the deterministic contribution to the pressure gradient. For example the flow in a pipe driven by gravity is equivalent to the flow driven by a constant pressure gradient. When the Reynolds number $Re < Re_c$ this equation gives a laminar velocity profile $\mathbf{U_L}(\mathbf{x}, \mathbf{t})$. At $Re > Re_c$ the laminar velocity profile is modified due to the interaction with turbulent velocity fluctuations.

It is customary to describe the dynamics of the intermediate scales by the Euler equation (the density $\rho = 1$):

$$\frac{\partial \mathbf{v}}{\partial t} + \mathbf{v} \cdot \nabla \mathbf{v} = -\nabla p \tag{2.1}$$

$$\nabla \cdot \mathbf{v} = 0$$

The Clebsch variables are defined as:

$$\mathbf{v} = \lambda \nabla \mu + \nabla \phi \tag{2.2}$$

Using the incompressibility condition, the potential ϕ can be expressed through λ and μ:

$$\phi = -\nabla^{-2} \nabla \cdot (\lambda \nabla \mu)$$

and thus:

$$\mathbf{v} = -\nabla^{-2} \nabla \times (\nabla \lambda \times \nabla \mu) \tag{2.3}$$

$$\omega = \nabla \lambda \times \nabla \mu \tag{2.4}$$

The Clebsch variables are transported by the flow and the Euler equation can be represented as:

$$\mathcal{D}\mu = \frac{\partial \mu}{\partial t} + \ \mathbf{v} \cdot \nabla \mu = 0; \ \mathcal{D}\lambda = \frac{\partial \lambda}{\partial t} + \mathbf{v} \cdot \nabla \lambda = 0 \tag{2.5}$$

It follows from equation (2.3) that the velocity field does not uniquely define the Clebsch field $(\lambda(x,t), \mu(x,t))$. In fact, a set of pairs of the Clebsch variables $(\lambda_i(x,t), \mu_i(x,t))$ can be used to express the velocity $\mathbf{v}(\mathbf{x}, \mathbf{t})$:

$$\mathbf{v} = \sum_{\mathbf{i=1}}^{\mathbf{M}} \lambda_\mathbf{i} \nabla \mu_\mathbf{i} + \nabla \phi \tag{2.6}$$

and

$$\omega = \sum_{i=1}^{M} \nabla \lambda_i \times \nabla \mu_i \tag{2.7}$$

where M is the number of Clebsch pairs necessary for the complete representation of velocity field.

The equations of motion for each pair (λ_i, μ_i), given by (2.5) with the subscript i specifying the pair, can be written in a Hamiltonian form since λ and μ are canonical variables. The Hamiltonian and the corresponding equations of motion are given below. The minimal number of canonical pairs needed to describe an arbitrary flow depends on the topology of the field $\mathbf{v}$. It a plausible conjecture that $M = 2$ is sufficient to represent a wide class of turbulent flows. Indeed, the velocity field in a three-dimensional incompressible flow has two independent components. This field, however, cannot be described by one pair of Clebsch variables due to the constraint $\mathbf{v} \cdot \omega = 0$ which tells us that, in fact, we have only one independent Clebsch variable. Introducing the second Clebsch pair we create two independent variables, sufficient for the description of the general velocity field with non-zero values of the local helicity. In this paper we will discuss only the case of $M = 1$ which corresponds to zero helicity $\int \mathbf{v} \cdot \omega \mathbf{dx} \equiv 0$, following directly from the definition (2.4). This restricts applicability of the analysis to flows in which the vortex lines do not have any knots. However, the results of this work may be readily generalized to the case of $M = 2$ corresponding to an arbitrary topology.

Introducing the complex variables $a(\mathbf{k})$ and $a^*(\mathbf{k})$

$$\mu(\mathrm{k}) = \frac{1}{\sqrt{2}}\Big(a(\mathrm{k}) + \mathrm{a}^*(-\mathrm{k})\Big); \lambda(\mathrm{k}) = \frac{\mathrm{i}}{\sqrt{2}}[\mathrm{a}(\mathrm{k}) - \mathrm{a}^*(-\mathrm{k})] \tag{2.8}$$

the Euler equation can be written in a Hamiltonian form:

$$i\frac{\partial a(\mathrm{k})}{\partial t} = \frac{\delta H}{\delta a^*(\mathrm{k})} \tag{2.9}$$

where the Hamiltonian H is:

$$H = \frac{1}{4}\int T_{12,34}\, a^*(\mathrm{k}_1)a^*(\mathrm{k}_2)a(\mathrm{k}_3)a(\mathrm{k}_4)\delta(\mathrm{k}_1 + \mathrm{k}_2 - \mathrm{k}_3 - \mathrm{k}_4)d\mathrm{k}_1, d\mathrm{k}_2\, d\mathrm{k}_3\, d\mathrm{k}_4 \tag{2.10}$$

The interaction potential is

$$T_{12,34} \equiv T(\mathrm{k}_1\mathrm{k}_2, \mathrm{k}_3\mathrm{k}_4) = \varphi_{13}\varphi_{24} + \varphi_{14}\varphi_{23} \tag{2.11}$$

where

$$\varphi(\mathrm{k}_1, k_2) \equiv \varphi_{12} = \mathrm{k}_1 + \mathrm{k}_2 - (\mathrm{k}_1 - \mathrm{k}_2)\frac{k_1^2 - k_2^2}{\mid \mathrm{k}_1 - \mathrm{k}_2 \mid^2} \tag{2.12}$$

In these variables:

$$\mathrm{v} = \int \varphi_{\mathrm{q},\mathrm{q}-\mathrm{k}} a^*_{\mathrm{q}} a_{\mathrm{q}-\mathrm{k}} d\mathrm{q} \tag{2.13}$$

The function $\varphi(k_1, k_2)$ is a discontinuous function at $k_1 = k_2$ since the diagonal elements of $\varphi(k, k)$ determine an arbitrary mean velocity in the flow $\mathrm{v}(\mathrm{k} = \mathbf{0})$. So, in what follows we set $\varphi(k, k) = 0$.

Substituting (2.10), (2.11), (2.12) into (2.9) the equation of motion for the "creation-annihilation" operators $a(\mathrm{k})$ is readily derived:

$$i\frac{\partial a(\mathrm{k})}{\partial t} = \frac{1}{2}\int T(\mathrm{k}\mathrm{k}_2, \mathrm{k}_3\mathrm{k}_4)a^*(\mathrm{k}_2)a(\mathrm{k}_3)a(\mathrm{k}_4)\delta(\mathrm{k} + \mathrm{k}_2 - \mathrm{k}_3 - \mathrm{k}_4)d\mathrm{k}_2 d\mathrm{k}_3 d\mathrm{k}_4 \tag{2.14}$$

The equation (2.14) conserves the total energy, since it is a Hamiltonian equation of motion. In addition, they conserve an infinite number of integrals of motion $\int F(\lambda,\mu)d\mathbf{r} = \mathbf{const}$. These integrals do not have simple interpretation in terms of the velocity field. In the present paper we concentrate only on one of the integral of motion:

$$N_0 = \frac{1}{2}\int(\lambda^2+\mu^2)d\mathrm{x} = \int \mathrm{a}^*(\mathrm{k})\mathrm{a}(\mathrm{k})\mathrm{dk} = \mathbf{const} \qquad (2.15)$$

The parameter N has the dimensionality of action and can be called the "hydrodynamic action" or number of quasi-particles (elementary excitations) describing turbulent flow. The relation (2.15) has the most important impact on what follows, so the elucidation of the physical meaning of the "quasi- particles" or waves and of the topological consequences of this conservation law remains a very important task. Due to the negative sign of the flux of the number of particles, their source is expected to be at the small scales.

3 Random Phase Approximation. Kinetic Equation

Let us single out the diagonal contributions to the equation of motion (2.14):

$$i\frac{\partial a(\mathrm{k})}{\partial t} - \omega(\mathrm{k})a(\mathrm{k}) = \int' T(\mathrm{k},\mathrm{k}_2,\mathrm{k}_3,\mathrm{k}_4)a^*(\mathrm{k}_2)a(\mathrm{k}_3)a(\mathrm{k}_4)\delta(\mathrm{k}+\mathrm{k}_2-\mathrm{k}_3-\mathrm{k}_4)\mathrm{dk}_2\mathrm{dk}_3\mathrm{dk}_4 \qquad (3.1)$$

where

$$\omega(\mathrm{k}) = \int T(\mathrm{kk}_2,\mathrm{kk}_2)\mathrm{a}^*(\mathrm{k}_2)\mathrm{a}(\mathrm{k}_2)\mathrm{dk}_2 \qquad (3.2)$$

and the symbol $'$ in the integral in (3.1) means that the diagonal contributions with $k = k_3$, $k_2 = k_4$ are not included. It will be shown in what follows that the integral

$$\overline{\omega}(\mathrm{k}) = \int T(k,k_2,k,k_2)n(\mathrm{k}_2)\mathrm{dk}_2 \qquad (3.3)$$

with

$$n(k) =< a^*(\mathrm{k})a(\mathrm{k}) > \tag{3.4}$$

converges when calculated on the solutions $n(\mathrm{k})$ of the kinetic equation derived below. This means that the main contribution to (3.3) comes from the region $k \simeq k_2$. In this work we are interested in statistically steady solutions $n(\mathrm{k})$, so $\overline{\omega(k)} = const$ is time-independent. Thus, we introduce the mean-field approximation[3]:

$$i\frac{\partial a(\mathrm{k})}{\partial t} - \overline{\omega(\mathrm{k})}a(\mathrm{k}) = \mathbf{S} \tag{3.5}$$

where the collision integral $S(\mathrm{k})$ is defined by the right side of equation (3.1). In the zeroth order of the expansion in powers of the non-linear interaction S we have:

$$a^0(\mathrm{k},t) = a(\mathrm{k})e^{-i\omega(\mathrm{k})t} \tag{3.6}$$

The bar over $\overline{\omega(k)}$defined by (3.3) is omitted in what follows. The statistical ensemble can be constructed by introducing an infinite set of realizations differing in the values of the initial phases $\varphi(\mathrm{k})$ in (3.6):

$$a^0(k,t) =\mid a(k) \mid e^{i\omega(\mathrm{k})t+i\varphi(\mathrm{k})} \tag{3.7}$$

The key element of the theory of weak turbulence, adopted in Ref.3 for consideration of strong turbulence is the assumption that all phases $\varphi(\mathrm{k})$ uncorrelated, i.e.:

$$< a(\mathrm{k}) >=<\mid \mathrm{a(k)} \mid \mathbf{e}^{\mathbf{i}\varphi(\mathbf{k})} >= \mathbf{0}$$

$$< a(\mathrm{k})a(\mathrm{k}') >=<\mid a(\mathrm{k}) \mid\mid a(\mathrm{k}') \mid exp(i(\varphi(\mathrm{k}) + \varphi(\mathrm{k}')) >= 0$$

$$< a(\mathrm{k})a^*(\mathrm{k}') >=<\mid a(\mathrm{k}) \mid\mid a(\mathrm{k}') \mid exp(i(\varphi(\mathrm{k}) - \varphi(\mathrm{k}')) >= \mathrm{n(k)}\delta(\mathrm{k} - \mathrm{k}')$$

All odd-order correlation functions of the fields $a(\mathrm{k})$ are equal to zero in this random phase approximation (RPA). As was mentioned above the averaging is performed over the ensemble of initial phases $\phi(k)$.

To derive equations of motion for the "occupation numbers" $n(\mathrm{k})$, let us multiply (3.5) and the corresponding equation for $a^*(\mathrm{k})$ by $a^*(\mathrm{k})$ and by $a(\mathrm{k})$, respectively. Then, the equation of motion for $n(k)$ reads:

$$\frac{\partial n(k,t)}{\partial t} = Im \int T_{kk_2,k_3k_4} J_{kk_2,k_3k_4} \delta(\mathrm{k}+\mathrm{k_1},-\mathrm{k_2}-\mathrm{k_3})\mathrm{dk_2dk_3dk_4} \quad (3.8)$$

where

$$J_4 = J_{kk_2,k_3k_4} =< a^*(\mathrm{k})\mathrm{a}^*(\mathrm{k_2})\mathrm{a}(\mathrm{k_3})\mathrm{a}(\mathrm{k_4}) > \quad (3.9)$$

Writing the equation of motion for J_4 as:

$$\frac{\partial J_4}{\partial t} =< \frac{\partial}{\partial t}(a^*(\mathrm{k})\mathrm{a}^*(\mathrm{k_2})\mathrm{a}(\mathrm{k_3})\mathrm{a}(\mathrm{k_4})) > \quad (3.10)$$

and expressing the time-derivatives in (3.10) using (3.6) we obtain in the random-phase approximation in the long time limit $t \to \infty$:

$$\frac{\partial n(k,t)}{\partial t} = \frac{\pi}{2} \int \mid T_{k_2,k_3k_4} \mid^2 J_4 \delta(\mathrm{k}+\mathrm{k_2}-\mathrm{k_3}-\mathrm{k_4})\delta(\omega(k)+\omega(k_2)-\omega(k_3)-\omega(k_4))d\mathrm{k_2}d\mathrm{k_3}d\mathrm{k_4} \quad (3.11)$$

with:

$$J_4 = n_3n_4(n_2+n_k) - n_2n_k(n_3+n_4) \quad (3.12)$$

Here $n(\mathrm{k_i}) = \mathrm{n_i}$. The δ function in the collision integral in (3.11), describing energy conservation per collision, appears in the equation of motion as a result of iteration:

$$J_4 =< a^*(k_1)a^*(k_2)a(k_3)a(k_4) > \int_0^t dt\ exp(it(\omega(k_1)+\omega(k_2)-\omega(k_3)-\omega(k_4)))$$

in the limit of large time t. The kinetic equation (3.10)-(3.11) has been analyzed and solved by Zakharov in the context of the weak turbulence theory (see excellent Review [2] and references therein). It has been shown that if

$$\omega(\mathrm{k}) \propto k^{\alpha} \tag{3.13}$$

there exist four scaling solutions:

$$n(k) = const \quad ; \quad n(k) \propto \frac{1}{\omega(k)} \tag{3.14}$$

and

$$n(k) \propto k^{-x} \tag{3.15}$$

with

$$x_1 = \frac{4}{3} + d; x_2 = \frac{4-\alpha}{3} + d \tag{3.16}$$

The solutions (3.14) correspond to a fluid in thermodynamic equilibrium, while the relations (3.15), (3.16) describe a non-equilibrium flow. From the definition of $\omega(\mathrm{k})$ given by (3.3) we find readily:

$$\alpha = -x + d + 2 = -x + 5 \quad (d = 3) \tag{3.17}$$

and the expressions for $n(\mathrm{k})$ can be obtained in a closed form:

$$n \propto k^{-13/3} \quad ; \quad \alpha = 2/3 \tag{3.18}$$

and

$$n \propto k^{-4} \; ; \quad \alpha = 1 \tag{3.19}$$

It can be checked easily that the total energy can be evaluated from the following relation:

$$E = \int \omega(\mathrm{k}) n(\mathrm{k}) d\mathrm{k} \tag{3.20}$$

which defines the energy spectra in terms of the Clebsch variables:

$$E(k) = 4\pi k^{d-1} \omega(k) n(k)$$

The relations (3.18) and (3.19) generate two solutions:

$$E(k) \propto \epsilon^{2/3} k^{-5/3} \tag{3.21}$$

and

$$E_n(k) \propto P k^{-1} \tag{3.22}$$

where P denotes the "particle" flux in the wave-number space. It has also been shown[2] that, while the energy flux is positive, i.e., the energy is cascading from the largest to the smallest scales, the flux of particles is in the opposite direction: from small to large scales (inverse cascade). The importance of this fact will be discussed below. Thus, as follows from (3.21) and (3.22), the small- and large-scale dynamics in turbulent flows are characterized by two different energy spectra. This is a completely new development which is discovered due to our use of the Clebsch variables. It is clear that the energy spectra (3.21) and (3.22) can readily be obtained from dimensional considerations which do not require one-loop approximation and kinetic equation (3.11)-(3.12).

Strictly speaking, Clebsch variables are formally defined for the inviscid Euler equation. However, it has been shown[3] that using the definitions (2.3), (2.4), the viscous hydrodynamics can be described by the equations (2.5) with the source term

$$I_c = O(\xi \nu \Delta \lambda)$$

where $\xi = O(\Delta^{-2} \frac{\Delta\omega}{\omega})$ is a complicated functional of the vorticity field ω. If ξ can be considered as a gaussian random function, then this term represents the small-scale source of the "quasi-particles", consistent with the results presented above. In the Fourier space $I_c = O(\nu k^2 a(k))$ which can

be assumed small in the inertial range. This fact is important for the application of the Clebsch formulation of hydrodynamics for investigation of turbulence problem.

Another problem with the Clebsch formulation is it's nonuniqueness: any velocity field v can be represented by an infinite number of different Clebsch fields (λ, μ). At the present time we do not know how to solve this problem, and therefore we neglect it for the time being and hope that one day the way to calibrate the Clebsch representation will be found.

4 Large-Scale Coherent State and Equations of Motion

All results described in the previous Sections were derived in the RPA combined with the mean field approximation introduced in the work of Yakhot and Zakharov[3]. This theory used the unjustified assumption of the close-to-gaussian statistics of the Clebsch variables and led to the explanation of various experimental observations. For example, the exponential distribution of the velocity differences is readily understood: The assumed PDF of the Clebsch field $P(a; a^*) \approx e^{-\frac{aa^*}{N}}$. Since $u = O(aa^*)$ then $P(U) \approx exp(-\frac{U}{U_{rms}})$. The actual derivation is rather difficult due to the complex form of the matrix element φ_{12} entering the expression of the velocity field in terms of Clebsch variables but the origin of the exponential distribution is clear from the above dimensional considerations. This theory failed to explain the experimentally observed gaussian statistics of velocity differences at the large scales and the "anomalous scaling" of the high-order moments S_n.

Let us reflect on the approximations involved in the derivation of the spectra in the previous Section. The close-to-gaussian probability distribution of the Clebsch field is, on the first glance, the crudest of all since it assumes weak interaction between modes $a(k)$. Still, this approximation qualitatively explained the experimentally observed close-to-exponential distibution of the velocity differences at the small scales.

Random phase approximation was a key element of the theory developed in Ref. (3). This approximation, which disregards the possibility of generation of the large-scale coherent structures, can serve only as a crude model for the small-scale dynamics. In reality turbulence is produced as a result of hydrodynamic instabilities of the large-scale ordered flows (structures) char-

acterized by very strong phase correlation. The well known examples include traveling waves and streaks in wall flows, convection rolls, Karman vortex streets in jets and mixing layers, Taylor vortices etc. In all these cases the structures, though strongly interacting with the random component of the velocity field, preserve the phase correlation even in high Reynolds number flows. The organized motions, reflecting the physical mechanisms of turbulence generation, create large-scale shear acting on the small-scale component of velocity fluctuations. This shear is not a result of pure nonlinear interaction and can be considered as a "dressed" external field. The dynamical consequences of the large-scale coherent component are not taken into account in the theories based on the random phase approximation.

Let $\mathbf{k_0^i}$ denote the wave-vector or set of wave-vectors corresponding to the basic flow structure. Then, the random phase approximation cannot be valid for $k \to k_0^i \to 0$. To incorporate coherent structures in the theory we relax the random phase approximation and introduce:

$$< a(k) >= \Sigma_i A(k)\delta(\mathrm{k} - \mathrm{k_0^i})$$

$$< a^*(k) >= \Sigma_i A^*(\mathrm{k})\delta(\mathrm{k} - \mathrm{k_0^i})$$

and

$$< a(k)a^*(k) >= \Sigma_i N_0^i \delta(\mathrm{k} - \mathrm{k_0^i}) + \mathrm{n(k)}$$

where $N_0^i =< A(k_0^i)A^*(k_0^i) >$ correspond to the coherent components of the Clebsch field while the modes $a(k)$ with $k > k_0^i$ describe fluctuations and can be considered in the random phase approximation so that $< a(k) >= 0$. This will be discussed in what follows. Although the detailed structure of the ordered component can be very involved and vary from flow to flow, here, as a first step, I consider a simplified model and investigate consequences of the very existence of the large scale coherent mode. Taking into account that

$$\varphi(\mathrm{k}, \mathrm{k_1}) \approx \mathrm{k} - \frac{\mathrm{k_1(k \cdot k_1)}}{\mathrm{k_1^2}} \approx \mathrm{k}$$

when $k << k_1$, the velocity definition in terms of the Clebsch field reads:

$$\mathbf{v(k) \approx V_0 + (A^*(k_0,k)a(-k) + A(-k_0,k)a^*(k)) + \int \varphi_{q,q-k} a^*_q a_{q-k} dk} \tag{4.1}$$

where $k_0^2 = O(L^{-2})$ and $\mathbf{k_0}$ can, in principle, slowly vary in time so that $< \mathbf{k_0} >= \mathbf{0}$. The coherent component of the velocity field V_0, derived from the definition (2.13), calculated on the coherent contributions to the Clebsch field $A(k_0)$ is:

$$\mathbf{V_0 = \Sigma \varphi_{k_0^i, k_0^j} A(k_0^i) A^*(k_0^j)}$$

where the summation is carried out over the wave-vectors $\mathbf{k_0^m}$ forming the coherent state. The vector $\mathbf{A(k_0,k) = \Sigma_i (k_0^i - \frac{k(k \cdot k_0^i)}{k^2}) A(k_0^i)}$. This relation introduces some violation of both isotropy and homogeneity, always present at the large scales in real-life flows. This anisotropy is not essential for the results derived below, since one can introduce an ensemble of the large-scale coherent structures and average the results derived for each realization over directions of $\mathbf{k_0^i}$ (This argument is due to G.Fal'kovich). In many flows the large scale structure has rather complicated topology and the anisotropy introduced by it is small. To proceed further we need information about physical properties of the large-scale coherent structures which has to emerge as a result of solution of the entire dynamical problem. Since at the present time we cannot develop a comprehensive theory, approximations based on a sensible physical picture are to be invoked. The coherent structures, often generated at the transition to turbulence, are long-living solutions of the dynamical problem and thus, it is reasonable to assume that they are stable or marginally stable in the limit $a(k) \to 0$. In other words

$$\frac{\delta H}{\delta a(k)} = 0$$

when $a(k) \to 0$. This means that the linear in $a(k)$ contributions to the Hamiltonian of the kind $\int dk O(\mathbf{V_0 \cdot A(k_0,k)a(k)}) = 0$ can be neglected. Thus, the Hamiltonian, which does not include linear in $a(k)$ contributions can be written as:

$$H = H_0 + H_2 + H_3 + H_4$$

$$H_0 = \Sigma\varphi_{\mathbf{k_0^i},\mathbf{k_0^j}} \cdot \varphi_{\mathbf{k_0^p},\mathbf{k_0^q}} A^*(k_0^i)A^*(k_0^p)A(k_0^j)A(k_0^q)$$

$$H_2 = \int dk\Big(\mid A(k_0,k) \mid^2 a(k)a^*(k) + \frac{1}{2}(A^2(k_0,k)a(k)a(-k) + (A^*(k_0,k))^2 a^*(k)a^*(-k))\Big)$$

$$H_3 = \int dkO\Big(\mathbf{A}(\mathbf{k_0},\mathbf{k}) \cdot \phi_{\mathbf{q},\mathbf{q}-\mathbf{k}}(a^*(q)a(q-k)a(k) + a^*a^*a + ...)\Big)$$

$$H_4 = S$$

The same result is derived directly from the Hamiltonian (2.10): as in the Bogolubov theory of weakly interacting Bose gas, the linear in $a(k)$ contributions are absent when $k_0^i << 1$ and $k = O(1)$ due to the impossibility to satisfy momentum conservation.

In general the large-scale field $\mathbf{A}(\mathbf{k_0},\mathbf{k})$, which is to be obtained as a solution of the full dynamical problem, is a functional of $a(k)$ and the derivation of $A(k;a(k))$ is a very difficult task. First, we consider the simpler case of low-Reynolds number flow, in which the coherent component of the velocity field does not strongly differ from the laminar velocity profile $\mathbf{U_L}(\mathbf{x},\mathbf{t})$. We can neglect the dependence of $\mathbf{A}(\mathbf{k_0},\mathbf{k})$ on $a(k)$ and treat the large-scale coherent component as an external field.

Due to quadratic in $a(k)$ contributions to the Hamiltonian, the equations of motion have linear terms:

$$i\frac{\partial a(k)}{\partial t} = \mid A(k_0,k) \mid^2 a(k) + \frac{1}{2}(A^*(k_0,k))^2 a^*(-k)) \equiv I_L$$

and

$$-i\frac{\partial a^*(k)}{\partial t} = \mid A(k_0,k) \mid^2 a^*(k) + \frac{1}{2}A^2(k_0,k)a(-k)) \equiv I_L^*$$

The physical meaning of I_L can be understood readily. Let us introduce the Reynolds decomposition of the velocity field:

$$\mathbf{v} = \mathbf{U} + \mathbf{v}'$$

where $\mathbf{U}$ and $\mathbf{u}'$ correspond to the mean (coherent) and fluctuating velocity fields respectively. This decomposition is difficult to realize in unsteady flows and it is used here only to illustrate the physical origin of the external field in the Clebsch formulation of hydrodynamics. Then, the Euler equation (2.1) can formally be rewritten:

$$\frac{\partial \mathbf{v}'}{\partial t} + \mathbf{v}' \cdot \nabla \mathbf{v}' + I_v = -\nabla p'$$

and

$$\frac{\partial \mathbf{U}}{\partial t} + \mathbf{U} \cdot \nabla \mathbf{U} + I_U = -\nabla P + \mathbf{F}$$

where

$$I_v + I_U = \mathbf{U} \cdot \nabla \mathbf{v}' + \mathbf{v}' \cdot \nabla \mathbf{U}$$

and $p' + P = p$. It is clear that these two equations are equivalent to the Navier-Stokes equations at the scales $l >> l_d$.

Taking into account that

$$A^2(k_0, k) = \Sigma_{ij}(\mathbf{k_0^i} \cdot \mathbf{k_0^j} - \frac{(\mathbf{k} \cdot \mathbf{k_0^j})(\mathbf{k} \cdot \mathbf{k_0^i})}{\mathbf{k^2}})\mathbf{A}(\mathbf{k_0^i})\mathbf{A}(\mathbf{k_0^j}) = \mathbf{O}(\mathbf{\Sigma_{ij}} \nabla_\mathbf{i} \mathbf{U_j})$$

we come to the conclusion that the linear contribution to the equation of motion for $a(k)$ comes from the large-scale shear. This result is expected, since it is this shear which strongly contributes to the turbulence production in the Navier-Stokes equations. Thus, the introduction of coherent and fluctuating components of the Clebsch field is equivalent to the Reynolds decomposition of the velocity field. It is clear from these relations that $\mathbf{A}$ can be treated as external field only if I_U is small enough to introduce large deviations from the laminar solution U_L.

If the amplitude of $A(k)$ is large the interaction Hamiltonians H_3 and H_4 can be taken into account perturbatively. The small coupling constant will be introduced below. Using the Bogolubov transformation[1,4]

$$a(k) = uc(k) + vc^*(-k)$$

and

$$a^*(k) = u^*c^*(k) + v^*c^*(-k)$$

the expression for H_2 can be diagonalized:

$$H_2 = \int e(k)c(k)c^*(k)dk$$

with

$$e^2(k) = u^2 - vv^*$$

$$u^2 = (\mid A(k_0, k) \mid^2)^2$$

$$v = A^2(k_0, k)$$

where $\mid A \mid^2 = \mid A_1 \mid^2 + \mid A_2 \mid^2 + \mid A_3 \mid^2$ and $A^2 = A_1^2 + A_2^2 + A_3^2$. From these expressions we can see that for the general structure of the field $\mathbf{A}(\mathbf{k_0}, \mathbf{k})$, the dispersion relation $e^2(k) > 0$ and thus, the coherent state is linearly stable as was assumed when the linear contributions to the Hamiltonian were neglected.

In a general case of high Reynolds number flow $\mathbf{A}(\mathbf{k_0}, \mathbf{k}) = \mathbf{A}(\mathbf{k_0}, \mathbf{k}, \mathbf{a}(\mathbf{k}))$ and the equations of motion, derived above, are incorrect. Following the theory of superfluidity, let us use the particle conservation law (2.15) and express $A(k_0^i)$ in terms of the external parameters of the problem and fluctuation $a(k)$:

$$\Sigma_{ij} A(k_0^i)A(k_0^j) = N_0 - \int a^*(k)a(k)d^dk$$

where $N_0 = const$, independent of $a(k)$. Due to the complexity of the matrix elements $\varphi_{k,k'}$ we cannot exactly express the Hamiltonian H in terms of N_0 and $a(k)$. However, the particle conservation relation can be used to estimate various contributions. The dangers of this approach are clear but at the present time this is all we can do. Thus,

$$H_2 \approx \int dk \Big(N a(k) a^*(k) + \frac{1}{2} (A^2(k_0, k) a(k) a(-k) + (A^*(k_0, k))^2 a^*(k) a^*(-k)) \Big)$$

where

$$N = O(k_0^2 N_0)$$

The corresponding $O((\frac{k_0}{k})^2)$ correction to H_4 is small in the limit $k_0 \to 0$. Using the same estimate we can express the operators $A(k)$ in H_0 in terms of N_0 and $A(k)$. The resulting Hamiltonian has constant $O(k_0^2 N_0^2)$ term and the $a(k)$-dependent contributions which simply modify all factors in H_2. The magnitudes of these factors can be important for the results of this work since, in principle, they can modify the frequency shift we are trying to calculate.

In the theory of weakly interacting Bose gas the condensate is considered at $k_0 = 0$ and the corresponding operators are taken as c-numbers, so that $A = A^* = \sqrt{N}$. In this case the frequency shift is equal to zero. This gives rise to phonons, characterized by linear in wave number energy spectrum $\omega(k) \propto k$. In the theory of turbulence the coherent state cannot occupy $k_0 = 0$ since the finite shear is necessary for the turbulence production. Thus, some violation of translational invariance is always expected at the large scales.

As was shown above, the particle conservation law gives some information about the product $A(k)A^*(k)$. In order to say anything about A^2 we have to solve the corresponding dynamic equations describing the large-scale coherent component of the Clebsch field. At the present time we cannot do it. However, it is reasonable to assume that:

$$N^2 \neq \mid A^2(k_0, k) \mid^2$$

Based on the particle conservation law, we estimate:

$$e^2(k) \approx N^2 - \mid A^2(k_0, k, a(k)) \mid^2 = O(k_0^4 N_0^2) > 0$$

If the large-scale flow is produced by the non-linear interactions without the large-scale symmetry breaking external field, then it is possible that $e(k) = 0$ and the results of this work should be modified.

In what follows we take the frequency shift $\Omega \equiv e(k) \approx k_0^2 N_0$ and, to avoid introduction of a new notation, set $a(k) \equiv c(k)$. This approximation totally neglects the geometric structure of the coherent state and the fact that it depends not only on the wave-vectors $\mathbf{k}_0^{\mathbf{i}}$ but also on the angles between vectors $\mathbf{k}$ and $\mathbf{k}_0^{\mathbf{i}}$. So, in what follows the dispersion relation $e(k)$ is taken into account in an average way, which is sufficient for the qualitative theory of "weakly interacting Clebsch gas" developed in this paper.

Since the fluctuations from the coherent state $< a(k) >=< a^*(k) >= 0$ the Fourier component of velocity $< v(k) >= 0$ for k large enough. Thus, I assume that the field $a(k)$ is isotropic and homogeneous. This assumption should come out as a result of a dynamical theory showing that anisotropic perturbations of the coherent state decay while the isotropic ones survive. This can be done easily considering linear stability of a basic flow of a given structure in Clebsch variables. However, in fully developed turbulence, the coherent and random components strongly interact: the large-scale turbulence- producing eddies are influenced by the small- scale velocity fluctuations and the resulting "turbulent profiles" arise from the complicated interactions. So, in this work I will not consider the nature of the coherent state and simply postulate its existence. As will be clear from what follows some of the consequences of the interaction between organized and random motions are of a general nature independent of the detailed structure of large-scale eddies.

The mean field equations of motion for the Clebsch variables are derived from the approximate Hamiltonian introduced above:

$$i\frac{\partial a(\mathbf{k})}{\partial t} - (\omega(k) + 2N_0 k_0^2) a(\mathbf{k}) = S \qquad (4.2)$$

The $O(aa)$ terms on the right-side of the equation of motion coming from H_3, violating particle conservation, are neglected in (4.2). However, they are very important since it is only due to these terms the constant nonlinear frequency shift in (4.2) cannot be removed by the trivial transformation

$$b(k) = a(k)e^{-iN_0k_0^2t}$$

Let us show that in the kinetic equation approximation, considered in this work, the $O(aa)$-contributions are negligibly small due to the absence of the resonant interaction on the dispersion relations $\omega(k)+const.$ Indeed, repeating the derivation of the kinetic equation we find an additional contribution to (3.8) of the type:

$$\frac{\partial n(k,t)}{\partial t} = Im \int T_{k,k_3k_4} J_{k,k_3k_4} \delta(\mathbf{k} - \mathbf{k_4} - \mathbf{k_3}) \mathbf{dk_3 dk_4} \qquad (4.3)$$

with

$$J_{k,k_3,k_4} = J_3 = O(< a^*(k)a(k_3)a(k_4) >)$$

Using the results of the previous Section we derive after the iteration:

$$J_3 \propto \int_0^t dt\ exp(it(\omega(k_3+k_4) - \omega(k_3) - \omega(k_4) - 2N_0k_0^2))$$

which disappears in the limit $t \to \infty$ due to the absence of the resonances. It can be shown[3] that elimination of the nonresonant terms can be done rigorously by introduction of the new operators $\alpha(k) = \bar{a}(k) + s$ where the linear shift s is chosen in such a way that the third-order contribution disappears from the resulting equation for $\alpha(k)$. In the case considered in this work this leads to a simple multiplication of the matrix element (2.11) by a constant factor which does not modify the scaling relations derived in this paper.

Thus, the kinetic equation corresponding to (4.2) is exactly the same as one derived in the previous section since the constant non-linear frequency shift disappears from the conservation laws. Solutions (3.18) and (3.19) stay intact but in addition to the energy spectra (3.21) and (3.22) we also have:

$$E_3(k) \propto k^{-\frac{7}{3}} \qquad (4.4)$$

and

$$E_4(k) \propto k^{-2} \tag{4.5}$$

corresponding to energy and particle conservation laws respectively. The origin of these spectra is clear: in general $E(k) \approx F^{\frac{1}{3}} n(k)/\tau(k)$ where F is the corresponding flux and τ is the characteristic time-scale. Due to the interaction with the "external field", we now have an additional wave-number-independent time $\tau = const$, leading to the energy spectra (4.4) and (4.5). We will see below that the 7/3-spectrum is indeed observed in shear flows at scales larger than those corresponding to the 5/3- Kolmogorov range. Since the limit $k \to 0$ is dominated by the $-7/3$- spectrum the second $E(k) \approx k^{-2}$-spectrum will not be considered in what follows. If $\Omega = N_0 k_0^2$ is not small, then the expansion parameter of the theory $\eta = \frac{\omega(k)}{\Omega} \to 0$ when $k \to 0$ since the dispersion relations corresponding to both spectra E_3 and E_4 are $\omega(k) \propto k^\alpha$ with $\alpha > 0$. In this case the solutions E_3 and E_4 are asymptotically exact. Let us estimate η for some well-known cases of turbulent flows. The mean dissipation rate $\bar{\epsilon} \approx u_{rms}^3/L$ where u_{rms} is the root-mean square velocity of turbulent fluctuations and L is the integral scale. The characteristic frequency of the coherent structure is simply given by the large-scale shear $\Omega \approx S \approx U/L$ where U is the characteristic velocity of coherent motion. Using these estimates we obtain $\eta \approx u_{rms}/U$. In wall flows $\eta \approx 10^{-1} - 10^{-2}$ in a typical laboratory situations and, according to the data $\eta \to 0$ when the Reynolds number $Re \to \infty$. The same estimate is applied to other wall flows and wakes behind bluff bodies. In Bernard convection $\eta \approx Ra^{-\frac{1}{14}}$ in the experimentally covered range of variation of the Rayleigh number $10^7 < Ra < 10^{14}$. In this flow U is the mean velocity of the coherent vortex ("wind") observed in high Ra flows. According to theoretical arguments in this case too, $\eta \to 0$ when $Ra \to \infty$. Existence of small parameter in this formulation of the theory of turbulence means that the fields $a(k)$ and $a^*(k)$ are close to gaussian when $k \to k_0 \to 0$. However, in jets the parameter $\eta \approx 10^{-1}$ and does not seem to decrease with increase of the Reynolds number. The experimentally observed close-to-gaussian large scale statistics of velocity field in these kind of flows should be related to numerical smallness of η and, unlike the wall flows, the extent of the range where the gaussian statistics is observed should not grow with Reynolds number.

The expansion parameter $\eta(k) = O(1)$ when $k \to \infty$. Still, this parameter will be considered small in what follows. This restricts the results of this

paper to not-too-large wave- numbers. The limits of validity of the theory will be discussed below.

5 Probability Distribution of the Velocity Differences

Let us consider the probability density of the velocity difference

$$U(X,x) = u(X+x) - u(X) = k_0\sqrt{N_0}\int (a(k) + a^*(k))(e^{ikx} - 1)dk$$

$$+ \int \varphi(k_1,k_2)a^*(k_1)a(k_2)(e^{i(k_1-k_2)x} - 1)d\mathrm{k_1}d\mathrm{k_2} \qquad (5.1)$$

where we have omitted the subscript x denoting the x-components of the velocity and wavevectors. It is well known that the odd moments $\overline{U^{2n+1}}$ are not equal to zero and that the PDF $P(U) \neq P(-U)$. However, this asymmetry is not very strong and it is absent when x denotes displacement in the direction perpendicular to the x-axis. In this work we shall discuss the behaviour of even moments only, leaving investigation of the odd-order moments to future publications. It is clear from the above definitions that

$$\overline{U^2} = U_R^2 + U_c^2$$

with

$$U_R^2 = \int \varphi^2_{k_1,k_2} n(\mathrm{k_1})n(\mathrm{k_2})\left(2 - 2\cos\left((k_1-k_2)x\right)\right)d\mathrm{k_1}d\mathrm{k_2} = O(x^{\frac{2}{3}}) \equiv \beta x^{\frac{2}{3}} \qquad (5.2)$$

and

$$U_c^2 = 4N_0k_0^2\int n(k)(coskx - 1)dk = \mathrm{O(x^{\frac{4}{3}})} \equiv \gamma(\frac{\mathrm{x}}{\mathrm{L}})^{\frac{4}{3}}. \qquad (5.3)$$

The proportionality coefficients β and γ are given by $\beta \approx \bar{\epsilon}^{\frac{2}{3}}$ and $\gamma \approx N_0k_0^2\bar{\epsilon}^{\frac{1}{3}}$. It will become clear below that in many cases $N_0k_0^2 \approx S$, where

S is the shear due to the coherent state which dominates the large-scale dynamics. The probability distribution function $P(U)$ is defined as

$$P(U) \propto \int \delta\Big(U - u(x) + u(x+r)\Big) dx$$

or, using the integral representation of the δ- function

$$P(U) \propto \int_{-\infty}^{\infty} d\alpha \;\; e^{i\alpha U} \int \; e^{-i\alpha U(x,r)} dx.$$

Introducing the ensemble of fluctuating Clebsch fields and assuming that the space and ensemble averaging procedures are equivalent leads to

$$P(U) = \int_{-\infty}^{\infty} d\alpha \; e^{i\alpha U} < \; e^{-i\alpha U(0,x)} > . \tag{5.4}$$

Our goal is to evaluate

$$I = < e^{-i\alpha U(0,x)} >$$

Assuming further that the statistics of the Clebsch fields $a(k)$ and $a^*(k)$ are near-gaussian for $k > k_0$, we can analyze the expression for I with $U(x)$ defined by (5.1). In principle the result of gaussian averaging can be formally expressed in terms of the corresponding determinants. The resulting formulae are very involved and it is difficult to extract any useful information from them. Here I will expand I in powers of $i\alpha U(x)$ and evaluate the outcome of gaussian averaging. First of all it is clear that if the quadratic contribution to (5.1) is small, the gaussian averaging can be done exactly with the result

$$I = exp(-\alpha^2 U_c^2/2)$$

which after substitution into (5.4) yields the experimentally observed gaussian distribution function

$$P(U) \propto exp(-U^2/8U_c^2)$$

for large values of the displacement $x/L \to 1$.

Now let us set for the time being $N_0 = 0$ and try to evaluate I. Due to the complicated functional shape of the matrix elements $\varphi(k_1, k_2)$, this is a rather difficult task. Expanding the exponent in I and examining the series in powers of α we find that the second order term is equal to

$$I_2 = -\frac{1}{2}\alpha^2 U_R^2.$$

The fourth order contribution is

$$I_4 = \frac{\alpha^4}{24}(3U_R^4 + 6ND_4)$$

where $6ND_4$ denotes six off-diagonal contributions to I of the kind

$$ND_4 = \int \varphi^0_{1,2}\varphi^0_{3,1}\varphi^0_{2,6}\varphi^0_{3,6} n_1 n_2 n_3 n_6 d\mathbf{k_1} d\mathbf{k_2} d\mathbf{k_3} d\mathbf{k_6}$$

$$\varphi^0_{i,j} = \varphi(k_i, k_j)(e^{i(k_i - k_j)x} - 1).$$

All others are obtained from this one by permutation of the subscripts. It can be shown easily that the $2n^{th}$ order term in the expansion has the form:

$$I_{2n} = \frac{(-1)^n}{2n!}(B_{2n-2}\frac{2n(2n-1)}{2}U_R^{2n} + G_{2n-2}\frac{2n(2n-1)}{2}ND_{2n})$$

where B_{2n-2} and G_{2n-2} denote the number of the corresponding contributions to I_{2n-2}. Neglecting the off-diagonal contributions we can sum up the remaining series with the result

$$I = \frac{1}{2}(1 + \frac{\alpha^2 U_R^2}{2})^{-1}.$$

If all terms in the expansion are assumed to be equal, then we have the same result with the coefficient 3/2 replacing 1/2 in the above relation. Substituting the expression for I into (5.4) and evaluating a simple integral yields the exponential probability distribution function

$$P(U) \propto exp(-\frac{\sqrt{2}U}{U_R}).$$

This relation resembles the experimentally observed $P(U)$ for small separations $x/L << 1$. The exact evaluation of the function I is a difficult problem because the number of contributions to I_n involving various combinations of wavevectors grows very rapidly with n. This indicates the possibility to evaluate I_n for $n >> 1$ using statistical methods of diagram calculations. Here I assume that when n is large the contribution of the off-diagonal terms is small due to the cancellations stemming from proliferation of $cos((k_i - k_j)x)$. So, I select an infinite subset of contributions to I with the correct asymptotic properties:

$$I = \frac{e^{-\frac{1}{2}\alpha^2 U_c^2}}{1 + \frac{\alpha^2 U_R^2}{2}} \tag{5.5}$$

The relation for $P(U)$ reads

$$P(U) = \int_{-\infty}^{\infty} d\alpha e^{i\alpha U} \frac{e^{-\frac{1}{2}\alpha^2 U_c^2}}{1 + \frac{\alpha^2 U_R^2}{2}}$$

It follows from the above considerations that this expression should be used only for the calculation of the high-order moments of velocity differences $\overline{U^{2n}}$ with $n >> 1$. Substituting (5.5) into the expression for $P(U)$ gives: $\int P(U)dU = 1$. Evaluation of the moments of velocity differences

$$\overline{U^{2n}} = \int_{-\infty}^{\infty} P(U)U^{2n}dU$$

using (5.4) and (5.5) is done readily. The result for the normalized moments R_n is:

$$R_{2n} = (2n-1)!!\frac{P^n}{P_n} \tag{5.6}$$

where

$$P^n = \int_0^\infty dt\, e^{-t}((x/L)^{\frac{2}{3}} + \frac{t}{C_0})^n \qquad (5.7)$$

The parameter $C_0 = \frac{2\gamma}{2\beta}$ and $P_n = (P^1)^n$. In the limit $x/L \geq 1$ and if the constant C_0 is large, this expression gives $R_n \approx (2n-1)!!$ corresponding to the close-to-gaussian statistics of the velocity differences. When $x/L << 1$, $R_{2n} = (2n-1)!!n!$ indicating strong deviations of $P(U)$ from gaussian. In wall flows, $\gamma \approx S$ and $\beta \approx 1/2\epsilon^{\frac{1}{3}}L^{\frac{2}{3}}$ where the shear $S \approx U/L$ and $\epsilon \approx u^3/L$ with U and u denoting the mean and rms fluctuating velocities, respectively. Not too far from the wall region of a boundary layer flow, $U \approx (10-20)u$ and $C_0 \approx 10-20$. Some of the normalized moments R_{2n}, given by (5.6) and (5.7) are plotted on Fig.1 ($C_0 = 20$). The most striking feature of the plots is that the transition between these two asymptotic values of R_n is very slow, covering almost two decades of the displacement x variation. Moreover, the transitional region can be accurately represented by the power law $R_n \approx x^{-\xi_n}$ with the "scaling exponents" ξ_n. This poser law is compared with the experimental data in the Table where the experimentally observed[5] values of the "exponents" ξ_n are presented. Relations (5.6) and(5.7) show that intermittency is the consequence of interaction of coherent and random components of the Clesch field. With decrease of the length-scale, the role of this interaction diminishes and PDF undergoes transition from gaussian to close-to-exponential. At the very small scales $x/L \to 0$, the normalized moments $R_n(x) \to const \approx (2n-1)!!n!$. However, this limit might be beyond experimental reach since proximity to the dissipation range, not considered in this work, can strongly influence the small-scale behaviour of the moments R_n. It follows from (5.7) that even in the same flow the measured deviations from the Kolmogorov scaling can vary from point to point depending on the ratio $S/\epsilon^{\frac{1}{3}}$ if the displacement is measured in the units of the integral scale $X = x/L$.

The results of this work can be explained in a very simple way. Let us consider, for example, the familiar case of a shear flow. At the large scales the dynamics are dominated by the shear S and the co-spectrum of the anisotropic state $k^2\overline{v_i(k)v_j(k)} = \epsilon^{\frac{1}{3}}k^2n(k)\Omega$ where the characteristic frequency is $\Omega = S$. With the expression for $n(k)$ derived in this work, the 7/3-energy spectrum is readily obtained in the interval $k_0 < k < S^{\frac{3}{2}}\epsilon^{-\frac{1}{2}}$. The anisotropy- generated 7/3-scaling of the co-spectrum does not enter the expression for the energy spectrum. However, it does not disappear from the expressions for the high-order moments leading to the non-trivial behaviour

of $R_{2n}(x)$. I believe that this mechanism is quite general and the long-living anisotropic large-scale fluctuations can produce similar effects in statistically isotropic flows. Indeed, if the large-scale shear has complex topology, the arguments leading to the $-7/3$ co-spectrum $E_{12}(k) \approx k^{-\frac{7}{3}}$ do not work since the problem loses strong anisotropy which is the essential part of the derivation. In addition, the introduction of the large-scale super-ensemble, discussed in Section 4, makes the results of this work applicable to the statistically isotropic flows which are slightly anisotropic in each realization. This physical assumptions are reflected in the scalar expression for the condensate contribution to the dispersion relation in the equation of motion (4.2).

According to this theory, anomalous scaling is not necessary to explain the experimental data and the measured "scaling exponents" are the artifacts of signal processing. I illustrate how deceiving the data can be with the following consideration: The moments of the velocity differences grow by factor $\approx n!$ when x/L decreases by two orders of magnitude. Using a familiar extrapolation, the "exponents" ξ_n are found from the trivial relation $100^{\xi_n} = n!$, so that

$$\xi_n = \frac{1}{2} log n! \tag{5.8}$$

This formula is compared with the experimental data in the Table.

6 Spectra of the Dissipation Rate Fluctuations

Planning to compare the results with experimental data in the next Section, here I reproduce the evaluation of the dissipation rate structure functions S_2^ϵ defined by the relation (1.4) published in Ref.(3). To begin the discussion, let us first recall the derivation of the Kolmogorov result $S_2^\epsilon \approx k^{-1}$. The dissipation fluctuation spectrum is:

$$E^\epsilon(k) \approx 4\pi k^{d-1} \frac{\overline{\epsilon(k)\epsilon(k')}}{\delta(\mathbf{k}+\mathbf{k}')} \tag{6.1}$$

Substituting the relation

$$\epsilon(k) = 2\nu \int_0^\infty q_i(k-q)_i v_j(q) v_j(k-q) d^3q \tag{6.2}$$

into (6.1) we obtain:

$$E^\epsilon(k) \approx \nu^2 k^2 \int_0^\infty (q_i(k-q)_i)^2 U(q) U(k-q) d^3q \tag{6.3}$$

where $U(k) = \frac{E(k)}{4\pi k^2}$. It is easy to see that the integral converges in both limits, yielding $E^\epsilon(k) \approx k^{\frac{5}{3}}$, which is grossly incorrect. The mistake can be traced to the assumption of gaussian statistics of the velocity field involved in the derivation of this relation. However, this assumption is plausible in the renormalization group sense, i.e., the deviations from gaussian statistics can be treated as small, provided the effective (renormalized) transport coefficients are used in the evaluation of the corresponding flow features. This statement is rather clear since in the inertial range of fully developed turbulent flow the characteristic time-scale of the velocity fluctuations at the scale $l \approx \frac{1}{k}$ is dominated by the non-linear interactions and can be represented using an effective (turbulent) viscosity ν_K. The ϵ-spectrum is given by:

$$E^\epsilon(k) \approx \nu_K^2(k) k^2 \int_0^\infty (q_i(k-q)_i)^2 U(q) U(k-q) d^3q \tag{6.4}$$

with $\nu_K \approx \epsilon^{\frac{1}{3}} k^{-\frac{4}{3}}$ in accord with the Kolmogorov theory. The integral (6.4) converges and (6.4) and (6.1) give the dissipation fluctuation spectrum in Kolmogorov turbulence:

$$E_K^\epsilon(k) \approx \epsilon^2 k^{-1} \tag{6.5}$$

Using the same procedure we can calculate $E_n^\epsilon(k)$ corresponding to the k^{-1}-spectrum. The only fundamental difference between this case and the one considered above is that the integral (6.3) calculated for the k^{-1}-spectrum is ultra-violet divergent and, thus, is equal to a constant which strongly depends on the value of k_d. Then, it is easy to find the dissipation rate spectrum in the gaussian random field: $E^\epsilon \approx k^2$. In a turbulent flow dominated by a k^{-1}-spectrum, a different procedure should be used. It follows from the relation (3.19) and the energy spectrum (4.1) that the effective viscosity ν_n in this case is:

$$\nu_n(k) \approx (\epsilon\nu)^{\frac{1}{4}} k^{-1} \tag{6.6}$$

and we derive readily:

$$E_n^\epsilon(k) \approx k^0 \tag{6.7}$$

In the general case of high Reynolds number statistically stationary turbulence the largest fraction of energy is contained in the $\frac{5}{3}$-Kolmogorov range dominating the large-scale velocity fluctuations. Indeed, in this case $\frac{E_K}{E_n} \approx \frac{Re}{lnRe} \to \infty$ when the Reynolds number $Re = \frac{u_{rms}L}{\nu} \to \infty$. The subscripts n and K hereafter denote parameters of the flow corresponding to the k^{-1} and Kolmogorov spectra, respectively. It is easy to see that $\frac{\epsilon_K}{\epsilon_n} = O(1)$ and thus, the energy dissipation is more or less equally distributed between two spectra. To estimate the ϵ-correlation function let us assume that the total dissipation rate $\epsilon = \epsilon_K + \epsilon_n$. This assumption is plausible within the framework of our weakly non-linear theory. Then we have:

$$E_{total}^\epsilon = E_K^\epsilon + E_n^\epsilon + E_{Kn}^\epsilon \tag{6.8}$$

where in the three-dimensional case:

$$E_{Kn}^\epsilon = k^2 \nu_K(k)\nu_n(k) \int_0^\infty (q_i(k-q)_i)^2 U_K(k) U_n(k) d^3q \approx k^{-\frac{1}{3}} \tag{6.9}$$

Statistical independence of the velocity fields described by the two spectra was assumed in the derivation of this relation. Thus, the Kolmogorov scaling (1.4) is "contaminated" by contributions coming from the second solution of the kinetic equation. This is a manifestation of small-scale intermittency. The predicted spectrum of the dissipation rate fluctuations consists of three ranges, characterized by the k^{-1}-spectrum at the largest scales and k^0-spectrum in the vicinity of the dissipation cut-off. The intermediate $k^{-\frac{1}{3}}$-range might be too narrow to be found in the available experimental data. It should be mentioned that the simple linear superposition of the dissipation rates corresponding to different spectral ranges introduced above is an approximation which can be rather crude. In a non-linear system a weighted superposition can modify the relative importance of different spectral contributions to the total dissipation fluctuation spectrum.

7 Discussion of the Experimental Data

According to the theory presented in this work the large-scale coherent state, contributing to turbulence production in some flows, is responsible for the observed close-to-gaussian probability distribution of velocity differences at large scales and the non-trivial behaviour of high-order moments S_n. To begin to test the main predictions of the theory we have to look for the energy spectrum $E(k) \propto k^{-\frac{7}{3}}$ at scales somewhat larger than those corresponding to the 5/3-inertial range spectrum. Experimental investigation of the large-scale dynamics is not a simple task. In a typical experiment the signal is acquired as a time sequence $v(x,t)$ at a given point x. The correlation functions are measured in the frequency domain:

$$F(\omega) = \int_{k_0} F(k, \omega + \mathrm{k} \cdot \mathbf{U}) dk$$

where the integration domain is limited by the box-size $O(k_0^{-1})$ and U is the mean velocity. The function $F(k,\omega) \approx k^x F(\frac{\omega}{k^z})$ where the scaling exponents x and z differ from flow to flow (the dynamic exponent $z = 2/3$ for Kolmogorov turbulence). The space correlation function is given by

$$F(k) = \int_{-\infty}^{\infty} F(k,\omega) d\omega$$

with the integration domain limited only by the data acquisition time which often can be made as long as desired. It clear from these two expressions that when $\omega >> O(k_0 U)$ and the integrals converge, the expressions for $F(\omega)$ and $F(k)$ are simply related since $\omega \approx k$. This is called the Taylor hypothesis which is very often used for interpretation of the data. However, this hypothesis fails at the large scales where $\omega \leq k_0 U$ since in this case ω disappears from the problem giving $F(\omega) = const$, observed in all experiments in the frequency domain. A few experiments conducted in both space and time domains revealed substantial differences in the large-scale behavior of the correlation functions.

The energy spectra, measured in the large NASA Ames wind tunnel[6] are presented on Fig.(2). We can see a decade of Kolmogorov 5/3-energy spectrum in some interval of scales. However, the co-spectra, presented on Fig.(3) show a decade of the 7/3-spectrum at the larger scales, in accord

with prediction in this work. As was mentioned above, the appearance of this spectrum in a shear flow is not surprising due to the an additional scale-independent time-constant. In another experiment[8] the second-order moment $S_2(x)$, measured in physical space using a particle-tracking technique, was best fitted by the 2/3-power law at the small scales and by 4/3-exponent at the large values of the separation x. The results are shown on Fig.4. We can see that when fitted by the Kolmogorov relation $S_2 = O(x^{\frac{2}{3}})$ the experimental and fitting curves barely touched each other. However, the data were well represented by the dependence $S_2 = ax^{\frac{2}{3}} + bx^{\frac{4}{3}}$, exactly as predicted in this paper. Even more striking conformation of the predictions derived in this work can be found in the sate-of -the-art (864^3 resolved Fourier modes) direct numerical simulations of the Taylor-Green vortex conducted by M.Brachet[7]. The calculated energy spectrum is presented on Fig.5. We can see that the large-scale part of $E(k)$ is dominated by the 7/3-scaling regime while the 5/3-Kolmogorov spectrum can be found at the larger values of wave numbers.

In the Navier-Stokes equations different components of the velocity field are coupled via non-linear interaction. It is a small miracle that the third-order structure function of the x-component of velocity field can be expressed in terms of the x-components only. This miracle is unlikely to happen in the high-order correlation functions which means that the S_n's with large n are composed of contributions obeying different scaling laws. Examples of the experimentally observed[9-11] compensated high-order moments are presented on Fig.(6). From comparison of the graphs of Fig.1 and Fig.6 we conclude that the high-order moments, derived in this paper, though not obeying any real scaling laws, exhibit much more of a "scaling range" than the experimentally observed ones.

To conclude the comparison of the predictions of the theory with experimental data, the measured correlation function[12,13] of the dissipation rate are shown on Fig.7. The predicted range $S_2^{\epsilon} \approx k^0$ in the vicinity of the dissipation scale is clearly seen.

8 Conclusions

The large-scale processes in all real-life turbulent flows are dominated by powerful, well-organized, long-living coherent structures. These structures participate in turbulence production and influence both global and small-

scale features of the flow. It is always assumed in developing the theory of turbulence that in the so-called inertial range the large-scale processes and those happening in the viscosity-dominated dissipation range can be safely neglected. The role of the large-scale coherent state in the statistical properties of velocity fluctuations has been analyzed in this work and it has been shown that, indeed, the influence of the coherent state diminishes with decrease of the length-scale. However, the transition is very slow and experimentally observed behaviour of the high-order structure functions can be mistakenly perceived as obeying non-trivial scaling laws.

The theory presented here is based on the assumption that even at the relatively high Reynolds numbers the coherent state in the external-field-driven flow reflects properties of this field. In principle, it is plausible to assume that the instability of the laminar velocity profile leads to a mean field having nothing in common with the laminar state of the flow due to the strong non-linear interaction between coherent and fluctuating components. In this case the details of the external field are forgotten even in moderate Reynolds number situations. In my opinion, in the real life flows this is not the case. The coherent structures, emerging at the transition to turbulence when $Re \approx Re_c$, persist even when $Re \gg Re_c$. This fact is readily understood: If the effect of the small-scale velocity fluctuations on the large-scale flow features can be described in terms of an eddy viscosity, then it is possible to show that the relevant effective Reynolds number $Re = \frac{u_{rms}L}{\nu_{eff}} = O(1) \approx Re_c$. Thus, the large-scale flow is always transitional and is strongly influenced by the driving mechanism. This fact can be easily verified for the wall-shear flows, convection, jets and mixing layers by simply using the data on the turbulent intensities (u_{rms}) in the definition of the turbulent viscosity $\nu_{eff} = \frac{\overline{v_i v_j}}{\frac{\partial U_i}{\partial x_j}}$. In all these cases the effective Reynolds number is close to critical and that is why the large-scale flow features resemble organized structures characteristic of transitional flows. Experimental manifestation of this fact can also be found in the data on the energy spectra as function of dimensionless frequency f. For example, in the wake behind the cylinder the spectrum $E(f)$ has a very sharp maximum at $f \approx 0.2$ independent on the Reynolds number in a very wide range of Re variation. Similar feature can be found in Benard convection where the characteristic velocity of the large-scale coherent vortex (wind) scale with the Rayleigh number as $U \approx Ra^{\frac{1}{2}}$ which corresponds to the simple relation $U \propto \sqrt{gL}$ where g is the gravitational acceleration driving the flow. As we

see, the external field g plays a very important part even at large Ra. These facts, in my opinion, support the main assumption that the coherent state can be treated as an external field.

According to the theory developed here, the existence of the large-scale coherent state explains the experimentally observed gaussian statistics of the velocity fluctuations. This fact has important implications for the problem of turbulence modelling. Indeed, the gaussian field cannot participate in the energy transfer from large to small-scale fluctuations. This means that only the fluctuations $v(k)$ with $k > (\frac{S^3}{\epsilon})^{\frac{1}{2}} >> k_0$ can give substantial contribution to the effective transport coefficient. The same estimate holds for the rate of diminishing of the large-scale generated anisotropy with decrease of the wave number. The anisotropy of the velocity fluctuations makes the energy transfer from large to small scales more difficult, which is another reason for the relatively weak contribution of the large scale velocity fluctuations to the effective transport. Thus, there exist some scale separation, characterized by the small parameter $u_{rms}/U \ll 1$ justifying the concept of turbulent viscosity which is so successful in the modelling of the large-scale features of turbulent flows.

The main unsolved problem with the Clebsch formulation of statistical hydrodynamics is non-uniqueness: it follows from (2.4) that any transformation $\lambda \to f(\lambda, \mu)$, $\mu \to \phi(\lambda, \mu)$ with

$$\frac{\partial f}{\partial \lambda}\frac{\partial \phi}{\partial \mu} = 1$$

does not change the velocity field. The parameter

$$N' = \int (f^2 + \phi^2) d^3x \neq N_0$$

This is a problem since N_0 is an important parameter of the theory determining the constant frequency shift Ω. At the present time we do not have a rigorous way to gauge the Clebsch field and determine N_0. However, the only large-scale physically relevant frequency $\Omega = N_0 k_0^2 \approx S$ which can serve as an estimate for N_0 since $k_0 = O(1)$. Thus, the large-scale dynamics are strongly influenced by the interactions of the fluctuating and coherent components of the Clebsch field.

It is possible that this is only a part of the picture. The viscosity-dominated

small-scale dynamics can produce another mechanism of deviation from Kolmogorov scaling. The physical reasons for this can be illustrated by the definition of the high-order moments of velocity differences:

$$S_{2n} = \overline{\prod(u(X_i) - u(X_i + x))}$$

in the limit when all $X_i \to X_j$ and $2 < i < 2n$. We can see that S_{2n} are mixed quantities, involving not only inertial range separation x but also dissipation range displacements $X_i - X_j \to 0$. Thus, S_{2n} are not pure inertial range properties of the flow and corrections to the Kolmogorov scaling are expected. If this is so, then we can predict a cross-over from the large-scale "scaling", dominated by the coherent structures, to another one reflecting intermittency of fully developed turbulence due to the viscous contribution to the equations of motion.

figure legends

Fig.1. a. Typical form of the normalized moment $R_{2n}(x)$ plotted for $n = 3$. b. Compensated moments $x^{\xi_{2n}} R_{2n}(x)/(2n-1)!!$. The values of ξ_{2n} for n=2,3,4,and 5 are given in the Table.

Fig.2 Energy spectra in the boundary layer of the wind tunnel. NASA Ames experiment Ref.(6). a. u^2; b. v^2; c. w^2. $R_\lambda = 1400$.

Fig.3 Co-spectra $E_{12}(k_1)$ measured at two different locations ($R_\lambda = 1450; 600; 1000; 500$) in the boundary layer for two values of free-stream velocity. Ref.(6). The data are presented in dimensionless coordinates.

Fig.4 Second-order structure function $S_2(x)$ Ref.(8) measured in the laboratory boundary layer. a.Fitted by the Kolmogorov scaling; b. The same data fitted by $S_2 = ax^{\frac{2}{3}} + bx^{\frac{4}{3}}$;

Fig.5. The energy spectrum $E(k)$ from direct numerical simulations of the Taylor-Green vortex by M.Brachet[7].

Fig.6. The experimentally measured compensated moments of velocity differences. a. Ref.9 (jets: $R_\lambda = 500; 800$); b.Ref.10 (wind tunnel); c. Ref.11 (boundary layer)

Fig.7. Second-order moment of the dissipation range differences S_2^ϵ. a. Ref.12 (atmospheric boundary layer); b. Ref.13 (laboratory boundary layer)

11 References

1. L.D. Landau and E.M. Lifshitz, Fluid Mechanics, Pergamon Press, Oxford, 1962

2. V.E.Zakharov, G.Falkovich and V.S.L'vov, "Kolmogorov Spectra in Weak Turbulence", Springer Verlag, Heidelberg, 1993

3. V.Yakhot and V.Zakharov, PhysicaD64, 379 (1993)

4. The detailed calculation of the diagonalization of quadratic Hamiltonian in a more general case will be published by V.Zakharov, Phys. Lett, 1993.

5. K.R.Sreenivasan, private communication, 1993

6. S.G.Saddoughi and S.V.Veeravalli, Center of Turbulence Research, Stanford University, Report, 1993

7.M.Brachet, private communication, 1993

8. K.R.Sreenivasan, private communication, 1993

9. F.Anselmet, Y.Gagne, E.J.Hopfinger and R.A.Antonia J.Fluid Mech. **140**, 63 (1984)

10. Y. Gagne, Thesis, University of Grenoble, 1987

11. K.R.Sreenivasan, private communication

12. J.R.Wilson and R.W.Burling, J.Fluid Mech. **41**, 141

13. K.R.Sreenivasan, private communication, 1993

Exponents ζ_{2n}

2n	Experiment[5]	Present	Extrapolation
4	0.14 ± 0.038	0.13	0.15
6	0.34 ± 0.042	0.33	0.39
8	0.60 ± 0.037	0.70	0.69
10	0.97 ± 0.037	1.10	1.04
12	1.15 ± 0.13	-	1.42

Fig. 1

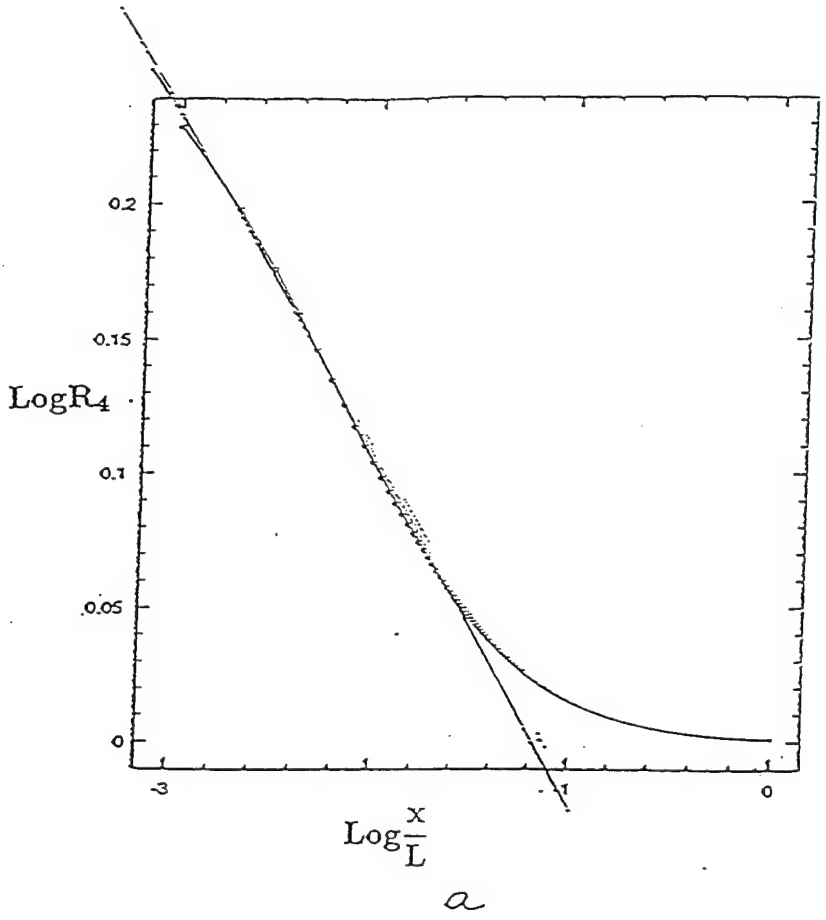
0.2
0.15
LogR4
0.1
.05
0
-3
-1
0
Log x/L

a

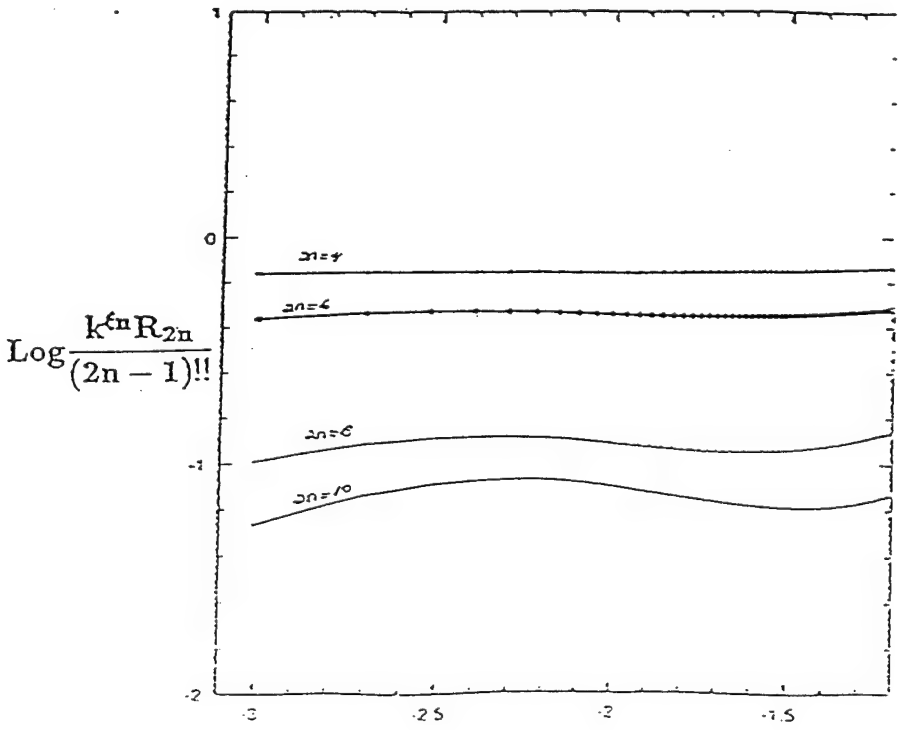
1
0
2n=4
2n=6
2n=8
2n=10
-1
-2
-3
-2.5
-2
-1.5
Log k^2n R2n / (2n-1)!!

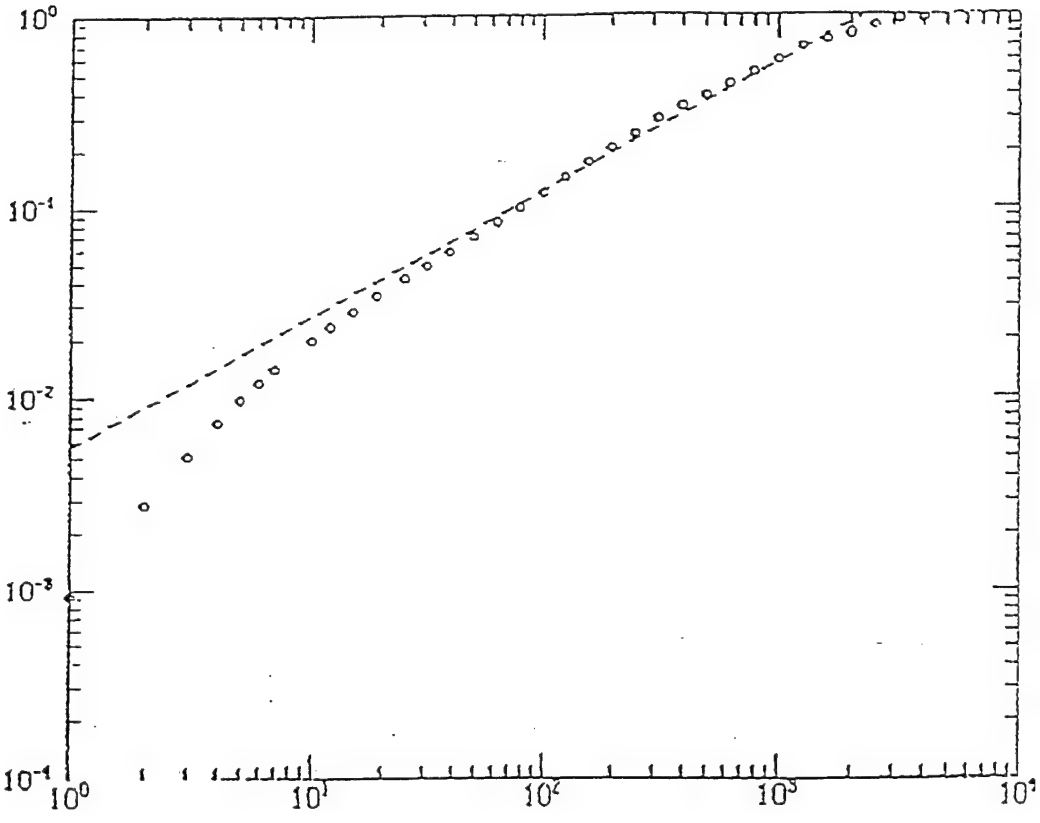

a

Fig. 2

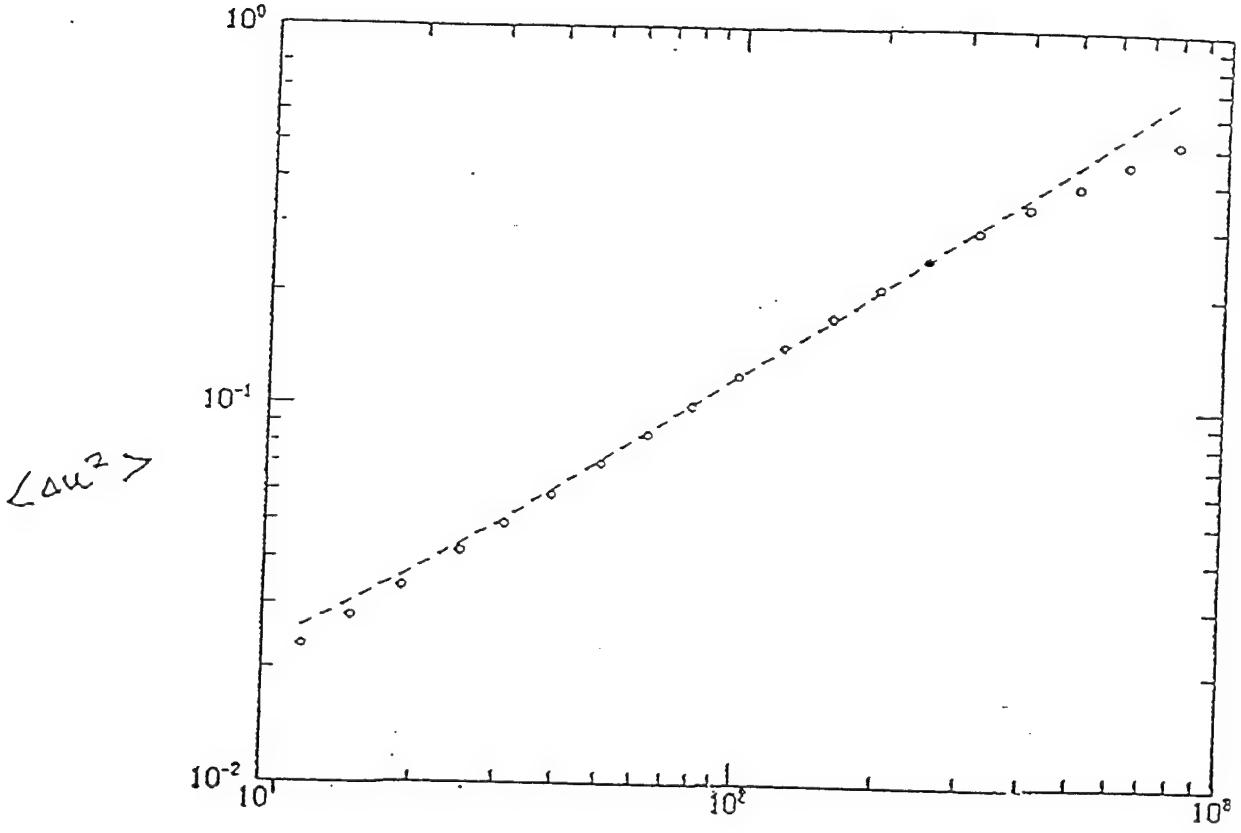

b

Fig.2

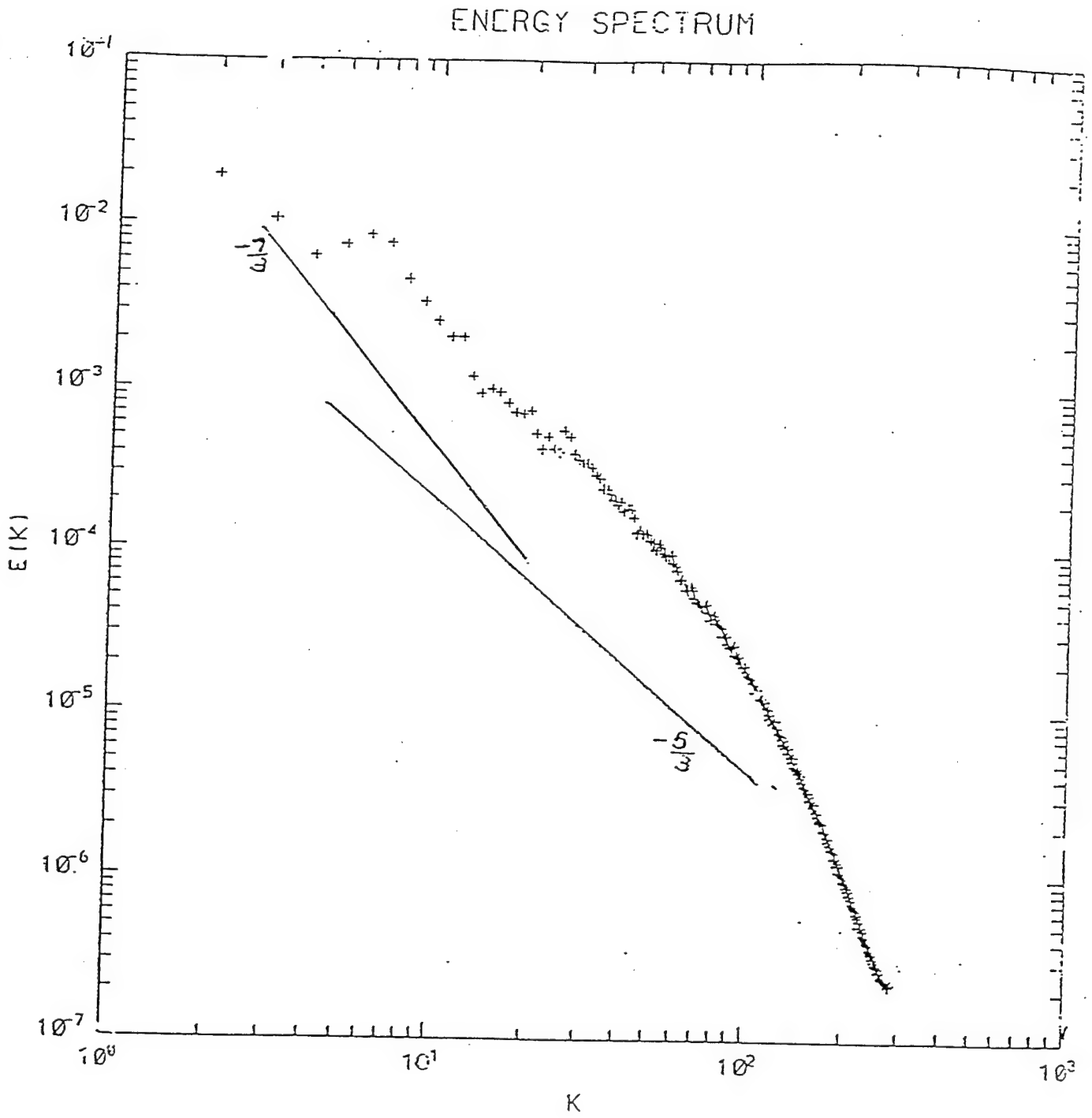
ENERGY SPECTRUM
E(K)
K
10^{-1}
10^{-2}
10^{-3}
10^{-4}
10^{-5}
10^{-6}
10^{-7}
10^{0}
10^{1}
10^{2}
10^{3}
$\frac{1}{\omega^{5/3}}$
$\frac{1}{\omega^{5}}$

Fig.3

Spectra of Fluctuations of Velocity, Kinetic Energy and Dissipation Rate in Strong Turbulence

Abstract. Following the ideas of operator product expansion, the velocity v, kinetic energy $K = \frac{1}{2}v^2$ and dissipation rate $\epsilon = \nu_0(\frac{\partial v_i}{\partial x_j})^2$ are treated as independent dynamical variables, each obeying its own equation of motion. The following relations $\overline{\Delta u(\Delta K)^2} \propto r$; $\overline{\Delta u(\Delta \epsilon)^2} \propto r^0$ and $\overline{(\Delta u)^5} \approx r\overline{\Delta\epsilon\Delta K}$ are derived. If velocity scales as $(\Delta v)_{rms} \propto r^{\frac{\gamma}{3}-1}$, then simple power counting gives: $(\Delta K)_{rms} \propto r^{1-\frac{\gamma}{6}}$ and $(\Delta\epsilon)_{rms} \propto 1/\sqrt{(\Delta v)_{rms}} \propto r^{\frac{1}{2}-\frac{\gamma}{6}}$. In the Kolmogorov turbulence ($\gamma = 4$) the intermittency exponent $\mu = \frac{\gamma}{3} - 1 = 1/3$ and $\overline{(\Delta\epsilon)^2} = O(Re^{\frac{1}{4}})$. The scaling relation for the ϵ-fluctuations is a consequence of cancellation of ultra-violet divergences in the equation of motion for the dissipation rate.

The Kolmogorov relation for the third order structure function in decaying homogeneous and isotropic turbulence[1], derived directly from the Navier-Stokes equations, reads:

$$S_3 = \overline{(u(X+r)-u(X))^3} = -6\overline{u(x)u(x)u(x+r)} = -\frac{4}{5}\bar{\epsilon}r + 6\nu_0\frac{dS_2}{dr} \qquad (1)$$

where $u(X)$ is the x-component of the velocity field $\mathbf{v}$,r is the displacement in the x-direction and $\bar{\epsilon} = \nu_0\overline{(\frac{\partial v_i}{\partial x_j})^2} = O(1)$. The correlation function $S_2 = \overline{(u(X)-u(X+r))^2}$. The mean dissipation rate $\bar{\epsilon}$ in the Kolmogorov derivation is defined as $\frac{\overline{\partial v^2}}{\partial t} = -2\bar{\epsilon}$. In a statistically steady flow driven by the force $\mathbf{f}$, $\frac{\overline{dv^2}}{dt} = 0 = -2\bar{\epsilon} + 2\overline{\mathbf{f}\cdot\mathbf{v}}$ and, in general, the Kolmogorov relation (1) must be modified. The Navier-Stokes equations driven by a force $\mathbf{f}$ are:

$$\frac{\partial v_i}{\partial t} + v_j\frac{\partial v_i}{\partial x_j} = -\frac{\partial p}{\partial x_i} + \nu\frac{\partial^2 v_i}{\partial x_j^2} + f_i \qquad (2)$$

with $\nabla\cdot\mathbf{v} = 0$. It follows from this equation[2] that

$$S_3 = -\frac{4}{5}\bar{\epsilon}r + \frac{6}{r^4}\int_0^r y^4\overline{\Delta u\Delta f}dy + 6\nu\frac{\partial S_2}{\partial r} \qquad (3)$$

where $\Delta f = f(X+r) - f(X)$. It is clear that if the energy source acts at the largest scales only, so that the Fourier transform $f(k) = 0$ for $k > k_0 \to 0$, then the relations (3) and (1) are identical for small enough values of the displacement r. Applying dimensional considerations to the expression (1) or (3) leads to the Kolmogorov law: $(\Delta u)_{rms} = O(\bar{\epsilon}^{\frac{1}{3}}r^{\frac{1}{3}})$. This relation defines the dimensionality of the velocity operator: the root-mean square velocity v_r averaged over a ball of a radius r scales as $v_r \propto r^{\frac{1}{3}}$. It is convenient to introduce the effective viscosity $\nu(r)$ defined from the equation for the velocity field $\mathbf{v}^<$, averaged over small-scale ($l < r$) fluctuations: $\mathbf{v}^<\cdot\nabla\mathbf{v}^< \approx \nu(\mathbf{r})\nabla^2\mathbf{v}^<$. Power counting gives: $\nu(r) \approx \bar{\epsilon}^{\frac{1}{3}}r^{\frac{4}{3}}$ in accord with Kolmogorov theory. The effective viscosity $\nu(r)$ takes into account the effects of the velocity fluctuations at scales $l < r$. Dimensional considerations, applied to relation (3) are a very crude approximation. In general, if $(\Delta u)_{rms} \propto r^{\frac{\gamma}{3}-1}$, then $\nu(r) \propto r^{\frac{\gamma}{3}}$, where the exponent γ is to be determined from the theory. The Kolmogorov spectrum, approximately supported by experimental data, corresponds to $\gamma = 4$. So, in what follows this value of parameter γ will be used for evaluation of the exponents following the general relations derived below. The

relation (1) or (3) gives an important constraint on the structure of turbulence theory. Fourier transform of $S_3(k) \propto \delta'(k) = 0$ for the wave-mumber k in the inertial range. This means that the largest scales in the flow play the most important part in dynamics of turbulence. To make this point even stronger, let us consider a flow driven by a white-in-time random force having non-zero Fourier component $f(k)$ at $k = k_0$. In this case the relation (3) gives

$$S_3 = -\frac{4\bar{\epsilon}}{5! k_0 r^4} \frac{\partial^3}{\partial q^3} \frac{sinqr}{q}$$

evaluated at $q = k_0$. Here $\bar{\epsilon} =< \mathbf{f} \cdot \mathbf{v} >$. This exact relation tells us that the integral scale k_0 cannot disappear from the problem as a result of Galileo-like transformations. The effects of the large scale dynamics on the scaling properties of both kinetic energy and dissipation rate will be investigated below.

It is also interesting to investigate the properties of fluctuations of the local values of kinetic energy $K = 1/2\ v_i^2(x)$ and dissipation rate $\epsilon = \nu_0 (\frac{\partial v_i}{\partial x_j})^2$. Power counting based on $u = O(r^{\frac{1}{3}})$ gives for the dimensionality of kinetic energy and dissipation rate: $K^2 = O(r^{\frac{4}{3}})$ and $\epsilon_r^2 = O(r^{-\frac{8}{3}})$ corresponding to the spectra $E_K(k) \propto k^{-\frac{7}{3}}$ and $E_\epsilon \propto k^{\frac{5}{3}}$. These relations strongly contradict all available experimental data. In this work, following the ideas of operator product expansion, we consider $\mathbf{v}$, K and ϵ as independent dynamical variables and derive scaling properties of fluctuations of kinetic energy (K) and dissipation rate (ϵ). The equation of motion for kinetic energy is:

$$\frac{\partial K}{\partial t} + v_j \frac{\partial K}{\partial x_j} = -\epsilon - \frac{\partial v_i p}{\partial x_i} + \nu_0 \frac{\partial^2 K}{\partial x_j^2} + v_i f_i \tag{4}$$

This is essentially an equation for a passive scalar (K) with various sources added to the right side. Repeating the procedure for the isotropic and homogenious flow, described in Ref. (2) and Monin and Yaglom[3], gives:

$$\overline{\Delta u (\Delta K)^2} = 4\overline{u(x)K(x)K(x+r)} \approx -\frac{4}{3} N_K r + F_K$$

where $F_K = O(\overline{\Delta \epsilon \Delta K} r)$ and $N_K = \nu_0 \overline{(\frac{\partial K}{\partial x_j})^2} + 4\overline{\epsilon(x) K(x)} = O(1)$. The $O(\overline{\Delta u \Delta p \Delta K})$ terms, coming from pressure contributions to (4), are small in the inertial range limit $r \to 0$. It will

be shown below that $F_K = O(r^{\frac{5}{3}})$ is also small in the inertial range when displacement r is small enough. This leads to the root-mean-square of kinetic energy fluctuations:

$$\overline{(\Delta K)^2} \propto r^{2-\frac{7}{3}} \approx \frac{N_K}{\bar{\epsilon}^{\frac{1}{3}}} r^{\frac{1}{3}}$$

and $E_K \propto k^{\frac{7}{3}-3} \approx k^{-\frac{5}{3}}$ for $\gamma = 4$. Again, application of the dimensional reasoning leading to this result is extremely dangerous. Here it is used only to illustrate how the arguments based on the weak coupling, when applied to relevant equations of motion, can lead to the non-trivial scaling. The correlation of kinetic energy fluctuatuins can be also derived from the following considerations: the Fourier transform of $\overline{(\Delta K)^2}$ involves the integral $\int < K(q_1)K(q_2)K(q_3)K(k-q_1-q_2-q_3) >$. If the main contribution to this integral comes from the largest scales, then it is easy to show that

$$\overline{(\Delta K)^2} \approx V_{rms}^2 \overline{(\Delta u)^2} \approx V_{rms}^2 \bar{\epsilon}^{\frac{2}{3}} r^{\frac{2}{3}} (\frac{r}{L})^{\frac{2(\gamma-1)}{3}-2}$$

It is interesting that these two expressions for the kinetic energy correlation functions coinside only when $\gamma = 4$. In what follows we set $\bar{\epsilon} = V_{rms} = L = O(1)$.

The spectrum of the dissipation rate fluctuations has to be calculated from the following equation of motion:

$$\frac{\partial \epsilon}{\partial t} + v_i \nabla_i \epsilon = F_\epsilon + \nu_o \nabla_i \nabla_i \epsilon \tag{5}$$

where

$$F_\epsilon = \overbrace{2\nu_o (\nabla_j v_i)(\nabla_j f_i)}^{P_\epsilon} - \overbrace{2\nu_o (\nabla_j v_i)(\nabla_j v_l)(\nabla_l v_i)}^{T_1}$$

$$- \overbrace{2\nu_o^2 (\nabla_j \nabla_l v_i)^2}^{T_2} - 2\nu_o (\nabla_j v_i)(\nabla_i \nabla_j p) \tag{6}$$

This equation leads readily to:

$$\overline{\Delta u (\Delta \epsilon)^2} = 4\overline{u(x)\epsilon(x)\epsilon(x+r)} \approx -\frac{4}{3} N_\epsilon r + \phi_\epsilon \tag{7}$$

where $N_\epsilon = \overline{F_\epsilon(x)\epsilon(x)} = O(1)$ and $\phi_\epsilon = O(\overline{\Delta F_\epsilon \Delta \epsilon} r)$. It will be shown below that $N_\epsilon \approx \frac{\bar{\epsilon}^2 K}{\nu(L)}$ where $\nu(L) \approx \bar{\epsilon}^{\frac{1}{3}} L^{\frac{4}{3}}$. Thus, all contributions to N_ϵ are $O(1)$ which justifies the estimate $N_\epsilon = O(Re^0)$. Our goal is to evaluate ϕ_ϵ which can be written as:

$$\phi_\epsilon = r \int dk (1 - e^{ikr}) \overline{F_\epsilon(\mathbf{k})\epsilon(-\mathbf{k})} \tag{8}$$

Thus, the problem is reduced to calculation of:

$$Y = \overline{F_\epsilon(\mathbf{k})\epsilon(-\mathbf{k})} = -\nu_0 \int d^3q d\Omega q_i (q+k)_i \overline{v_m(\mathbf{q},\Omega) v_m(\mathbf{k}+\mathbf{q}, \omega+\Omega) F_\epsilon(\mathbf{k})} \tag{9}$$

The procedure leading to calculation of Y in the one-loop approximation was developed in Refs. (4). The main steps are: First we average the expression F_ϵ over the small-scale velocity fluctuations $v(\mathbf{k})$ with wave numbers $\Lambda < k < \Lambda_0 \approx k_d$. It is assumed that $k << \Lambda$. The main result of this averaging is in "dressing" the bare viscosity: everywhere we have to substitute ν_0 by the renormalized value $\nu(\Lambda) \approx \bar{\epsilon}^{\frac{1}{3}} \Lambda^{-\frac{4}{3}}$. Thus, the small- scale averaging procedure leads to the expressions (6)-(9) but with $\mathbf{v}^<$ instead of $\mathbf{v}$ and $\nu(\Lambda)$ instead of ν_0. Using this result and the fact that the Reynolds number based on $\nu(\Lambda)$ and $v^<$ is $O(1)$ when Λ is in the inertial range, we derive an estimate:

$$Y \approx \bar{\epsilon} < F_\epsilon(\mathbf{k}) > \tag{10}$$

This is clear since the largest contribution to the integral

$$I_Y = \nu(\Lambda) \int d^3q d\Omega q_i (q+k)_i \overline{v_m^<(\mathbf{q},\Omega) v_m^<(\mathbf{k}+\mathbf{q}, \omega+\Omega)}$$

taken over the interval $0 < q < \Lambda$ comes from the interval $k << q \approx \Lambda$. In this approximation in the long-time limit $\omega \to 0$

$$I_Y \approx \nu(\Lambda) \int dq q^2 E(q) \approx \bar{\epsilon} = O(1)$$

which is independent of Λ. Correction to (10), coming from the fluctuating contribution to $\epsilon = \bar{\epsilon} + \delta\epsilon$, will be discussed below. The details of evaluation of $< F_\epsilon(\mathbf{k}) >$ are given in Ref. (4). It has been shown that all contributions to $< F_\epsilon >$, defined by (6), are ultra-violet

divergent, i.e. the integrals depend on the u.v. cut-off k_d. However, an accurate evaluation of the integrals revealed that all divergent terms in (6) cancel in the one-loop approximation and the resulting expression is independent of the ultra-violet cut-off. It is easy to see from (6) that in the zeroth order the u.v. divergent corrections to P_ϵ and T_2 in (6) cancel each other, reflecting the fact that the mean rates of production and destruction of ϵ are equal in statistically steady state[4]. It has also been shown[4] that the divergent terms in P_ϵ, T_1, T_2 and the pressure contributions to (6), appearing in the first order of the iteration procedure sum up to zero. The first nonvanishing correction to

$$T_2 \approx \nu^2(\Lambda) \int q^2(\mathbf{k}-\mathbf{q})^2 v_i^<(q) v_i^<(k-q) d^3q d\Omega_q$$

appears in the second order of the iteration procedure, which uses the Navier-Stokes equations symbolically written as:

$$v^< \approx fG + \frac{1}{2} P(\mathbf{k}) G \int v^<(q) v^<(k-q) dq$$

This correction is equal to:

$$F_\epsilon(\mathbf{k}) \approx \nu^2(\Lambda) \int q^2(\mathbf{k}-\mathbf{q})^2 P(\mathbf{q}) P((\mathbf{k}-\mathbf{q})) G(q) G(k-q) v^<(Q) v^<(q-Q) v^<(p) v^<(k-q-p) dq dp dQ \tag{11}$$

where $P(\mathbf{k}) = O(\mathbf{k})$, $k = (\mathbf{k}, \omega)$ and $G(k,\omega) = (-i\omega + \nu(\Lambda)k^2)^{-1}$. Relation (11) represents the operator F_ϵ in terms of $\mathbf{v}^<$. To evaluate expressions (9), (10) and (8) we have to calculate $\overline{F_\epsilon}$. The estimate can be derived readily: iterating (11) using zero-order solution:

$$\overline{v_i(k,\omega) v_j(k',\omega')} \propto \bar{\epsilon} k^{-3} G G^* \delta(\mathbf{k}+\mathbf{k}') \delta(\omega+\omega')$$

gives:

$$\bar{F}_\epsilon(\mathbf{k}) \approx \frac{\bar{\epsilon} K(k)}{\nu(\Lambda)} \tag{12}$$

where

$$K(k) \approx \frac{1}{4}\left(\left(\int d^3q d\Omega_q v_i^<(\mathbf{q},\Omega_q) v_i^<(\mathbf{k}-\mathbf{q},\omega-\Omega_q)\right)^2\right)^{\frac{1}{2}}$$

Substituting (10),(12) into (8) gives for $\Lambda \approx r^{-1}$ and $\omega \to 0$:

$$\overline{\Delta u(\Delta\epsilon)^2} = 4\overline{u(x)\epsilon(x)\epsilon(x+r)} \approx -\frac{4}{3}N_\epsilon r + \phi_\epsilon \approx r\frac{\bar{\epsilon}^2(\Delta K)_{rms}}{\nu(r)} = O(\bar{\epsilon}^2 V_{rms} r^0) \qquad (13)$$

It is interesting that the scaling of the right side of (13) is independent of the value of γ. This result can be obtained from (11) on the basis of dimensional considerations: the one-loop iteration introduces a factor $\bar{\epsilon} = O(1)$ and $\int G^4 d\Omega$ gives $\nu^3(\Lambda)$ in the denominator. The remaining $O(v^2)$ contributions give ΔK in relation (13). Thus, it follows from (7) and (13) that:

$$\overline{(\Delta\epsilon)^2} \propto 1/(\Delta u)_{rms} \propto r^{1-\frac{\gamma}{3}} \equiv r^{-\mu} \approx r^{-\frac{1}{3}} \qquad (14)$$

This expression defines the so-called intermittency exponents μ. The corresponding spectrum E_ϵ is: $E_\epsilon(k) \propto k^{\frac{\gamma}{3}-2} \propto k^{-\frac{2}{3}}$. For the mean value of the dissipation rate fluctuations we have: $\overline{(\Delta\epsilon)^2} \propto k_d^{\frac{1}{3}} \propto Re^{\frac{1}{4}}$

The approach, developed in this work can be used for derivation of the scaling propeties of various composite operators. For example, the energy equation (4) leads to:

$$\frac{\partial}{\partial r}\overline{\Delta u(\Delta K)^2} + \frac{4}{3}N_K \approx -\overline{\Delta\epsilon\Delta K} \qquad (15)$$

This relation was obtained above taking into account that in the case of the large-scale white-in-time random force $< f_i v_i K(x+r) >= \bar{\epsilon} K(x+r)$ and neglecting the pressure contributions. The left side of (15) is $O(\frac{\partial}{\partial r}(V^2\overline{(\Delta u)^3} + \overline{(\Delta u)^5})) + \frac{4}{3}N_K$, where $V^2 = O((\bar{\epsilon}L)^{\frac{2}{3}}) = O(1)$. Using (1) we come to the conclusion that if the r-independent contributions to the left side of (15), corresponding to the constant in the wave-number space flux of K, cancel each other, the remaining terms give:

$$\overline{\Delta\epsilon\Delta K} \approx \frac{\partial}{\partial r}\overline{(\Delta u)^5} \propto (\frac{r}{L})^\beta \qquad (16)$$

with $\beta = 2/3$ if the Kolmogorov prediction for the fifth-order structure fuction is used. The corresponding co-specrum $E_{\epsilon,K} \propto k^{-\frac{5}{3}}$. Using (16) we can show that the contribution to (13), coming from the ϵ-fluctuations, neglected in (10), which is $O(r\frac{\overline{\epsilon\Delta\epsilon\Delta K}}{\nu(r)} \approx r^{\frac{1}{3}})$ is small when $r \to 0$. The relation (16) was verified in numerical experiments on the random force-driven three-dimensional turbulence in Ref. 5. The theoretical understanding of (16) was developed jointly with the authors of ref. 5.

All operators $\mathbf{v}$, K and ϵ, considered in this work are goverened by the equations of motion which do not change under Galileo transformations and $K' = K + \frac{1}{2}U^2 + \mathbf{v}\cdot\mathbf{U}$. It is clear that the scaling of $\overline{(\Delta K')^2}$ with r is the same as that of $\overline{(\Delta K)^2} \approx r^{\frac{2}{3}}$. Indeed, we can write: $\overline{(\Delta K')^2} = \overline{(\Delta K)^2} + \frac{1}{2}U^2\overline{(\Delta u)^2} \propto r^{\frac{2}{3}}$. The Kolmogorov relation following directly fron the equation for K':

$$\overline{\Delta u'(\Delta K')^2} = -\frac{4}{3}N_{K'}r + F_{K'}$$

where $u' = u + U$. Since $\Delta u' = \Delta u$ we have: $\overline{(\Delta K')^2} \propto r^{\frac{2}{3}} \propto \overline{(\Delta K)^2}$. As was shown above, the scaling exponent of the right side of relation (13) is invariant under Galileo transformation. However, the proportionality coefficient is transformed as $a' = a + O(U^2)$, i.e., strictly speaking, the relation (13) violate Galileo invariance. This can be an artifact of the low-order diagrammatic approximation used in the derivation of (13) which, in principle, can yield incorrect scaling exponents. So, it is gratifying to know that in the calculation presented here, this is not the case.

Let us explore the possibility that Galileo invariance is broken by powerfull large-scale structures, always present in real-life turbulent flows. It is known from experimental data that the large scale velocity field is described by close-to-gaussian statistics. To illustrate the physical meaning of the results derived in this work let us write the energy equation:

$$\frac{\partial K}{\partial t} + v_j\frac{\partial K}{\partial x_j} + V_j\frac{\partial K}{\partial x_j} = -\epsilon \tag{17}$$

where the forcing, pressure and viscous terms are omitted for simplicity. The large-scale gaussian velocity field $\mathbf{V}$ is assumed constant in each realization. The non-linear contribution to (17) can be treated perturbatively. It is easy to see that in the zeroth order:

$$K(k,t) = K(k,0) - \int_0^t \epsilon(k,\tau) e^{i\mathbf{V}\cdot\mathbf{k}\tau} d\tau$$

Multiplying this equation by $\epsilon(-k,0)$ and averaging independently over the gaussian field V and the small-scale ϵ-fluctuations we obtain in the long-time limit $t \to \infty$:

$$\overline{\epsilon(-k,0)K(k,0)} \approx \int_0^t \overline{\epsilon(k,\tau)\epsilon(-k,0)} exp(-\frac{1}{4}\overline{V^2}k^2\tau^2) d\tau$$

This integtal is evaluated easily when $kV_{rms} \to \infty$:

$$\overline{\epsilon(-k,0)K(k,0)} \approx \frac{1}{kV_{rms}} \overline{\epsilon(k,\frac{1}{kV})\epsilon(-k,0)} \approx \frac{1}{kV_{rms}} \overline{\epsilon(k,0)\epsilon(-k,0)} \qquad (18)$$

Setting $\tau = (kV_{rms})^{-1} = 0$ in the second equality in (18) means that the dynamics of the dissipation rate is characterized by the longer time-scale or in the other words ϵ, though advected by the large scales is dominated by the local interactions. This statement will be justified below. Thus, the scaling exponent μ of the dissipation rate fluctuations correlation function is given by $-\mu = \beta - 1$, where the exponent β is defined by relation (16). This result holds if the neglected non-linear contribution to the energy equation can be represented in the eddy-viscosity approximation $\nu(k,t)k^2K(k,t)$, provided $kV_{rms} >> \nu(k,t)k^2$. An attempt to explain experimentally observed large-scale gaussian statistics of the velocity fluctuations as a result of the symmetry breaking by the large-scale coherent structures, was made in Ref. 6.

The relation (18) can be directly obtained from the so called $K - \epsilon$ model, wich is extremely successfull in describing large-scale properties of complex turbulent flows. In this model the effective viscosity $\nu \approx \frac{(K^<)^2}{\epsilon^<}$ where the operators $< K >_{ss} = K^<$ and $< \epsilon >_{ss} = \epsilon^<$ with symbol $<>_{ss}$ denoting small scale averaging[4]. The model, which is the result of cancellation of the ultra-violet divergences[4], is:

$$\frac{\partial K}{\partial t} + v_j \frac{\partial K}{\partial x_j} = -\epsilon \qquad (19)$$

$$\frac{\partial \epsilon}{\partial t} + v_i \nabla_i \epsilon \approx -C_2 \frac{\epsilon^2}{K} \qquad (20)$$

where, to simplify notation, we set $K = K^<$, $\epsilon^< = \epsilon$ and neglected the diffusion terms in both equations, The constant factor $C_2 \approx 1.7$ (see Ref.4). These equations give readily

$$\frac{\partial}{\partial r}\overline{\Delta u \Delta K \Delta \epsilon} \approx \overline{(\Delta \epsilon)^2} \tag{21}$$

leading to the relation (18), provided the left side of (21) is dominated by the large- scale advection with velocity V_{rms}. The relation (21) is based on the assumption that $\overline{(\epsilon^<)^2} \approx \overline{(\Delta \epsilon)^2}$ if $\epsilon^<$ stands for the dissipation rate field averaged over the scales $l < r$. It is important to notice the difference between (13) and (21). The expression (13), written in terms of Fourier transforms, involves the dissipation rate spectrum $E_\epsilon \propto k^{-\frac{2}{3}}$ and, as a consequence the integral is infra-red convergent, i.e. the resulting expression does not involve both infra-red and ultra-violet cut- offs. In this case $(\Delta u)_{rms} \propto r^{\frac{1}{3}}$ is to be used for estimation of the dissipation rate scaling. On the other hand, the relation (21) involves the co-spectrum $E_{\epsilon,K}$ contributing to the strong infra-red divergence of the corresponding integral, which leads to the choice $(\Delta u)_{rms} \approx V_{rms} = O(1)$, yielding the same result for the dissipation rate spectrum. It is interesting that the relation (21) is invariant under random Galileo transformation.

The main result of this work is the derivation of the experimentally observable correlation functions:

$$\overline{\Delta u (\Delta K)^2} \approx N_K r \tag{22}$$

$$\frac{\partial}{\partial r}\overline{\Delta u \Delta \epsilon \Delta K} \approx \overline{(\Delta \epsilon)^2} \tag{23}$$

$$\overline{\Delta u (\Delta \epsilon)^2} \approx \bar{\epsilon}^2 V_{rms} r^0 \tag{24}$$

$$\overline{(\Delta u)^5} \approx r \overline{\Delta \epsilon \Delta K} \tag{25}$$

$$r\overline{(\Delta \epsilon)^2} \approx V_{rms} \overline{\Delta \epsilon \Delta K} \tag{26}$$

Since the effective Reynolds number in the inertial range is $O(1)$ these relations lead approximately to: $(\Delta K)_{rms} \propto r^{\frac{1}{3}}$ and $(\Delta \epsilon)_{rms} \propto (\Delta u)_{rms}^{-\frac{1}{2}} \propto r^{-\frac{1}{6}}$. One interesting consequence of relation (13) was noticed by M.Nelkin: if the Kolmogorov hypothesis

$$\epsilon(x)\epsilon(x+r) \approx \epsilon_r^2 \approx \frac{(\Delta u)^6}{r^2}$$

where ϵ_r is the value of the dissipation rate ϵ averaged over the sphere of radius r surrounding the point x, is correct, then $\overline{(\Delta u)^7} \propto r^2$. Simple power counting, involved in derivation of these scaling relations, implies weak coupling and thus is a very dangerous procedure. The derived numerical values of the exponents, corresponding to the mean field theory, are not to be taken too seriosly despite their close agreement with experimental data.

To conclude: Derivation of the non-trivial spectrum of the dissipation rate fluctuations directly from the Navier-Stokes equations based on a finite order of the renormalized perturbation expansion seems to be impossible. However, even one-loop approximation, applied to the high-order equation of motion for the local values of the dissipation rate, gives a strong intermittency with exponent $\mu = 1/3$ in good agreement with experimental data. This result is a direct consequence of exact cancellation of the ultra-violet divergences in the ϵ-equation, discovered in Ref. (4) in the context of derivation of the $K - \bar{\epsilon}$ model for the description of the large-scale features of turbulent flows. One consequence of the anomalous scaling of K and ϵ may play an important part in developement of turbulence theory: the only dimensionless coupling constant, based on the Kolmogorov scaling, is local Reynolds number $Re = \frac{v_r r}{\nu(r)} \approx \left(\frac{\bar{\epsilon} r^4}{\nu^3(r)}\right)^{\frac{1}{2}} = O(1)$. The non-trivial scaling, derived in this work, leads to appearence of new dimensionless parameters $Re_K \approx \frac{K_r r^2}{\nu^2(r)} \approx Re^0 (\frac{r}{L})^{-\frac{1}{3}} \to 0$ and $\mathrm{Re}_\epsilon = \frac{\epsilon_r r^4}{\nu^3(r)} \to 0$ in the infra-red limit $r \to \infty$. The role of these small parameters in the high-order contributions to the renormalized perturbation expansion is under investigation.

The expression (14) leads to the the relation between the shape of the energy spectrum in turbulent flows and the small-scale intermittency exponent μ. Let $E(k) \propto k^{1-\frac{2\gamma}{3}}$, so that: $u_{rms} \propto r^{\frac{\gamma}{3}-1}$. This relation tells us that $\gamma = 3$ is a crossover value of parameter γ: the small scale intermittency exist for $\gamma > 3$ and the intermittency exponent $\mu = \frac{\gamma}{3} - 1$ reaches value $\mu = 1/3$ on the Kolmogorov spectrum ($\gamma = 4$). It is interesting that at $\gamma > 3$, the kinetic energy of the flow is dominated by the large-scale dynamics, while when $\gamma < 3$ the main contribution to turbulent energy comes from small scales. This result stresses the dominant role of the large-scale dynamics in the intermittency of the dissipation rate fluctuations.

It clear that the dissipation rate ϵ is a strongly fluctuating operator. Then, the natural question to ask is: How can the Kolmogorov law be even approximately correct? A possible

answer can be found in the fact that $\bar{\epsilon} = \overline{P} = \overline{f_i v_i}$ where $\overline{P}$ is the mean rate of the energy injection which is equal to the mean energy flux in the wave-number space. The operator P describes the large-scale property of the system which fluctuates much less than the small-scale dominated dissipation rate ϵ. It can be seen from the derivation of relation (3) that it is the energy flux and not the dissipation rate that enters the relation for the third-order structure function. This may by the reason why the Kolmogorov law can be correct despite very strong fluctuations of the dissipation rate.

The method presented in this work can be directly applied to the equation for a passive scalar T, advected by turbulent velocity field. In this case cancellation of u.v. divergences in the scallar dissipation rate equation should lead to the following correlation functions: $\overline{\Delta u(\Delta K_T)^2} = O(r)$ and $\overline{\Delta u(\Delta N_T)^2} = O(r^0)$ where $K_T = T^2$ and $N_T = (\nabla T)^2$. The power counting gives then $\Delta K_T \propto r^{\frac{1}{3}}$ and $\Delta N_T \propto r^{-\frac{1}{6}}$. These relations are invariant under Galileo transformations. It is interesting that the reported experimentally observed intermittency exponent for the fluctuations of the scalar dissipation rate is $\mu_T \approx 0.35$ which is extremely close to the prediction of this work: $\mu_T \approx 1/3$, provided the velocity field is characterized by the Kolmogorov spectrum.

Most stimulating discussions with V.Borue, M.Nelkin, R.H.Kraichnan, A.Polyakov, U. Frisch, M.Vergassola, S.Orszag, K.R.Sreenivasan, E.Jackson, L.Smith and I.Starosel'skii are gratefully aknowledged.

references

1. A.N.Kolmogorov, Dokl. Akad. Nauk SSSR 32, 19, (1941)

2. V.Yakhot, Phys.Rev.Lett.69, 769(1992)

3. A.S.Monin and A.M.Yaglom, Statistical Fluid Mechanics, V2, The MIT Press, Cambridge, 1975

4. V. Yakhot and L.M. Smith J.Scient.Comp.7, 35, (1992)

5. V.Borue and S.A.Orszag, Phys. Rev. Lett., submitted

6. V.Yakhot Phys.Rev.E, in press

Kolmogorov turbulence in a random-force-driven Burgers equation: anomalous scaling and probability density functions

Abstract

High-resolution numerical experiments, described in this work, show that velocity fluctuations governed by the one-dimensional Burgers equation driven by a white-in-time random noise with the spectrum $\overline{|f(k)|^2} \propto k^{-1}$ exhibit a biscaling behavior: All moments of velocity differences $S_{n\leq 3}(r) = \overline{|u(x+r)-u(x)|^n} \equiv \overline{|\Delta u|^n} \propto r^{n/3}$, while $S_{n>3}(r) \propto r^{\xi_n}$ with $\xi_n \approx 1$ for real $n > 0$ (Chekhlov and Yakhot, Phys. Rev. E **51**, R2739, 1995). The probability density function, which is dominated by coherent shocks in the interval $\Delta u < 0$, is $\mathcal{P}(\Delta u, r) \propto (\Delta u)^{-q}$ with $q \approx 4$. A phenomenological theory describing the experimental findings is presented.

Our recent study [1] of the one-dimensional Burgers equation

$$\frac{\partial u}{\partial t} + u\,\frac{\partial u}{\partial x} = f + \nu\,\frac{\partial^2 u}{\partial x^2} \tag{1}$$

driven by a white-in-time random force defined by the correlation function

$$\overline{f(k,t)f(k',t')} \propto D(k)\,\delta(k+k')\,\delta(t-t') \tag{2}$$

with $D(k) = \epsilon_0\,k^{-1}$ and $\epsilon_0 = O(1)$ was motivated by an interest in dynamical processes which involve an interplay between chaotic and coherent phenomena. It has been shown that the velocity field $u(x,t)$ consists of random-in-time and random-in-space fluctuations superimposed on the relatively strong and long-living shocks. Numerical simulations yielded the energy spectrum $E(k) \propto \overline{|u(k)|^2} \propto k^{-x}$ with $x = 5/3 \pm 0.02$, characteristic of Kolmogorov turbulence [2] and the Eulerian correlation function $C(k,\omega) = \overline{|u(k,\omega)|^2} \propto k^{-7/3}\,\Phi(\omega/k^z)$ with the dynamic exponent $z = 2/3$. This result shows that in this system the kinematic transport of the small-scale velocity fluctuations by the large-scale structures is very weak. Investigation of the velocity structure functions $S_n(r) = \overline{[u(x+r)-u(x)]^n} \equiv \overline{(\Delta u)^n}$ with integer n revealed strong deviations from the Kolmogorov picture of turbulence: all moments $S_{n>3}(r) \propto r^{\xi_n}$ with $\xi_n \approx 1$, characteristic of strong shocks. Thus, the system governed by (1) – (2) shows both "normal" (Kolmogorov) and anomalous scalings with the latter dominated by the coherent structures (shocks). In this work we are interested in the details of the probability density functions (PDF's) characterizing the fluctuations generated by (1) – (2) and in the role the structures play in the determination of the PDF's shape. The PDF $\mathcal{P}(\Delta u, r)$ is defined such that $\mathcal{P}(X,r)\,dX$ is the probability of finding a velocity difference $\Delta u = u(x+r) - u(x)$ within the interval $(X, X+dX)$ for infinitesimally small dX. A spectral code with 12288 Fourier modes was used in the numerical experiment. Equation (1) with a hyperviscous (instead of viscous) dissipation term was solved. The details of the numerical procedure are reported in [1].

The most prominent feature of Burgers equation is a tendency to create shocks and, consequently, to increase the negative velocity differences $\Delta u < 0$ and to decrease the positive ones $\Delta u > 0$ [3]. Thus, strong asymmetry of the curve $\mathcal{P}(\Delta u, r)$ is expected. The two-point PDF $\mathcal{P}(\Delta u, r)$ was measured for a set of separations r covering a variety of scales in

the system in the following way. The range of variation of the velocity difference, $-5 < \Delta u/u_{rms} < 5$, was divided into 10^4 bins. The data were collected during a time longer than 10 largest eddy turnover times (corresponding to $O(10^7)$ time-steps) and were distributed among the appropriate bins to generate a histogram. Fig. 1 presents $\mathcal{P}(\Delta u, r)$ for the inertial range separations $r/dx = 200, 250, 300, 350, 400$, where $dx = L/12288$ is the mesh size and $L = 2\pi$ is the system size. It follows from $(1) - (2)$ that: $\overline{(\Delta u)^3} \propto \epsilon_0 \, r \, log \; r k_d$ and that is why this PDF has a shifted maximum, approximately at $\phi = (\Delta u)/R^{1/3} \approx 0.5$. Here the function $R(r)$ defined as $R(r) \equiv \int \overline{[f(x+y) - f(x)]^2} \, dy$, was also directly measured. It is fully force-dependent and in a system with viscosity it may be analytically calculated for the inertial-range values of separation r, giving $R(r) \propto \overline{(\Delta u)^3} \propto \epsilon_0 \, r \, \log(r \, k_d)$, where $k_d \to +\infty$ is a dissipative cutoff wavenumber. Technically speaking, the system considered in this work does not have a real "inertial range" since the mean dissipation rate $\bar{\epsilon} = O(\epsilon_0 \, log(L \, k_d))$ depends on the ultra-violet cut-off k_d. This dependence, however, is weak and in what follows we take $k_d = O((\epsilon_0/\nu^3)^{1/4})$.

The tail of the PDF $\mathcal{P}(\Delta u, r)$ for $\Delta u < 0$ is shown on Fig. 2 for various magnitudes of the displacement r in the universal range. One may observe from this figure that the PDF for $\Delta u < 0$ may be well approximated as:

$$\mathcal{P}(\Delta u, r) \propto (\Delta u)^{-q}, \tag{3}$$

with $q \approx 4$. We have also found that $\mathcal{P}(\Delta u, r)$ for $\Delta u > 0$ is well fitted by the exponential:

$$\mathcal{P}(\Delta u, r) \propto e^{-\alpha \frac{(\Delta u)^3}{r}}, \tag{4}$$

with the constant α to be determined from the theory. The dynamic argument leading to (3) will be presented below. The results shown on Figs. 1, 2 are highly nontrivial because the observed algebraic decay of the PDF $\mathcal{P}(\Delta u, r)$ as $\Delta u/(\Delta u)_{rms} \to -\infty$ leads to the divergence of the moments $S_n(r)$ for $n > 3$ for the inviscid case. However, as we also observed, the single point PDF $\mathcal{P}(u)$ is a very rapidly decreasing function which is close to the Gaussian and that is why the occurrence of shocks with an amplitude $\Delta u > U_0 \approx (\bar{\epsilon} \, L \, log(L \, k_d))^{1/3}$ is highly improbable and one can expect the PDF $\mathcal{P}(\Delta u, r)$ to decrease sharply for $\Delta u < -U_0$. This is sufficient for the existence of all moments $S_n(r)$. A full analytical theory leading

to an expression for $\mathcal{P}(\Delta u, r)$, which unifies both asymptotics (3) and (4) will be published elsewhere [4].

To develop a phenomenological theory we assume that the flow can be represented as a superposition of coherent and random components. The coherent contribution is visualized as a "gas of shocks" and a single structure (shock) can be approximated by the exact tanh-solution of the unforced problem [3]. In particular, let us assume that solution for the normal (not the hyper-) viscosity case has the form

$$u(x,t) = -\sum_{i=0}^{N} U_i \tanh\left[\frac{(x-a_i)\,U_i}{2\nu}\right] + \phi(x,t). \tag{5}$$

The first contribution to the right side of (5) describes the slowly varying coherent "gas of shocks", whereas the second represents the effects unaccounted for by the first term. Here a_i and U_i denote the coordinates of the centers of the shocks and the shock amplitudes respectively. The physical picture behind this representation is the following: the forcing produces the low energy excitations which coagulate into ever stronger well separated shocks due to the non-linear interactions. It will be clear below that the detailed shape of the shock assumed in (5) is unimportant. The most essential feature of the tanh-solution (5) is that the shock width $l_i \approx \nu/U_i$, which means that the stronger the shock, the more narrow it is.

Statistics of the dissipation rate fluctuations were investigated in detail in Ref. 1. It has been shown that the energy dissipation takes place mainly ($\approx 99\%$) inside the well separated strong shocks. Thus, it follows from (5) that the dissipation rate in interval of length r is

$$\epsilon_r = \frac{1}{4\,r\,\nu}\int_{x=0}^{r} dx \sum_{i,j=0}^{N} \frac{U_i^2\,U_j^2}{\cosh^2 Y_i \cosh^2 Y_j}, \tag{6}$$

where we denote $Y_i = (x-a_i)\,U_i/(2\nu)$. The principle contribution to the sum comes from the strong and narrow shocks, and, therefore, we can neglect the nondiagonal terms with $i \neq j$. Taking the integral for inertial-range values of r we have

$$\epsilon_r \propto \sum_{i=0}^{N} \frac{U_i^3}{r} \approx \frac{\overline{U^3}}{r}. \tag{7}$$

On the other hand, it can be directly shown from (1) – (2) that

$$\epsilon_r = \epsilon_0\, ln\left(\frac{L\,U_0}{\nu}\right). \tag{8}$$

Introducing the PDF $\mathcal{P}(U,r)$ to find a shock with amplitude U in the interval of the length r we obtain from the last two relations

$$\int_{\frac{\nu}{L}}^{U_0} U^3\,\mathcal{P}(U,r)\,dU \propto \epsilon_0 r\, ln\left(\frac{L\,U_0}{\nu}\right), \tag{9}$$

from which we readily establish the form of $\mathcal{P}(U,r)$

$$\mathcal{P}(U,r) \propto \frac{\epsilon_0\, r}{U^4}. \tag{10}$$

Since $\mathcal{P}(U,r) = \mathcal{P}(U)\,r/L$, the relation (10) establishes the shape of PDF $\mathcal{P}(U) \propto U^{-4}$ to find a shock of the amplitude U. Note that r/L is the probability to find a shock center within the interval of the length r which is in turn placed in the larger interval of the length L. The low integration limit $U \approx \nu/L$, corresponds to the amplitude of the "weakest structure", contributing to ϵ_r. Formula (10) is a consequence of relations (7) and (8), and is valid in the logarithmic case when the forcing function is defined by (2). It is only in this case that we can establish the form of the PDF.

Thus, according to the data presented in Fig. 1 and the theoretical considerations developed above, the PDF of velocity differences can be represented as:

$$\mathcal{P}(\Delta u,r) = a\,R^{-\frac{1}{3}}\,F(\frac{\Delta u}{R^{\frac{1}{3}}}) \tag{11}$$

in the interval $O(-1) < x \equiv \Delta u/R^{1/3} < \infty$, where function $R(r)$ is defined above, a is a numerical constant and $F(x)$ is a scaling function (see, [5]) which is assumed to go rapidly to zero when $|x|$ is large. In the interval $x \ll -1$, and $|\Delta u| < O(U_0)$, where the PDF is dominated by the well-separated shocks, we have:

$$\mathcal{P}(\Delta u,r) = b\,\frac{\epsilon_0\, r}{(\Delta u)^4}, \tag{12}$$

where b is a constant. When $\Delta u \ll -U_0$, the PDF is a rapidly decreasing function of $\Delta u/U_0$. The moments of velocity difference are evaluated readily with the result:

$$S_n(r) = \int (\Delta u)^n\,\mathcal{P}(\Delta u,r)\,d\Delta u = b_n\,r\,\epsilon_0\,\frac{U_0^{n-3} - (\epsilon_0 R)^{\frac{n}{3}-1}}{n-3} + B_n(\epsilon_0\,R)^{\frac{n}{3}}, \tag{13}$$

where the amplitudes B_n depend on the shape of the scaling function $F(x)$. The constants $b_n \propto (-1)^n$ for integer n and for the noninteger values of n the structure functions $S_n = \overline{|\Delta u|^n}$

so that relation (13) should include the absolute value of the first term in the right side. It follows from (11) – (13) that all moments $S_n(r)$ with $n > 3$ are completely determined by the upper cut-off in (13)

$$S_n(r) \propto \epsilon_0 r \frac{U_0^{n-3}}{n-3}, \tag{14}$$

which is in excellent quantitative agreement with [1], whereas for $0 \leq n \leq 3$:

$$S_n(r) \propto (\epsilon_0 R)^{\frac{n}{3}}, \tag{15}$$

as in the Kolmogorov theory of turbulence [2]. Thus, the anomalous scaling of the velocity structure functions $S_n(r)$ appears only for $n > 3$. It should be stressed that, in accord with (13), in the logarithmic case considered in this work the contribution from the shocks to the moments $S_{n<3}$ is smaller than the one from the scaling component of the PDF only by factor $1/\log(r\, k_d)$ which makes the experimental investigation of the details of the crossover very difficult.

The prediction (13) has been tested in [1]. It has been shown that $S_{2n}(r) \propto r^{\xi_{2n}}$ with $\xi_{2n} \approx 0.91$ for $n > 2$, indicating that these correlation functions are dominated by coherent shocks. The results of the measurements of the structure functions $S_n(r)$ with $n = 1/3, 2/3, \ldots, 6/3$, presented on Fig. 3, are in good agreement with the scaling law (15). The general structure of the moments of velocity differences given by expression (13)–(15) is similar to the outcome of the recent theories of the random- force- driven Burgers equation by Polyakov [4] (1d) and Bouchaud [5] ($d \to \infty$) cases. The Polyakov theory confirmed our qualitative argument leading to the algebraic decrease of the PDF in the interval $\Delta u < 0$.

Fig. 4 presents the PDF of the shock amplitudes. The problem of the shock location was solved in the following simple but reliable way. At each spatial point x the local gradient of the solution $u(x)$ was measured. Then, if $u'(x) \geq 0$, it was assumed that this point x is outside of a shock, otherwise x lies inside of a shock. Once inside a shock, one can march in x until the gradient becomes zero, and thus the boundaries of the shock may be located, and so forth. Note that the shock amplitude obtained in this way has been corrected to exclude the Gibbs phenomenon typical in spectral approximations of discontinuous functions. To reduce

the statistical noise in $\mathcal{P}(U)$ in Fig. 4, a simple smoothing procedure was applied: $\mathcal{P}(U)$ was averaged over eight surrounding points. The result presented in Fig. 4 demonstrates that

$$\mathcal{P}(U) \propto U^{-4} \tag{16}$$

is observed for all $|U/U_{rms}| > 0.5$. The fact that $\mathcal{P}(\Delta u) \approx \mathcal{P}(U)$ when $\Delta u < 0$ tells us that in this range $\mathcal{P}(\Delta u)$ is dominated by the well-separated shocks. This confirms the main assumption of the phenomenological theory presented above. It follows from Figs. $1-4$ and relation (12) that the anomaly in the high-order moments results only from the slow (algebraic) decrease of the PDF in the interval $\Delta u < 0$. As was pointed out above, in this case one expects a cut-off at some $\Delta u \approx U_0$.

We have also investigated the problem (1), (2) driven by the white-in-time random forces with $D(k) \neq 0$ only for $k < 5$ and $D(k) \propto k^{-3/2}$ [6]. The outcome of the simulations in both cases revealed the algebraically decreasing $\mathcal{P}(\Delta u, r) \propto r/|\Delta u|^q$ for $\Delta u/(\Delta u)_{rms} \ll -1$, with the exponent q, related to the functional form of $D(k)$. The former case of the large-scale driven Burgers equation was investigated in a recent paper by Bouchaud et. al. [5] using a replica tric in the limit of the space dimensionality $d \to \infty$. Although the scaling of the moments of velocity differences, obtained in Ref. 5 is the same as the one observed in our simulations, the shape of the PDF in the 1d-case, numerically found by us, differs dramatically from $\mathcal{P}(\Delta u, r) = (1-r)\,\delta(\Delta u - r) + \beta\, r\, F(\Delta u/U_0)$, derived in Ref. 5. Here $F(x)$ is a scaling function and β is a number. This means that the physical mechanisms, responsible for the anomalous scaling in the one and multi-dimensional systems are different and understanding of the transition between the two behaviors is an extremely interesting challenge. The detailed theoretical and numerical investigations of the different cases of forcing functions will be published elsewhere [6].

References

[1] A. Chekhlov and V. Yakhot, Phys. Rev. E, **51**, R2739 (1995).

[2] A. Kolmogoroff, C. R. (Doklady) de l'Acad. des Sci. de l'URSS, **30**, 301 (1941); *ibid* **32**, 16 (1941).

[3] J. M. Burgers, *The Nonlinear Diffusion Equation. Asymptotic Solutions and Statistical Problems.* (Reidel, Dordrecht, 1974); J. Krug and H. Spohn, in *Solids Far From Equilibrium: Growth, Morphology and Defects*, edited by C. Godriche (Cambridge University Press, Cambridge, England, 1992).

[4] A. Polyakov, unpublished (1995).

[5] J. P. Bouchaud, M. Mézard, and G. Parisi, Phys. Rev. E, in press (1995).

[6] V. Yakhot and A. Chekhlov, unpublished (1995).

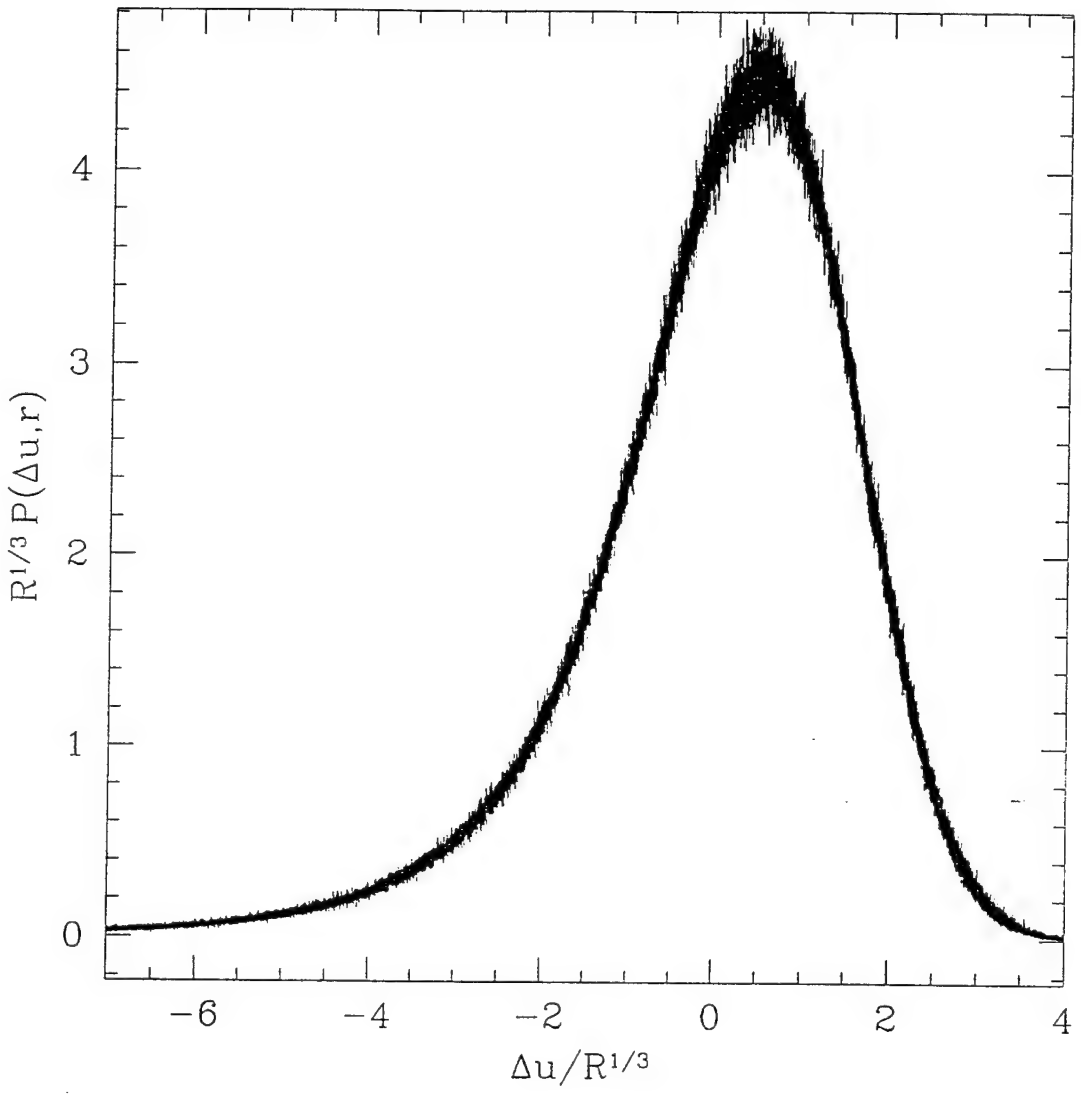

Figure 1: Normalized two-point PDF $F(\Delta u/R^{1/3}) = R^{1/3}\,\mathcal{P}(\Delta u, r)$ for separations $r/dx =$ 200, 250, 300, 350, 400 within the universal range. The collapse of various curves supports the choice of the scaling variable $\phi = (\Delta u)/R^{1/3}$, where function $R(r)$ is defined in the text.

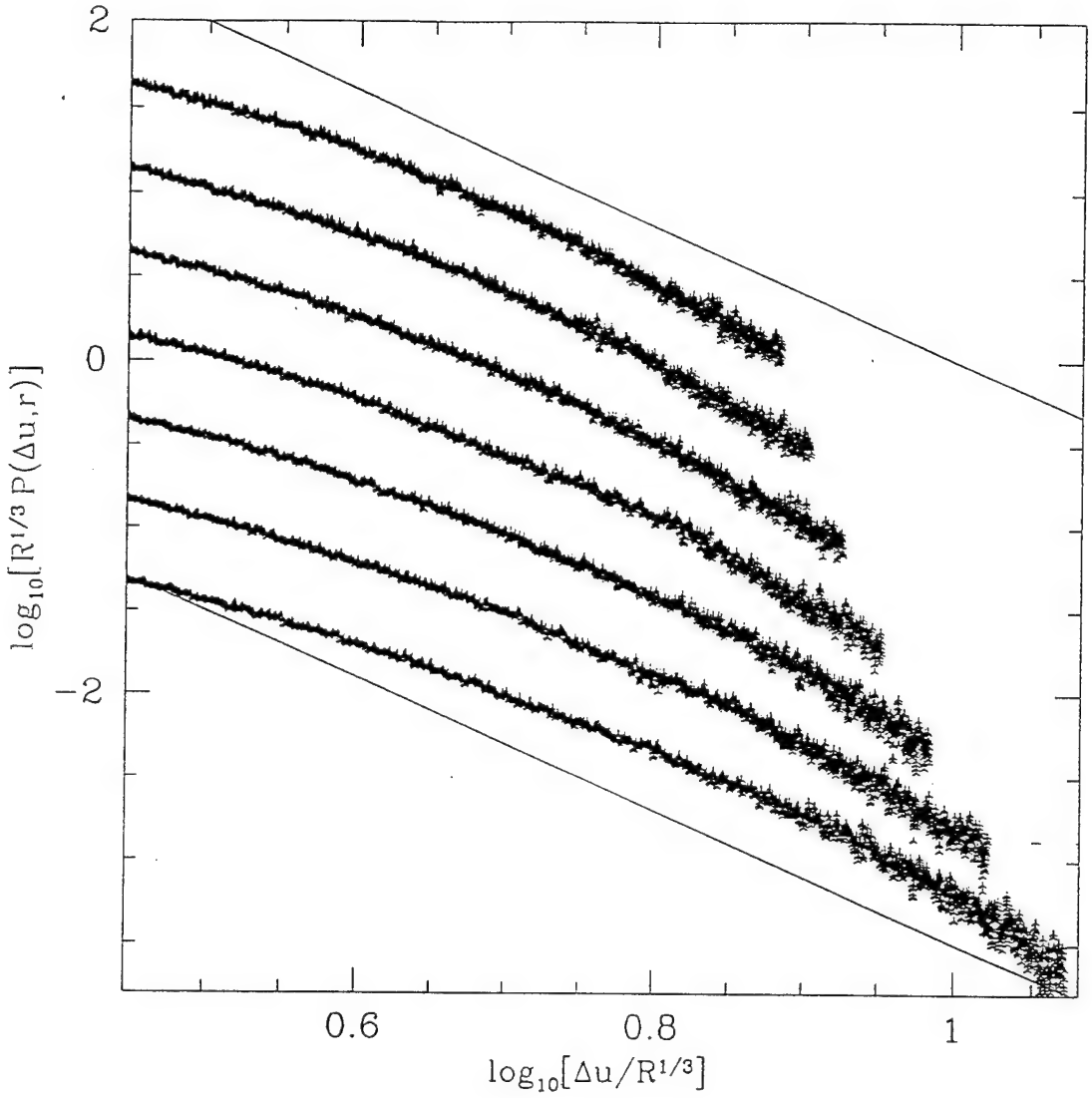

Figure 2: The tail of the two-point PDF $\mathcal{P}(\Delta u, r)$ (points) for separations $r/dx = 150, 200, 250, 300, 350, 400, 450$ within the universal range, plotted on a logarithmic-logarithmic scale. The slope of the solid lines is equal to -4. The graphs for different values of r are arbitrarily shifted along the vertical axis for clarity.

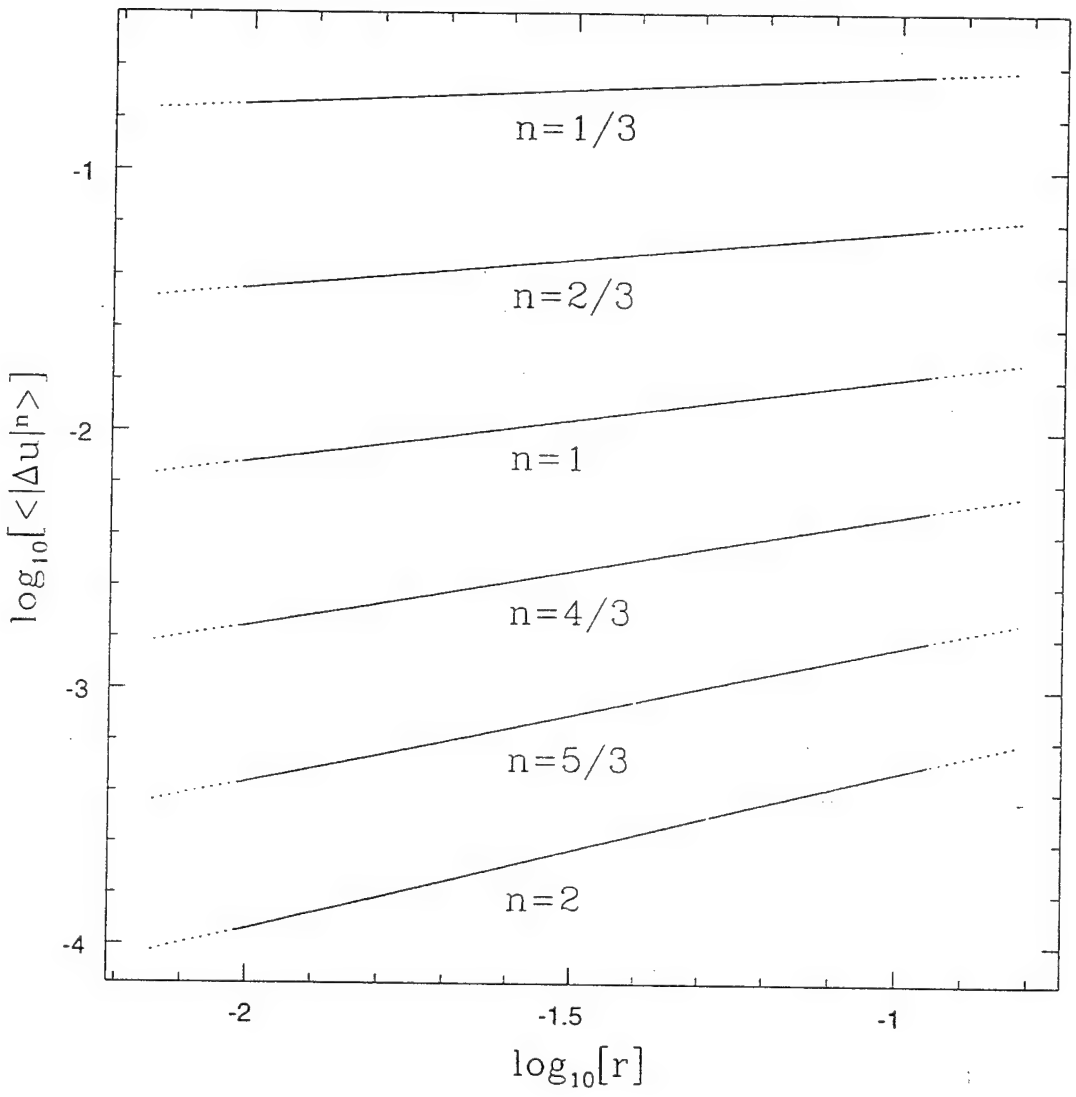

Figure 3: Velocity structure functions $\overline{|\Delta u|^n}$ for noninteger values $n = 1/3, 2/3, \ldots, 6/3$ (dotted curves). Slopes of the linear least square fits (solid lines) from top to bottom respectively are: 0.111, 0.222, 0.330, 0.433, 0.531, 0.620.

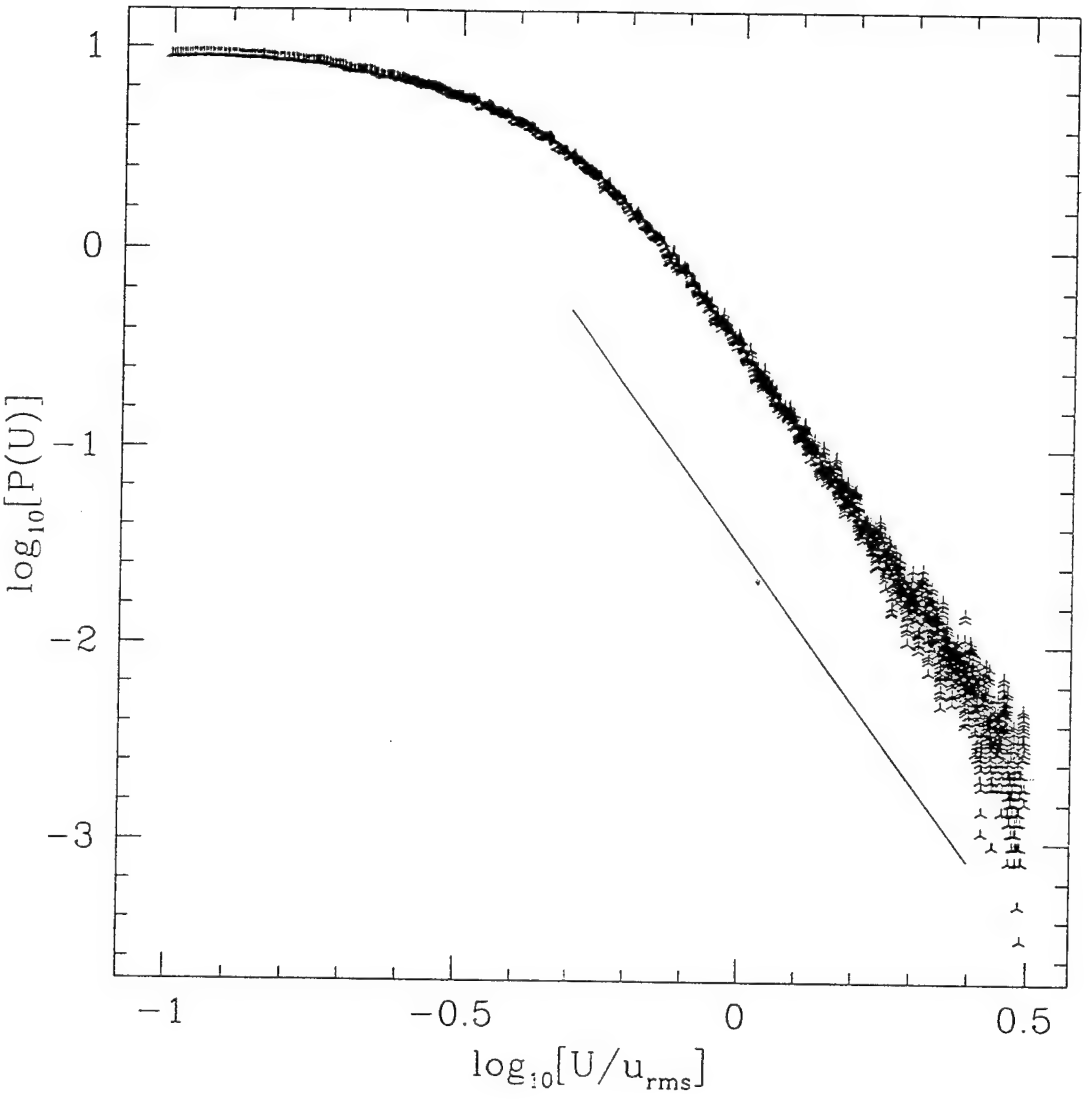

Figure 4: PDF of shock amplitudes, $\mathcal{P}(U)$ on a logarithmic-logarithmic scale (points). The slope of the solid line is equal to -4.

Kolmogorov's refined similarity hypothesis for hyperviscous turbulence

Abstract

Kolmogorov's refined similarity hypothesis (RSH) is tested in high resolution numerical simulations of forced three-dimensional homogeneous turbulence. High Reynolds numbers are achieved by using hyperviscous dissipation $(-1)^{h+1}\Delta^h$ $(h = 8)$ instead of Newtonian $(h = 1)$ dissipation. It is found that, in the inertial range, RSH is reasonably well satisfied for low order moments with noticeable systematic corrections for higher order moments. Within the constraints imposed by the use of hyperviscosity our data nearly eliminate trivial kinematic dependencies between longitudinal velocity differences and the energy dissipation rate thus helping to reveal the true dynamical nature of the RSH.

One of the most interesting properties of fully developed turbulence is small scale intermittency which manifests itself through the scale dependence of the probability distribution function (PDF) $\mathcal{P}(\Delta u_r/r^{1/3})$ of longitudinal velocity differences ($\Delta u_r = (u_i(x+r) - u_i(x))r_i/r$). In order to take account of this intermittent behavior, Kolmogorov [1] introduced the refined similarity hypothesis (RSH) which relates velocity differences Δu_r and the locally-averaged energy dissipation rate

$$\mathcal{E}_r(x) = \int F_r(\mathbf{x}-\mathbf{y})\mathcal{E}(\mathbf{y})d^3y \tag{1}$$

where $\mathcal{E}(\mathbf{y})$ is the local energy dissipation rate and F_r is a low-pass spatial filter with scale r and normalized, $\int F_r(x)d^3x = 1$. The RSH states that the joint one-point PDF of Δu_r and $\mathcal{E}_r$ has the form

$$\mathcal{P}(\Delta u_r, \mathcal{E}_r) = \mathcal{P}_v(V_r \equiv \frac{\Delta u_r}{r^{1/3}\mathcal{E}_r^{1/3}})\mathcal{P}_\mathcal{E}(\mathcal{E}_r) \tag{2}$$

and that, in the inertial range, the PDF $\mathcal{P}_v(V_r)$ is independent of scale and Reynolds number. RSH is the basis of nearly all existing cascade models of turbulence (see, e.g. [2]).

Recently, RSH was independently checked experimentally by four groups [3-6] all concluding that, on the level of the first conditional moment, RSH has solid experimental support, i.e. the conditional average of $\langle |V_r| \, | \mathcal{E}_r \rangle$ is relatively independent of $\mathcal{E}_r$. In all these works, a one-dimensional surrogate of real dissipation was used and local averaging of $\mathcal{E}$ was understood as one-dimensional averages. It was suggested in [7] that at least part of observed correlations between Δu_r and $\mathcal{E}_r$ come from the measurement procedures that emphasize the kinematic dependence between these two quantities. Thoroddsen [8] attempts to verify the RSH by eliminating kinematic dependencies by using pseudo-dissipation defined via the transverse velocity component. It was suggested in [8] that with this definition of the dissipation rate the validity of RSH is questionable. Existing numerical simulations [9], [10] give only partial support of RSH, but unfortunately employed many of the same simplifications to calculate $\mathcal{E}_r$ as used in experiments (with either the one-dimensional pseudo-dissipation $15\nu(\partial u/\partial x)^2$ or anisotropic one-dimensional local-averaging being used). Recent numerical simulations [11] aimed to eliminate kinematic factors but give only weak support of RSH.

In this work, we present evidence supporting RSH at least at the level of low order moments that is free from the kinematic constraints discussed above. In previous works [12], [13], [14] we have already demonstrated that for the same numerical resolution, we can effectively increase the extent of the inertial range of three-dimensional turbulence by an order of magnitude by using alternative forms of dissipation. Some evidence was given that three-dimensional inertial-range dynamics is relatively independent of the form of the hyperviscosity, although it may depend on the nature of the force. In this Rapid Communication, we address the problem of validation of RSH.

The hyperviscosity-modified Navier-Stokes equations are:

$$\partial_t u_i + u_j \partial_j u_i = -\partial_i p + (-1)^{h+1} \nu_h \Delta^h u_i + f_i \tag{3}$$

where the pressure p is calculated from the incompressibility condition $\partial_i u_i = 0$. We include a white-in-time Gaussian force which is nonzero only at some characteristic scale $k_f = 1$ and a hyperviscosity dissipation (as in [12] we use $h = 8$). The various characteristics of the statistically stationary state in this case can be found in [12]. We solve (3) using a pseudospectral parallel code and perform two series of runs with resolutions $(N = 128)^3$ and 256^3 for a periodic box with size $L = 2\pi$ in each direction. The total averaging times are 200 and 30 in units $\tau_0 \approx 1/v_{rms}$, respectively. The Reynolds number [12] is $R_\lambda \approx 50(k_d/k_f)^{2/3}$, where k_d is the wave-number where $k^2 E(k)$ is maximum ($k_d \approx 41, 82$ for 128^3 and 256^3). The hyperviscous energy dissipation rate is

$$\mathcal{E} = \nu_h \Delta^{h/2} u_i \Delta^{h/2} u_i \tag{4}$$

The local space-average in (1) is performed as a convolution in Fourier space by using an isotropic three-dimensional top-hat filter $F_r(\mathbf{k}) = 3(\sin\xi - \xi\cos\xi)/\xi^3$ with $\xi = r|\mathbf{k}|/2$. This filter exactly corresponds to the definition of local space-averaging used by Kolmogorov [1]. The midpoint of the velocity difference Δu_r coincides with the center of the spherical averaging cell of radius $r/2$. The definition of dissipation (4) and this measurement procedure nearly eliminate the possible kinematic dependencies discussed above. The measurements

are carried out for $r = \pi/k_c$ with $k_c = 4, 8, ...N/8$ which correspond to scales inside of the inertial range [12].

In Fig. 1 we plot the joint probability distribution functions $\mathcal{P}_{\rm u}(\Delta u_r/r^{1/3}, \mathcal{E}_r^{1/3})\ (a,b)$ and $\mathcal{P}_{\rm v}(V_r, \log_{10}\mathcal{E}_r)\ (c,d)$ for two spatial resolutions and filter sizes: $k_d = 41, 82$ and $k_c = 4, 32$. While isocontours of $\mathcal{P}_{\rm u}$ indicate a noticeable dependence between velocity differences and the dissipation rate, isocontours of $\mathcal{P}_{\rm v}$ show that V_r and $\log_{10}\mathcal{E}_r$ are nearly statistically independent in accordance with the RSH. To quantify this we calculate conditional moments of V_r conditioned on $\mathcal{E}_r$. Various moments are plotted in Fig. 2 and 3 as functions of $(\log_{10}\mathcal{E}_r - \langle\log_{10}\mathcal{E}_r\rangle)/\sigma_r$ (σ_r^2 is the variance of $\log_{10}\mathcal{E}_r$). The curves for different r and k_d nearly collapse using the above scaling. These figures show that the conditional moments of V_r are only weakly dependent on $\log_{10}\mathcal{E}_r$ and the RSH in the form (2) is approximately satisfied. The conditional mean $\langle V_r\,|\mathcal{E}_r\rangle$ is nearly equal to zero in contrast with the results of [6]. The conditional variance $\langle V_r^2\,|\mathcal{E}_r\rangle \approx 2.2$, close to the results of [3] and [10]. The conditional flatness (Fig. 2(b)) and conditional sixth order moments (Fig. 2(c)) are only weakly dependent on $\log_{10}\mathcal{E}_r$ and are close to Gaussian values (3 and 15, respectively) in agreement with [3], [6], [10]. The first and third conditional moments of $|V_r|$ normalized by conditional variances (Fig. 3(a,b)) are spectacularly independent of $\log_{10}\mathcal{E}_r$ (partially due to the normalization by $\langle V_r^2\,|\mathcal{E}_r\rangle$). The conditional skewness (Fig. 3(c)) has a substantially stronger dependence on $\log_{10}\mathcal{E}_r$. Also in accordance with Kolmogorov's 4/5 law [3] $\langle V_r^3\rangle$ is nearly equal to $-4/5$.

In Fig. 4(a,b) we plot the PDFs of $\log_{10}\mathcal{E}_r$ as a function of $(\log_{10}\mathcal{E}_r - \langle\log_{10}\mathcal{E}_r\rangle)/\sigma_r$, superimposed for different r and Reynolds numbers. All curves nearly collapse in the core region with the variance $\tilde{\sigma}_r^2$ of $ln\mathcal{E}_r$ proportional to $-\mu\ln(r)$ (here $\mu \approx 0.15$ is called the intermittency exponent). The PDFs of $\log_{10}\mathcal{E}_r$ are quite close to Gaussian. With our data set it is possible to obtain moments $\langle\mathcal{E}_r^n\rangle$ in the range $-2 \le n \le 4.5$ and within this range the PDF of $\mathcal{E}_r$ may be considered log-normal. If the flatness and sixth moments of Δu_r grow when r decreases the corresponding quantities for V_r grow more slowly and may even slightly decrease when R_λ increases (see Fig. 4 (c,d)). Note that according to RSH the

correlation coefficient ρ between $|\Delta u_r|$ and $\mathcal{E}_r^{1/3}$ should not be equal to one. Indeed from (2), $\rho = (1-A)^{1/2}/(B-A)^{1/2}$ with $A = \left\langle \mathcal{E}_r^{1/3} \right\rangle^2 / \langle \mathcal{E}_r^{2/3} \rangle$ and $B = \langle V_r^2 \rangle / \langle |V_r| \rangle^2$. From the data plotted in Fig. 3, 4, $A \approx 1 - \tilde{\sigma}_r^2/9$, $B \approx 1.56$ and $\rho \approx 0.45\tilde{\sigma}_r$. In accord with the RSH, the correlation coefficient ρ' between $|V_r|$ and $\log_{10} \mathcal{E}_r$ is close to zero (see Fig. 4(e)).

If the PDFs of $\log_{10} \mathcal{E}_r$ and V_r are close to Gaussian and RSH holds, isocontours of $\mathcal{P}_v$ will have the form of circles. That is not exactly so, as may be seen from Fig. 1. Our data not only allows us to validate RSH on the level of lower order moments, but also reveals systematic corrections to RSH. Indeed according to the results plotted in Fig. 2 (c) $\langle V_r^6 \, | \mathcal{E}_r \rangle \propto a(1 - b \ln \mathcal{E}_r / \tilde{\sigma}_r)$ where $a \approx 160$ and $b \approx 1/15$. That leads to systematic corrections to $\langle \Delta u_r^6 \rangle \propto r^2 \langle \mathcal{E}_r^\alpha \rangle$ with $\alpha \approx 2 - b/\tilde{\sigma}_r$ and RSH is strictly speaking violated. The situation is even worse for higher order moments. We do not know whether these systematic corrections to higher order moments are universal and/or hyperviscosity independent.

One may expect that RSH should not only be applicable to velocity differences, but to other inertial range quantities as well. To illustrate this idea we measure the joint probability distribution of subgrid-scale kinetic energy $\mathcal{K}_r$ and $\mathcal{E}_r$. We define $\mathcal{K}_r$ as $\mathcal{K}_r = (u_i u_i)_r - (u_i)_r (u_i)_r$ with the same local-averaging procedure as in (1) and with the same top-hat filter F_r. We have checked that our results are relatively independent on the form of filter. According to RSH we may expect that

$$\mathcal{P}(\mathcal{K}_r, \mathcal{E}_r) = \mathcal{P}_\mathcal{K}\left(\frac{\mathcal{K}_r}{r^{2/3}\mathcal{E}_r^{2/3}}\right)\mathcal{P}_\mathcal{E}(\mathcal{E}_r) \tag{5}$$

In Fig. 5(a) we plot $\mathcal{P}(\ln \mathcal{K}_r, \ln \mathcal{E}_r)$ for $k_c = 16$ and $k_d = 41$. A strong correlation between $\mathcal{K}_r$ and $\mathcal{E}_r$ is observed. It turns out that the probability distribution of $\mathcal{K}_r$ is also approximatly log-normal with $\overline{\sigma}_r$, the variance of $\ln \mathcal{K}_r$, nearly equal to $\tilde{\sigma}_r$, the variance of $\ln \mathcal{E}_r$ independently of k_c and k_d. Therefore, if RSH in the form (5) is correct the isocontours of $\mathcal{P}(\ln(\mathcal{K}_r/\mathcal{E}_r^{2/3}), \ln \mathcal{E}_r)$ should have the form of circles. That this is indeed nearly so can be seen from Fig. 5(b).

For further analysis it is convenient to introduce the variables $\xi = (\ln \mathcal{E}_r - \langle \ln \mathcal{E}_r \rangle)/\tilde{\sigma}_r$ and $\eta = (\ln \mathcal{K}_r - \langle \ln \mathcal{K}_r \rangle)/\overline{\sigma}_r$ with $\overline{\sigma}_r \approx \tilde{\sigma}_r$. We verified that, in these variables, the joint

PDF of $\mathcal{K}_r$ and $\mathcal{E}_r$ in the inertial range has the simple approximate form

$$\mathcal{P}(\mathcal{K}_r, \mathcal{E}_r) \propto \exp\left[-\frac{\xi^2+\eta^2}{2(1-c^2)} + \frac{c\xi\eta}{(1-c^2)}\right] \tag{6}$$

independently of k_c and k_d. Here $\langle\xi^2\rangle = \langle\eta^2\rangle = 1$ and $c = \langle\xi\eta\rangle$ is the correlation coefficient. It is clear from (6) that ξ and $\eta - c\xi$ or equivalently $\mathcal{K}_r/\mathcal{E}_r^c$ and $\mathcal{E}_r$ are independent variables. The RSH in the form (5) holds provided $c = 2/3$; this turns out to be approximately true according to our data. It follows from (6) that the conditional averages $\langle\eta|\xi\rangle = c\xi$ and $\langle\xi|\eta\rangle = c\eta$. Using the fact that ξ and η are nearly Gaussian variables and that $\overline{\sigma}_r \approx \tilde{\sigma}_r$ we obtain

$$\langle\mathcal{K}_r|\mathcal{E}_r\rangle \propto \mathcal{E}_r^{2/3} \quad \text{and} \quad \langle\mathcal{E}_r|\mathcal{K}_r\rangle \propto \mathcal{K}_r^{2/3}. \tag{7}$$

The conditional averages $\langle\mathcal{K}_r|\mathcal{E}_r\rangle$ and $\langle\mathcal{E}_r|\mathcal{K}_r\rangle$ are plotted in Fig. 5c and Fig. 5d respectively. It may be seen that (7) is approximately satisfied independently of k_c and k_d (with the first expression in Eq. (7) that directly tests RSH valid with noticeably higher accuracy). The results (7) are in good agreement with recent experimental findings of Meneveau and O'Neil [15]. Thus, RSH for $\mathcal{K}_r$ is approximately valid in the form (5); it can not be inverted in the sense that $\langle\mathcal{E}_r|\mathcal{K}_r\rangle$ does not scale as $\mathcal{K}_r^{3/2}$.

We also checked that RSH holds for other inertial range quantities such as locally-averaged strain and vorticity that are defined as $(S_{ij})_r = [(\partial_i u_j + \partial_j u_i)/2]_r$ and $(\omega_i)_r = \varepsilon_{ijk}\partial_j(u_k)_r$. Here the same filtering procedure is assumed. Precisely, we verified that the joint PDF of $\mathcal{E}_r$ and $S_r^2 = (S_{ij})_r(S_{ij})_r$ has the form (5): $\mathcal{P}_S(S_r^2/\mathcal{E}_r^{2/3})\mathcal{P}_\mathcal{E}(\mathcal{E}_r)$. The same decomposition is true for the joint PDF of $\mathcal{E}_r$ and locally-averaged vorticity $\omega_r^2 = (\omega_i)_r(\omega_i)_r$: $\mathcal{P}_\omega(\omega_r^2/\mathcal{E}_r^{2/3})\mathcal{P}_\mathcal{E}(\mathcal{E}_r)$. As in the case of subgrid-scale kinetic energy, the RSH for large-scale strain and vorticity can not be inverted.

In conclusion, we find that in the inertial range, RSH in the form (2) is reasonably well satisfied for low order moments of velocity differences with noticeable systematic corrections for higher order moments. We have also shown that RSH is as well applicable to other inertial range quantities such as subgrid-scale kinetic energy, locally-averaged strain and

vorticity. Our use of hyperviscosity and an accurate averaging procedure allows us to nearly eliminate kinematic dependencies between velocity differences and the dissipation rate, thus helping to reveal the dynamical nature of RSH. On the other hand, our results also give more confidence in the hypothesis that inertial-range dynamics is relatively independent of the form of hyperviscosity.

REFERENCES

[1] A.N. Kolmogorov, J. Fluid Mech. **13**, 82 (1962).

[2] M. Nelkin, Advances in Physics, **43**, 143 (1994).

[3] G. Stolovitzky, P. Kaliasnath, K.R. Sreenivasan, Phys. Rev. Lett., **69**, 1178 (1992).

[4] A. Praskovsky, Phys. Fluids A**4**, 2589 (1992).

[5] S.T. Thoroddsen, C.W. Van Atta, Phys. Fluids A**4**, 2592 (1992).

[6] Y. Gagne, M. Marchand, B. Castaing, J. Phys. II France **4**, 1 (1994).

[7] G. Stolovitzky, K.R. Sreenivasan, Rev. Mod. Phys. **66**, 229 (1994).

[8] S.T. Thoroddsen, Phys. Fluids **7**, 691 (1995).

[9] S. Chen, G. Doolen, R. Kraichnan, Z.-S. She, Phys. Fluids A **5**, 458 (1993);

[10] L.-P. Wang, S. Chen, J. Brasseur, J. Wyngaard, J. Fluid Mech. to appear.

[11] S. Chen, G. Doolen, R. Kraichnan, L.-P. Wang, Phys. Rev. Lett. **74**, 1755 (1995).

[12] V. Borue, S. Orszag, Europhys. Lett. **29**, 687 (1995).

[13] V. Borue, S. Orszag, Phys. Rev. E **52**, R856 (1995).

[14] V. Borue, S. Orszag, J. Fluid. Mech. to appear.

[15] C. Meneveau, J. O'Neil, Phys. Rev. E **49**, 2866 (1994).

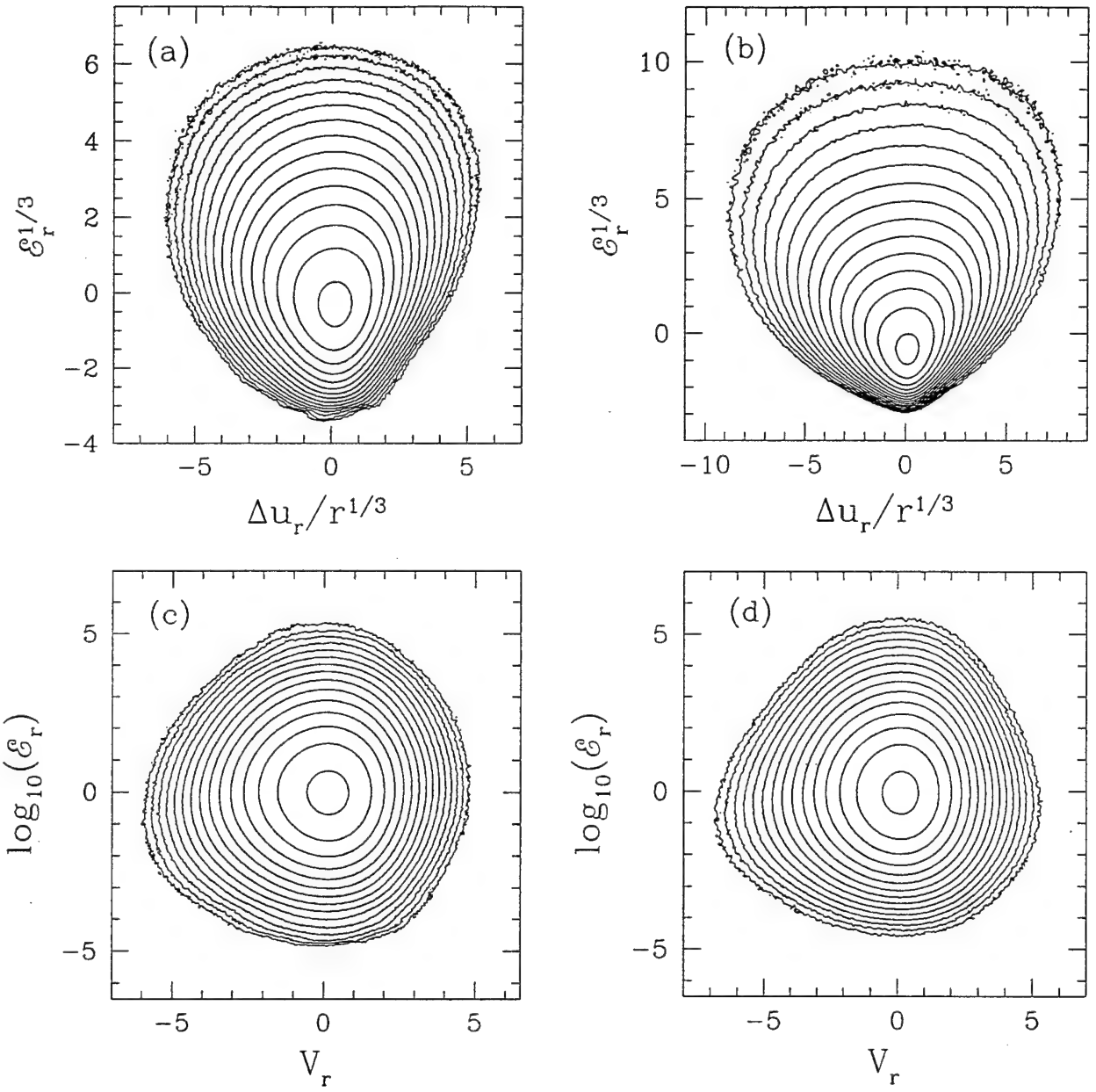

FIG. 1. Joint PDFs between (a,b) $\Delta u_r/r^{1/3}$ and $\mathcal{E}_r^{1/3}$; (c,d) V_r and $\log_{10}\mathcal{E}_r$. Means are subtracted and variables are normalized by their variances. (a,c) $k_c = 4$ and resolution 128^3. (b,d) $k_c = 32$ and resolution 256^3. The total number of points is $\approx 10^{10}$. Curves show isocontours of $\log_{10}\mathcal{P}$ in increments of 0.4.

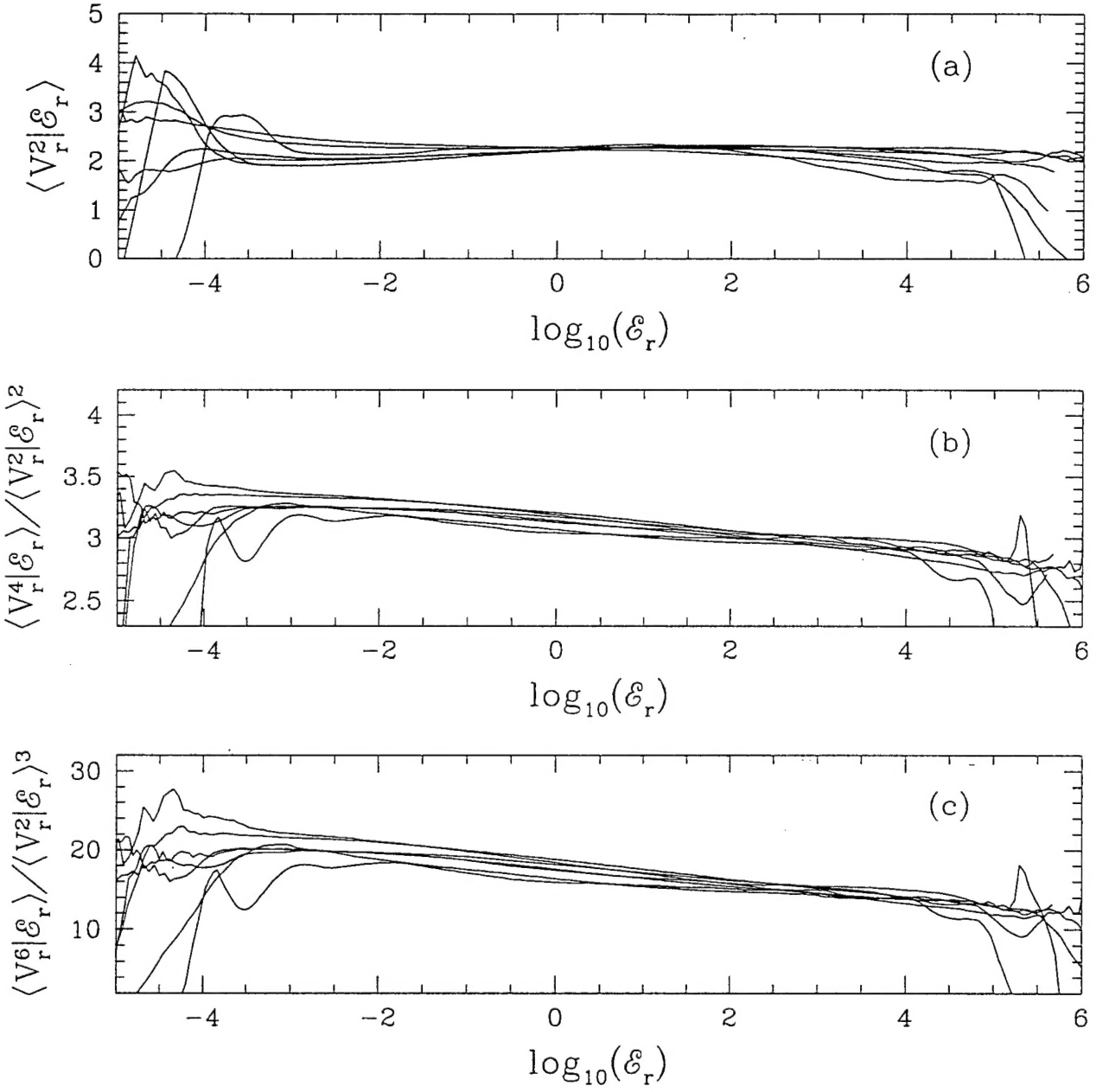

FIG. 2. (a) Conditional averages of $\langle V_r^2 \,|\mathcal{E}_r\rangle$; (b) conditional flatness $\langle V_r^4 \,|\mathcal{E}_r\rangle \,/\, \langle V_r^2 \,|\mathcal{E}_r\rangle^2$; (c) conditional sixth order moments $\langle V_r^6 \,|\mathcal{E}_r\rangle \,/\, \langle V_r^2 \,|\mathcal{E}_r\rangle^3$. Curves are obtained for 128^3 and 256^3 resolutions with $k_c = 4, 8, 16$ and $k_c = 4, 8, 16, 32$, respectively. All curves are superimposed with the dissipation rate plotted as $(\log_{10} \mathcal{E}_r - \langle \log_{10} \mathcal{E}_r \rangle)/\sigma_r$ (σ_r^2 is the variance of $\log_{10} \mathcal{E}_r$).

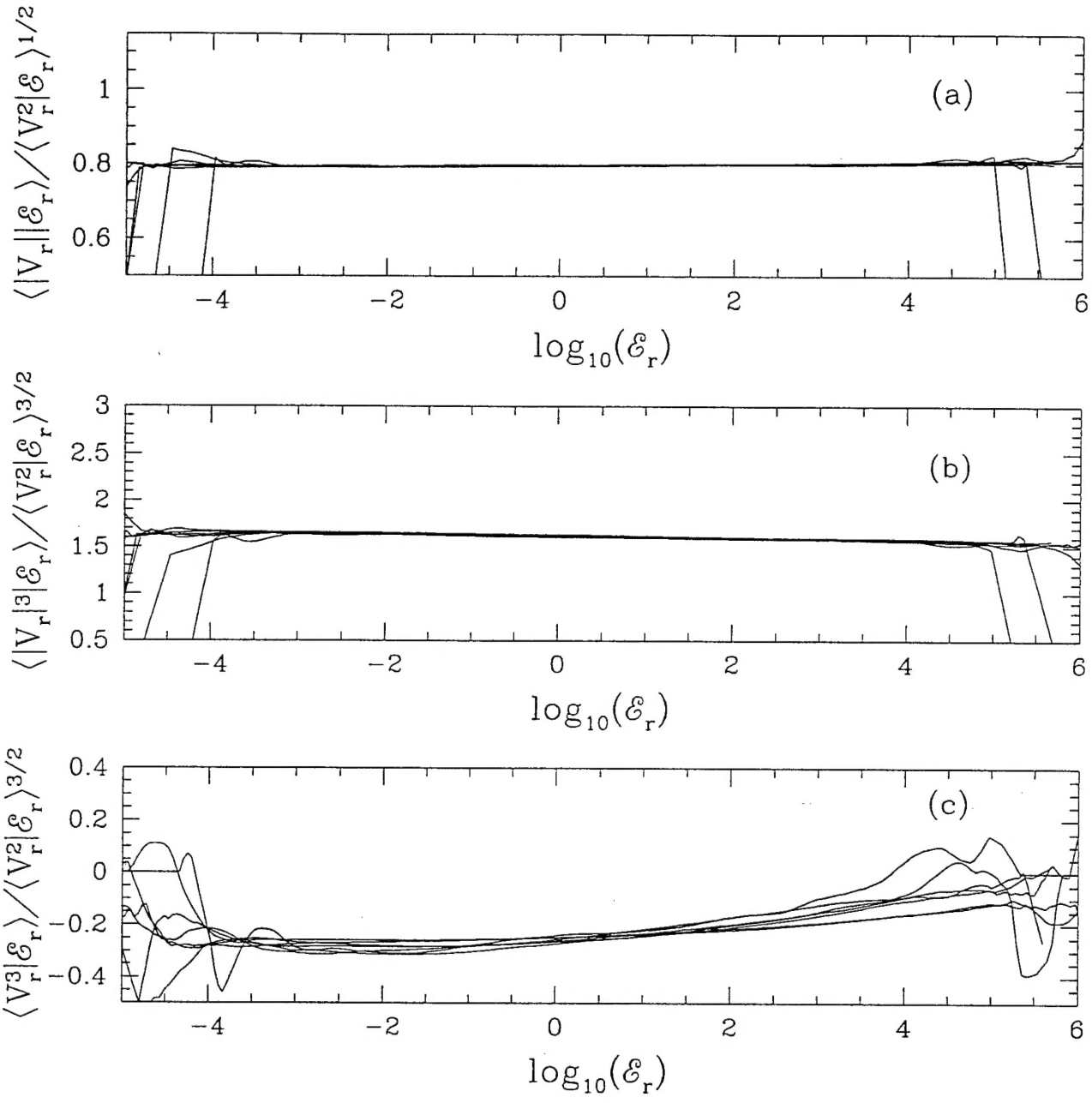

FIG. 3. (a) Conditional averages of $\langle |V_r|\,|\mathcal{E}_r\rangle\,/\,\langle V_r^2\,|\mathcal{E}_r\rangle^{1/2}$; (b) conditional third order moments $\langle |V_r|^3\,|\mathcal{E}_r\rangle\,/\,\langle V_r^2\,|\mathcal{E}_r\rangle^{3/2}$; (c) conditional skewness $\langle V_r^3\,|\mathcal{E}_r\rangle\,/\,\langle V_r^2\,|\mathcal{E}_r\rangle^{3/2}$. Curves are obtained for 128^3 and 256^3 resolutions with $k_c = 4, 8, 16$ and $k_c = 4, 8, 16, 32$, respectively. All curves are superimposed with the dissipation rate plotted as $(\log_{10}\mathcal{E}_r - \langle\log_{10}\mathcal{E}_r\rangle)/\sigma_r$ (σ_r^2 is the variance of $\log_{10}\mathcal{E}_r$).

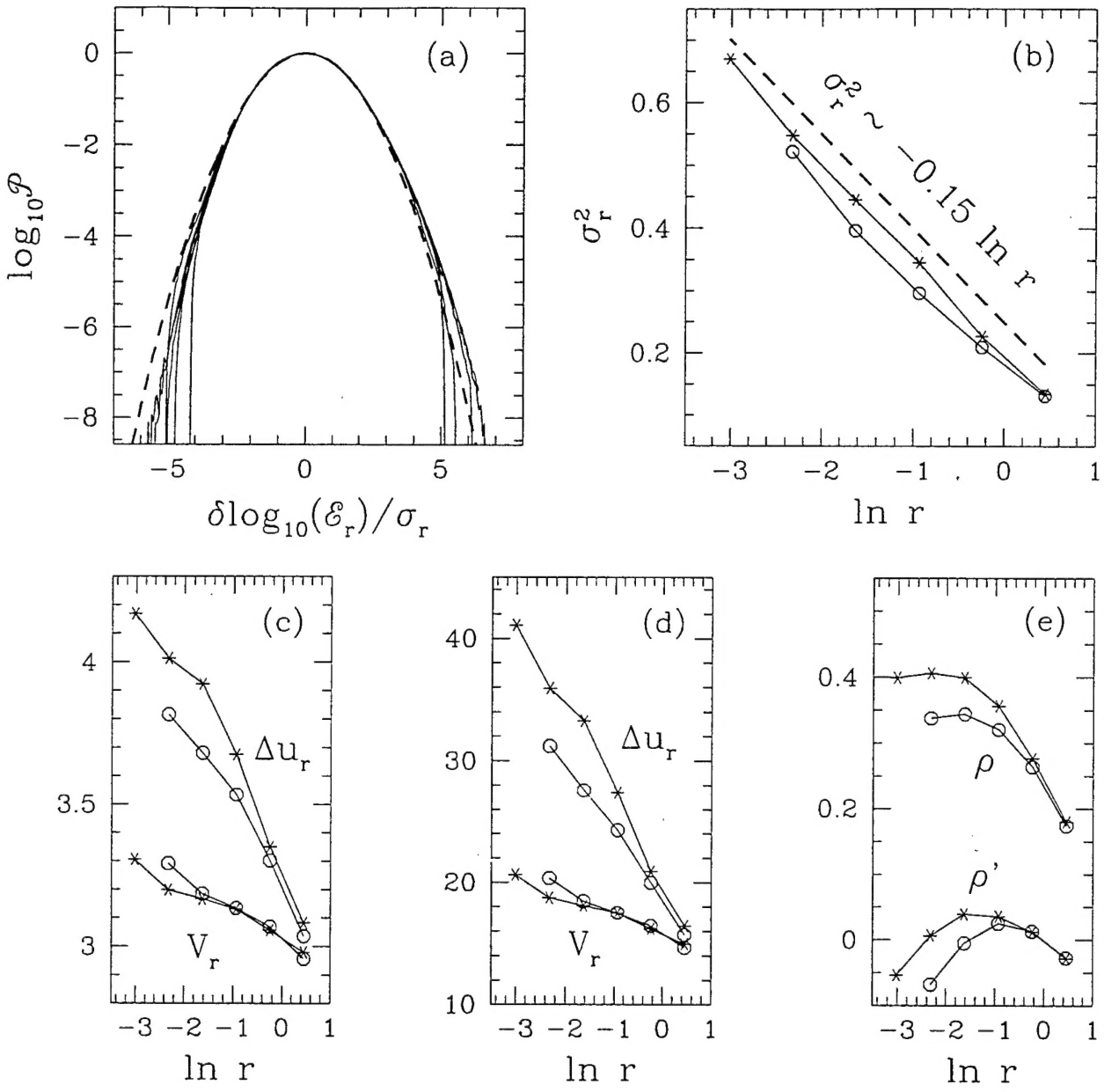

FIG. 4. (a) PDFs of $\log_{10}\mathcal{E}_r$; $\log_{10}\mathcal{P}$ is plotted as a function of $(\log_{10}\mathcal{E}_r - \langle\log_{10}\mathcal{E}_r\rangle)/\sigma_r$. (b) Variance $\tilde{\sigma}_r^2$ of $\ln\mathcal{E}_r$ as a function of filter size $\ln(r)$; the dashed line is $\tilde{\sigma}_r^2 \propto -0.15\ln(r)$. (c) Flatness of velocity differences Δu_r and V_r as a function of filter size $\ln(r)$. (d) Sixth order moments $\langle\Delta u_r^6\rangle/\langle\Delta u_r^2\rangle^3$ and $\langle V_r^6\rangle/\langle V_r^2\rangle^3$ as a function of filter size $\ln(r)$. (e) Correlation coefficients ρ between $|\Delta u_r|$ and $\mathcal{E}_r^{1/3}$ and ρ' between $|V_r|$ and $\log_{10}\mathcal{E}_r$ as functions of filter size $\ln(r)$. The measurements are performed for 128^3 and 256^3 resolutions and $k_c = 4, 8, 16$ and $k_c = 4, 8, 16, 32$, respectively. All data are superimposed in (a). In $(b-e)$ stars represent data for 256^3 resolution and circles represent data for 128^3 resolution.

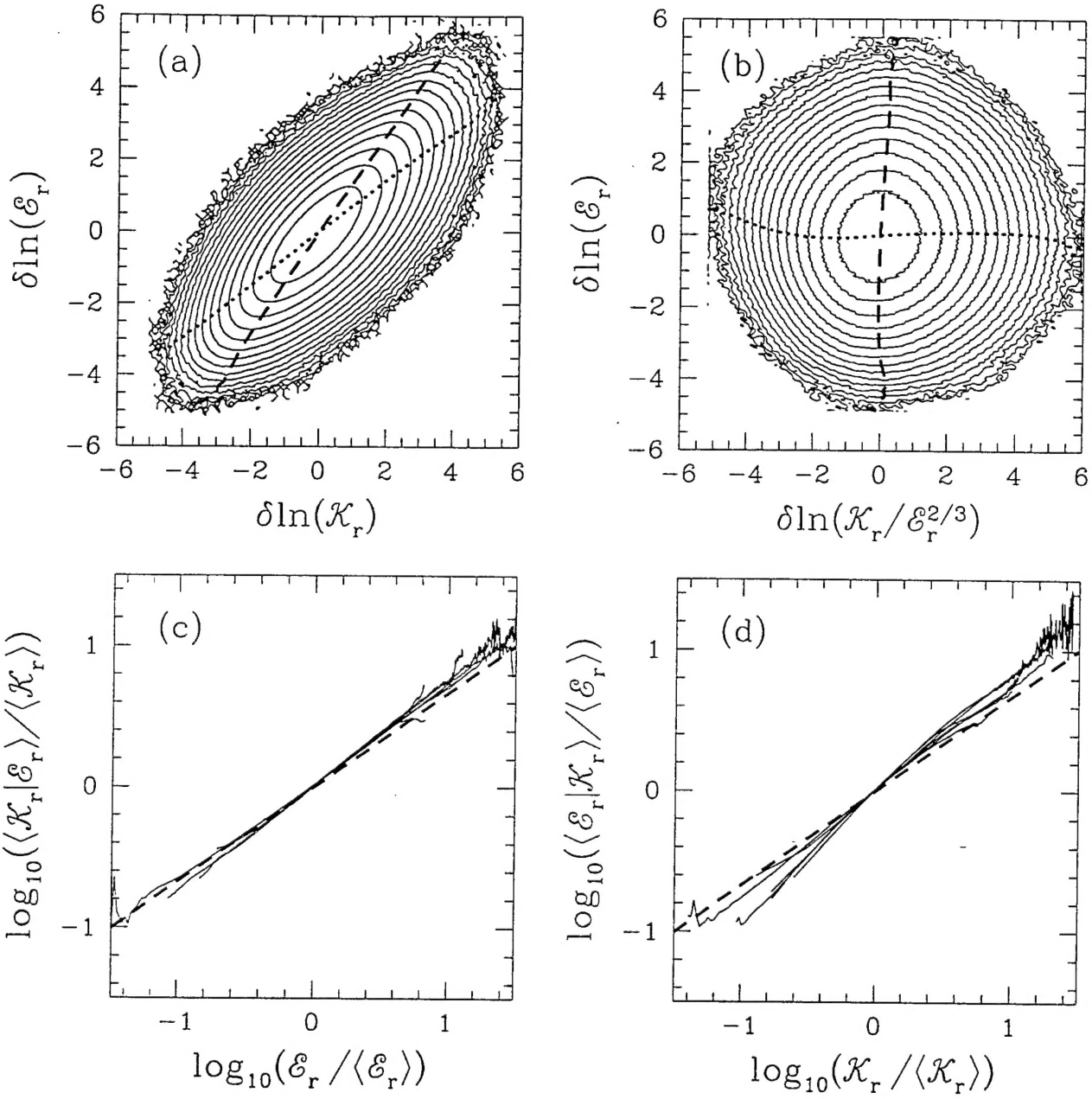

FIG. 5. Joint PDFs between (a) $\ln\mathcal{K}_r$ and $\ln\mathcal{E}_r$, (b) $\ln(\mathcal{K}_r/\mathcal{E}_r^{2/3})$ and $\ln\mathcal{E}_r$. Means are subtracted and variables are normalized by their variances. $k_c = 16$ and $k_d = 41$. Curves show isocontours of $\log_{10}\mathcal{P}$ in increments of 0.4. Dotted curves are conditional averages of abscissas conditioned on ordinates and dashed curves are visa versa. $\log_{10} - \log_{10}$ plots of (c) conditional averages of $\langle\mathcal{K}_r\,|\mathcal{E}_r\rangle\,/\,\langle\mathcal{K}_r\rangle$ as a functions of $\mathcal{E}_r/\,\langle\mathcal{E}_r\rangle$; dashed curve corresponds to $\mathcal{E}_r^{2/3}$; (d) conditional averages of $\langle\mathcal{E}_r\,|\mathcal{K}_r\rangle\,/\,\langle\mathcal{E}_r\rangle$ as a functions of $\mathcal{K}_r/\,\langle\mathcal{K}_r\rangle$; dashed curve corresponds to $\mathcal{K}_r^{2/3}$. Curves are obtained for 128^3 and 256^3 resolutions with $k_c = 4, 8, 16$ and $k_c = 4, 8, 16, 32$, respectively. All curves are superimposed.